Electrochemical study and corrosion modeling of chromium alloy steels exposed to sulfide containing environment

By

© Ladan Khaksar

A thesis submitted to the

School of Graduate Studies

In partial fulfillment of the requirements for the degree of

Doctor of Philosophy

Faculty of Engineering and Applied Science

Memorial University of Newfoundland

February 2018

St. John’s, Newfoundland

"Dedicated to my best friend, Soroosh, and my parents, sister and brother for their patience and support"

ABSTRACT

Corrosion, the destructive result of a chemical reaction between a metal or metal alloy and its environment in sour systems (H_2S dominant) has progressively become a greater concern to the oil and gas industry as a result of production from increasingly sour environments. In this study, the effects of the principal H_2S corrosion product, iron sulfide, on the corrosion resistance of alloy steel were initially investigated, followed by the study of the corrosion behavior of alloy steels in the presence of elemental sulfur, which is often present in sour systems. A new experimental method was applied to synthesize the iron sulfide layer on the steel surface with no H_2S in the environment. Attempts were also made to develop an accurate computational model to predict the corrosion rate of alloy steel in various environmental conditions.

A series of experiments was performed to study chloride concentration, temperature, immersion time and pH effects on the corrosion behavior of alloy steel in the simulated sour environment. Various analyzing methods, such as scanning electron microscopy and X-ray diffraction, were applied to investigate the results which suggest that each factor can significantly affect the electrochemical behavior of alloy steel, especially in the presence of H_2S corrosion products. The corrosion of alloy steel in the presence of elemental sulfur was also studied using the cyclic polarization technique. In general, it was shown that the presence of deposited layers of elemental sulfur on the surface of 13% Cr steel will increase the corrosion rate by decreasing the scaling tendency of corrosion products on the surface, especially at higher temperature.

The experimental data were analyzed and used to develop an analytical model to show the effects of corrosion products, chloride concentration, pH and temperature on the likelihood of corrosion of 13% chromium steel.

ACKNOWLEDGMENTS

I would like to express my great gratitude to my advisor, Dr. John Shirokoff, for his continuous support in my research and academic life. He always guided me through the problems encountered in my study with unimaginable patience. I feel so lucky to have him as an academic adviser during the last years.

Great thanks go to Dr. Bruce Colburne who was my co-supervisor in this project for his great support and guidance. He was always there for me through all the encountered problems during these years.

Many thanks go to my committee member, Dr. Kelly Hawboldt, for her instructions, time and patience during my Ph.D. studies.

Also I would like to thank Dr. Amy Hsiao, my former supervisor, who was the first person in Canada that trusted me and gave me the opportunity of being a PhD student here, in Memorial University of Newfoundland.

I would like to acknowledge the financial support through the Ocean Industries Student Research Award (OISRA) provided by Research and Development Corporation (RDC) Newfoundland and Labrador as well as the financial support provided by Memorial University of Newfoundland, and Suncor energy.

TABLE OF CONTENTS

LIST OF TABLES

LIST OF FIGURES

ABBREVIATIONS AND SYMBOLS

SSC	Sulfide Stress Cracking
CRA	Corrosion Resistant Alloy
FSPO	Floating Production Storage and Offloading
LPR	Linear Polarization Resistance
XRD	X-ray Diffraction
SEM	Scanning Electron Microscope
EDX	Energy Dispersive X-ray Spectroscopy
NACE	National Association of Corrosion Engineers
UNS	Unified Numbering System
AISI	American Iron and Steel Institute
CAMI	Coated Abrasive Manufacturers Institute
CE	Counter Electrode
RE	Reference Electrode
WE	Working Electrode
LPR	Linear Polarization Resistance
PDF	Powder Diffraction Files

JCPDS Joint Committee on Powder Diffraction Standards

ICDD International Center for Diffraction Data

BCC Body Center Cubic

CR Corrosion Rate

MSS Martensitic Stainless Steels

API American Petroleum Institute

OCP Open Circuit Potential

AFM Atomic Force Microscope

RSM Root Square Mean

ANN Artificial Neural Network

GRG Generalized Reduced Gradient

English Letters

M Molar

g Gram

L Liter

A Ampere

mA Mili Ampere

nA Nano Ampere

°C	Degrees Celsius
V	Voltage
i	Current
S	Second
pH	Measure of hydrogen ion concentration
mm	Millimeter
cm	Centimeter
h	Hour
ksi	kilo pound per square inch
Mpa	Megapascal
°F	Degree Fahrenheit
E	Potential
E_p	Pitting potential
E_{corr}	Corrosion potential
E_{pro}	Protection potential
I_{pass}	Passive current
R_a	Roughness average

1. INTRODUCTION

1.1. Background

The worldwide demand for petroleum is growing tremendously and this drives the oil and gas industry to exploit the remaining crude oil and natural gas reserves. According to the International Energy Agency, 70% of crude oil and 40% of natural gas reserves are defined as having a high content of organosulfur compounds which cause “reservoir souring”[1, 2]. This phenomenon is known to decrease the value of exploitation and production assets, increase operational costs and, at worst, result in the shutdown of wells due to the severe impacts of corrosion [3]. In 2008, internal corrosion was the cause of 26% of sour gas incidents in Alberta. Also in 2010, 64% of pipeline incidents on sour gas pipelines in British Columbia were the result of internal corrosion [4].

Crude oil corrosivity problems have been studied since the 1950s, mostly because of their severity and economic impacts on production and refining operations; however, without taking into account the progress made in understanding the role of different parameters on the corrosion process, modern scientific society cannot yet give exact answers enabling the understanding and prediction of petroleum corrosivity [5]. Various problems are encountered in the process of production and refining of sour crudes and corrosion is called as a major one. The costs of lost time, the replacement of construction materials, and the constant personnel involvement in corrosion control are essential. If these are not

controlled, the results can be fatal. The construction materials, uniqueness in refining, transportation, operation conditions and the petroleum mixture, especially the frequent variation in crude or blend oil transported or processed, increase the problem of correlating corrosion of a facility to a certain type of crude oil. Additionally, a wide variety of parameters, such as sulfur content, water content, presence of carbon dioxide and hydrogen sulfide, velocity, temperature and pressure influence the crude corrosion process. Some of those parameters, for instance carbon dioxide, affect the general corrosion of steel, whilst hydrogen sulfide is more localized and can cause sulfide stress corrosion cracking, hydrogen embrittlement, hydrogen induced cracking or stress orientated hydrogen induced cracking which are all localized corrosion. Although, hydrogen sulfide will not necessarily cause a proportional increase in the general corrosion rate, but rather will make susceptible materials prone to catastrophic failure [6].

Generally both CO_2 and H_2S are acid gases that are produced in the hydrocarbon phase which can render the associated water (condensed or formed) corrosive and lead to severe degradation. Each of these gases occurs naturally in some of the producing reservoirs or may result from external contamination of the reservoir, such as in the case of reservoir souring that may result when seawater is injected for secondary recovery or with the use of gas injection for reservoir pressure maintenance. Corrosion resulting from each of these two acidic gases has unique characteristics and, as a result, has received considerable industry attention, both to understand the corrosion mechanisms associated with the particular acid gas and the options available to mitigate the resulting corrosion [7]–[12]. Selection of materials to combat corrosion relies mainly on the type of

corrosion anticipated (e.g. whether general or localized), the confidence in predicting the rate and type of corrosion, risk of failure and life cycle cost. While the primary concern in selection of materials in systems containing H_2S is sulfide stress cracking (SSC), the issue of corrosion should not be underestimated.

There is ongoing research to investigate the effects of hydrogen sulfide on the corrosion process in a hydrocarbon environment [13]. Nonetheless, review of related literature has highlighted a gap in knowledge of a model to predict the internal corrosion rate of sour gas pipelines. To fill this gap, a prediction model should be developed to help in reducing the internal corrosion rate, optimizing the lifetime and in making decisions about material selection. The developed model provides a decision-making tool for material selection, which can accurately predict and determine the internal corrosion rate in the presence of hydrogen sulfide corrosion products. The model should be able to predict the influences of dissolved corrosion products, temperature, pH, and chloride concentration on the internal corrosion rate of Corrosion Resistant Alloys (CRAs).

1.2. Relevance of Project to Newfoundland and Labrador's Ocean Industries

The offshore oil and gas industry is of critical importance to the Newfoundland and Labrador economy [8]. One of the most productive oilfields in Newfoundland and Labrador is the Terra Nova oilfield. This oilfield is situated on the Grand Banks, about 350 kilometers east-southeast of St. John’s, Newfoundland and 35 kilometers southeast of the Hibernia Oil Field. Terra Nova’s life-of-field production is estimated at approximately 516 million barrels, with production from the Graben, East Flank and Far

East blocks [14]. In May 2011, Steve Williams, Suncor's chief operating officer, said that Suncor Energy, the operator of the Terra Nova oilfield, is dealing with sour gas problems at some of its production wells off Newfoundland and Labrador. A few month later, Rick George, Suncor president and CEO, during a conference call with analysts said: "What we've done is shut down the affected wells and the facilities in which we were testing H_2S while we developed a mitigation plan" [15]. The shutdown of some wells at Terra Nova cut the oilfield's total production in half during the first three months of the year and the total production dropped 49 percent to 4 million barrels of crude [14].

The Terra Nova facilities production supply and offloading (FPSO) was designed specifically for the North Atlantic environment, which includes ice-reinforcement and a global dynamic positioning system. This system allows the vessel to position itself for more favorable wave headings. There are more than 40 kilometers of flexible pipe that convey hydrocarbons between the wells and the vessel [16]. As a result of the literature review of similar cases in other provinces, described in the introduction, it is observed that these pipelines are extremely vulnerable to internal corrosion and consequently, failure, due to the reservoir souring process.

H_2S dissolves in water to form acid solutions that are corrosive to stainless steel. The corrosion rate is influenced by a number of complex factors, including water phase composition (acid gases content and dissolved minerals), temperature, flow regime, flow velocity, and the condensation rate from the vapor phase [17]. In the wells which are facing with reservoir souring in the Terra Nova field, it is expected that the corrosion mechanism in pipelines is primarily due to the presence of H_2S and its corrosion

products. This can cause, in steel, hydrogen induced cracking and sulfide stress corrosion cracking [18]. In harsh environments, corrosion remains a key obstacle to sustaining operational success in hydrocarbon production and its continued occurrence affects the economy and has consequences for the safety of people and the integrity of facilities [5]. A central element in the design of facilities and corrosion mitigation is the correct choice and deployment of materials which are both economical and suitable to provide satisfactory performance over the design life [16]. This project deals with a prediction model for the internal corrosion in sour gas pipelines to predict the corrosion profile in pipelines and help making informed operational decisions to prevent unsafe conditions while maintaining the profitability of offshore oil facilities. The development of the proposed prediction model for internal corrosion in sour gas pipelines will benefit the province of Newfoundland and Labrador by promoting inherently safer processing of natural resources in a cost-effective manner.

1.3. Knowledge and technological gap:

The corrosion of various steel, by H_2S containing media has been investigated since the 1940s [19]. Recently more attention has been focused on the corrosion of alloy steels such as molybdenum and chromium steels because of their wide application in the oil and gas industry, especially in an H_2S containing environment [8], [20]–[24]. The understanding, prediction, and control of H_2S corrosion of alloy steels are some of the key challenges for oil and gas production. With regard to this matter, many researchers have studied the H_2S corrosion mechanism with a special emphasis on the importance of

the electrochemical corrosion mechanism [25]. Despite the relative abundance of experimental data on H_2S corrosion, most of the literature is still confusing and contradictory, due to the complexity of the H_2S corrosion mechanism. One of the most persistent and complex aspects of the corrosion mechanism is corrosion products analysis, which should be purposed to identify the corrosion mechanism. Comprehensive investigation of corrosion products is the key to develop prediction models of the corrosion rate in an H_2S containing environment. Even small changes in experimental conditions can lead to various corrosion products, which have been investigated in numerous studies. It is important to note that, in contrast to one single type of iron carbonate formed in CO_2 corrosion, many types of iron sulfide, FeS, may form during H_2S corrosion, such as amorphous ferrous sulfide, mackinawite, cubic ferrous sulfide, smythite, greigite, pyrrhotite, troilite, pyrite, and marcasite [10], [26]–[30]. It has been reported that the evolution of H_2S corrosion products on the steel surface progresses from iron-rich to sulfur-rich phases in oxygen-free solution [31]. Mackinawite is formed by both solid-state and precipitation processes, whereas cubic FeS and troilite are the subsequent phases on an iron surface exposed to saturated aqueous H_2S at 21°C and pH 4 [32]. Multilayer corrosion product films have been investigated in a CO_2/ H_2S environment, and iron sulfide films have been found to cause a substantial rate reduction [33]. Mackinawite cracking leads to the nucleation of other types of iron sulfides and under different conditions [34], however, detailed studies on the effect of those products on the corrosion resistance of alloy steel are still insufficient. It has been reported that the protective thin iron sulfide film could be formed at the steel surface via solid-state

formation, resulting in a lower corrosion rate in the presence of trace amounts of H_2S [35]. Some reports have mentioned that this thin sulfide film might be mackinawite (FeS_{1-x}) [25], [35]–[37]. Hence, providing direct evidence that confirms the existence of thin mackinawite film on the alloy steel surface is one of the main goals of this study. In this study, sour corrosion is considered as a series of corrosion mechanisms that are defined by the formation of a type of FeS. An investigation has reported that there are three types of FeS that are commonly found in oilfield corrosion; these are pyrite, pyrrhotite and mackinawite [38]. Pyrite, an ordered solid solution of FeS and elemental sulfur, is found only when elemental sulfur is present in the system. Pyrrhotite is a non-stoichiometric form of FeS that forms in most sour environments. Mackinawite is a semi-stable form of FeS that forms under the special conditions of low H_2S activity in the environment, which will be referred to herein as slightly sour. This research deals with the condition where mackinawite is found, the chemistry of mackinawite formation and the impacts that mackinawite formation has on the corrosion rates. The corrosion mechanism for higher H_2S environments, where pyrrhotite is produced, has been reported elsewhere [25], [39], [40]

Beside the importance of investigation of iron sulfide, another substantial and common deposited corrosion product in oil and gas pipelines is elemental sulfur. The primary source of elemental sulfur in sour gas wells is the oxidation of hydrogen sulfide. This may occur as a result of an ingress of oxygen, the presence of reducible high oxidation state metals, such as ferric ion in iron (III) oxide, or be related to reservoir thermochemical sulfate reduction [41], [42]:

$$8\ H_2S + 4\ O_2 \rightarrow 8\ H_2O + S_8 \quad (1.1)$$

$$8\ Fe_2O_3 + 24\ H_2S \rightarrow 16\ FeS + 24\ H_2O + S_8 \quad (1.2)$$

$$2\ SO_4^{2-} + 6\ H_2S \rightarrow S_8 + 4\ H_2O + 2\ OH^- \quad (1.3)$$

In each of the above reactions, the sulfur has been represented as S_8, corresponding to its stable/dominant allotrope at temperatures approaching 160°C; note that it is molten at temperatures above 115°C (α-sulfur) [41], [43]. Other possible sulfur formation processes include H_2S dissociation at elevated temperatures or microbial sulfate reduction[44]. Typically, elemental sulfur is carried by the sour gas from the production zone well casing to the pipelins, however, as pressures and temperatures decrease, this sulfur will be deposited. In aqueous conditions, contact of sulfur with mild steel has resulted in the onset of catastrophic corrosion processes [45]. In 1700, Lemery reported the relationship between the corrosion of steels and elemental sulfur for the first time [1]. In the 1980s, severe corrosion was also observed on pipeline steel exposed to mixtures of elemental sulfur and H_2S in several important industrial areas, especially in sour gas and oil production fields and transport systems [46]. Elemental sulfur can be deposited in pipelines and facilities during sour gas production and increase the risk of corrosion failure of tubing and pipelines in a high H_2S and CO_2 environment [47]. The more content of H_2S in the gas, the more likely elemental sulfur precipitation will occur, especially in gas wells with more than 30% H_2S [5]. There has been a large number of works on H_2S corrosion and protection [8]–[11]. In recent years, Fang reported the corrosion behavior of carbon steels at different temperatures by molten covering sulfur on

steel surfaces [48], [49], however, there are not still enough investigations on corrosion process in the presence of elemental sulfur and iron sulfide deposition on the steel surface. In this research, the effects of deposited elemental sulfur on the corrosion behavior of molybdenum and chromium alloy steels have been investigated through corrosion simulation tests, and electrochemical measurements.

1.4. Research objectives

1) The initial objective is to identify and prioritize key contributing issues that need to be addressed to fill gaps in the knowledge, technology, and methodology associated with corrosion degradation in sour gas pipelines.

2) The principal objective is to develop a model to predict the corrosion profile of Corrosion Resistant Alloys (CRAs) based on the risk of pitting corrosion and the localized breakdown susceptibility of oxide film due to the presence of dissolved hydrogen sulfide (H_2S).

A new technique for corrosion prediction in sour gas pipelines is the main expected output of this research. Another valuable outcome would be enhancing pipelines safety and consequently decreasing sour pipeline incidents. These results would help to safeguard people and the environment and increase the profitability of sour oilfields.

1.5. Scope of work

The scope of this project covers both prediction and mitigation of corrosion process hazards in offshore pipelines which may result in release of chemicals and loss of

productivity. This work aims to better understand how reservoir souring propagates through a deteriorating process and cause loss, where loss is defined as the discrepancy between the current situation and the ideal situation. Development of an analytical model for prediction of corrosion rate is also included in the scope of this work. The project includes two major phases:

Phase I: Identification of corrosion factors and mechanisms due to reservoir souring: A three-pronged approach will be used to identify the corrosive factors contributing to the operational performance of offshore sour gas pipelines in sour environments:

• A detailed literature review will be conducted to determine what corrosive factors have been identified from earlier studies. Moreover, a complete and vigorous review of existing corrosion prediction models in sweet oil operations will be performed to determine how they are designed and how mitigation measures are enforced to avoid operational failures.

• The next step covers a thorough examination of the identified causes of the sour corrosion process in offshore pipelines operating in harsh environments. This activity includes identifying how and to what extent each cause affects both corrosion resistance and the microstructural properties of sour gas pipelines.

• Finally, the results will be shared with industry representatives and other relevant experts to gather opinions on the completeness of the identified causes of the sour corrosion process in offshore pipelines. The developed cause and effect diagram will

considered by the industry partner as based on real experiences, lessons learned, and industry needs.

Upon approval of Phase I by the industry partner, the results will be used in the next phase of the project to develop the corrosion prediction model, including the prediction model for corrosion due to the presence of hydrogen sulfide and elemental sulfur in harsh environment applications.

Phase II: Development of corrosion prediction model for sour gas pipelines in harsh environment applications:

The scope of Phase II includes the following:

• Developing a corrosion prediction model for offshore pipelines in sour environments. The developed model will perform the required analysis by answering these questions: 1) what is the final corrosion rate in a certain environmental condition? 2) What is the effect of deposited corrosion products on the corrosion mechanisms? Answers should take the correlation between corrosion and reservoir souring variables into consideration.

• Testing the project outcomes. Based on the availability of required information, the developed model will be applied to a simulated or a real-life case study and the results will be shared with the industry partner to assess the sensitivity, effectiveness and practical applicability of the model. Various comparisons to other existing analytical modeling tools and best practices will be provided to ensure the highest standards are applied during the modeling procedure.

1.6. Uniqueness of Proposed Research

Even though numerous predictive models have been and are being developed, most of the available predictive models for H_2S corrosion tend to be either very concentrative in their interpretation of results or focus on a narrow range of parametric effects, thereby limiting the scope of the model's application for a realistic assessment of corrosivity and corrosion rates. Often, data required by the models are not easily accessible or available to the operators who need to employ a model, thereby limiting the applicability of the models to situations of reduced practical importance. In this context, the issue of the H_2S corrosivity assessment of corrosion resistant alloys can be re-stated in terms of the following critical requirements:

- Utilize existing lab/field data and theoretical models to obtain a realistic assessment of corrosivity and corrosion rates.

- Develop an analytical approach that integrates both numerical (lab trends) and heuristic (field data and experience) information and knowledge about corrosivity prediction.

1.7. Research method and experimental design

According to NACE MR0175/ISO15156, one of the most common steel alloys for tubular and tubular components in sour service is UNS G41XX0, formerly AISI 41XX [26]. This steel typically consists of 0.80–1.1 Cr, 0.15–0.25 Mo, 0.28–0.33 C, 0.40–0.60 Mn, 0.035 P, 0.040 S, 0.15–0.35 Si, and balanced Fe. In the first two chapters, the

working electrodes are machined from the parent material, 4130 alloy steel, into cylinders having dimensions of approximately 9 mm length and 9 mm diameter.

Among all types of Corrosion Resistant Alloys (CRA) used today in the oil and gas industry, martensitic stainless steels (MSS) are some of the most reliable and applicable ones. These steels have significant CO_2 corrosion resistance due to the addition of a minimum of 11% chromium content to their composition. NACE and American Petroleum Institute (API) standards suggest a number of MSS for oil and gas industry applications; among all of them, 13% chromium steel is the most recommended [1]. According to the industrial partner's request, the corrosion samples are made from conventional 13% Cr steel, grade 420. In the second two chapters, the working electrodes are machined from the parent material, 13% chromium steel, into cylinders having dimensions of approximately a 9 mm length and 9 mm diameter.

Prior to the experiments, all specimens are polished with Coated Abrasive Manufacturers Institute (CAMI) grit designations 320, 600 and 1000 corresponding to average particle diameters 36.0, 16.0, and 10.3 microns and finally 6-micron grit silicon carbide paper, and then cleansed with deionized water until a homogeneous surface is observed. Then the specimens are quickly dried using cold air to avoid oxidation.

Due to the inherent safety concerns associated with H_2S gas, an alternative method of FeS film deposition is employed [27]. The alternative method provides an acidic electrolyte solution which has the potential to form a thin FeS layer on the steel surface, like its occurrence in a sour oil pipeline.

In order to measure the corrosion parameters, electrochemical techniques such as Linear Polarization resistance (LPR), potentiodynamic polarization and cyclic polarization are applied. Electrochemical corrosion measurements, and in particular, LPR, provide information about the corrosion rate of an electrochemical system [21]. In this method the polarization curves represent the evaluation of current density (i) developed on the steel surface as a function of the applied potential (E). The current density is directly related to the nature and the rate of electrochemical reactions which occur at the interface between the steel surface and the aggressive solution.

For this study, corrosion and electrochemical experiments are conducted in a multi-port glass cell with a three electrodes setup, at the atmospheric pressure based on the ASTM G5-82 standard for potentiodynamic anodic polarization measurements [22]. The applied sweep rate for these measurements is 0.5mV/s. An Ivium Compactstat Potentiostat monitoring system is used to perform electrochemical corrosion measurements. The pH is adjusted by adding deoxygenated hydrochloric acid or sodium hydroxide. During the electrochemical measurements, a graphite rod is used as the counter electrode (CE) while saturated silver/ silver chloride (Ag/AgCl) is installed as the reference electrode (RE) and 4130 molybdenum alloy and conventional 13% Cr steel samples are chosen as working electrodes (WE).

1.8. Organization of thesis

This thesis is written in manuscript format (paper-based). Table 1.1 shows the papers published during the course of this research and the outline of each chapter.

Table 1.1. Organization of thesis

Chapter Title	Supporting Paper Title
Chapter 1: Introduction	Not applicable (NA)
Chapter 2: Electrochemical and microstructural analysis of FeS	Electrochemical and microstructural analysis of FeS films from acidic chemical bath at varying temperatures, pH and immersion times, *International Journal of Corrosion*, 2016
Chapter 3: Corrosion Behavior of Cr-Mo Low Alloy Steel	Effect of Elemental Sulfur and Sulfide on the Corrosion Behavior of Cr-Mo Low Alloy Steel for Tubing and Tubular Components in Oil and Gas Industry, *Journal of Material Science and Engineering by MDPI*, 2017 Corrosion behavior of Cr-Mo low alloy steel in direct contact with elemental sulfur, *2nd International Conference on Smart Material Research (ICSMR 2016), Istanbul, Turkey* (Received best oral presentation award)
Chapter 4: Corrosion Behavior of 13% chromium steel	Effect of various corrosion films on electrochemical behavior of conventional 13% Cr steel exposed to chloride containing environment, *Journal of Innovations in Corrosion and Materials Science by Bentham Science*, 2017 Corrosion behavior of conventional 13% Cr steel exposed to chloride containing environment, *56th annual Conference of Metallurgists, Vancouver, Canada, 2017*
Chapter 5: Proposed model of corrosion rate of 13% chromium steel in harsh environment	Development of a model for prediction of corrosion rate of 13% chromium steel exposed to different environmental conditions, *Global Journal of Engineering Science and Research, 2017*
Chapter 6: Conclusions and Recommendations	NA

Chapter 2 proposes the synthetization of a FeS corrosion product layer on a 4130 alloy steel surface by chemical bath deposition of iron and sulfur ions at acidic pH levels under varying environmental conditions, without the presence of H_2S in the solution.

Chapter 3 discusses the effect of elemental sulfur deposition on the corrosion resistance of 4130 molybdenum alloy steel in different environmental conditions. This chapter highlights the effects of immersion time and pH on the corrosion behavior of alloy steel.

Chapter 4 studies the effects of elemental sulfur and FeS layers on the corrosion behavior of 13% chromium steel with particular emphasis on the role of temperature and chloride concentration and the morphological measurement of corrosion products.

Chapter 5 uses the empirical approaches, optimal solutions, curve fitting and neural networks to predict the corrosion rate of 13% chromium steel in a simulated sour environment by considering the presence of various sour corrosion product layers on the surface of material.

Chapter 6 reports the summary of the thesis and the main conclusions drawn through this work. Recommendations for future work are presented at the end of Chapter 7.

1.9. References

[1] D. A. Jones, *Principles and prevention of corrosion*, Second. Rio de Janeiro: Prentice Hall, 1996.

[2] M. Schofield and J. Stott, "Assessing the Magnitude and Consequences of Reservoir Souring," in *Deepwater drilling and completions conference*, Texas, USA, 2012, pp. 76–79.

[3] P. Evans, "Reservoir souring challenges and solution from operators' perspective," in *International Symposium on applied microbiology and molecular biology in oil system*, Rio de Janeiro, Brazil, 2013.

[4] "Mitigation of Internal Corrosion in Sour Gas Pipeline Systems,", CAPP Standard, Calgary, 2009.

[5] D. Duissenov, "Production and processing of sour crude and natural gas - challenges due to increasingly stringent regulations," M.Sc. thesis, Norwegian University of Science and Technology, 2013.

[6] B. Kermani, J. Martin, and K. Esaklul, "Material design strategy: effects of H_2S/CO_2 corrosion on materials selection," in *61st annual corrosion conference and exposition*, San Diego, USA, 2006, no. 6121.

[7] M. B. Kermani and A. Morshed, "Carbon Dioxide Corrosion in Oil and Gas Production — A Compendium," *Corrosion*, vol. 59, no. 8, pp. 659–683, 2003.

[8] *Petroleum and Natural Gas Industries – Materials for use in H_2S -containing Environments in Oil and Gas Production*, CAPP Standard, December 2005.

[9] S. D. Cramer and B. S. Covino, Eds., *ASM Handbook of Corrosion: Fundamentals, Testing, and Protection*, 10, illust ed. ASM International, 2003.

[10] L. Smith and B. B. Craig, "Practical Corrosion Control Measures for Elemental Sulfur Containing Environments," *Corrosion*, no. 5646, p. 20, 2005.

[11] R. H. Hausler, "Contribution to the Understanding of H_2S Corrosion," *Corrosion*, no. 4732, pp. 1–25, 2004.

[12] R. N. Tuttle, “Corrosion in Oil and Gas Production,” *Soc. Pet. Eng.*, pp. 756–762, 1987.

[13] L. Smith and K. De Waard, “Corrosion prediction and materials selection for oil and gas producing environments,” *Corrosion*, no. 5648, pp. 1–14, 2005.

[14] “Suncor energy’s public quarterly report. Terra Nova Developments,” St.John’s, 2014.

[15] M. Baird, “Terra Nova production drops,” *The Telegram*, 2011. [Online]. Available: file:///C:/Users/Ladan/Desktop/RDC/Terra Nova production drops - Business - The Telegram.html.

[16] S. Lundrigan, H. Greene, B. Burton, and S. Mapplebeck, “Terra Nova Calcium Nitrate Storage Tank,”, BHS consultant technical report, St.John’s, 2013.

[17] M. Lepoutre, “Technical challenges for tight & sour gas,” in *19th World Petroleum Congress*, Spain, 2008.

[18] “Sulfide stress cracking,” 2012. [Online]. Available: http://www.documentation.emersonprocess.com/groups/public/documents/reference/d351798x012_09.pdf. 2012.

[19] Y. Zheng, B. Brown, and S. Nesic, “Electrochemical Study and Modeling of H_2S Corrosion of Mild Steel,” *NACE Int.*, no. 2406, pp. 1–22, 2013.

[20] Y. Miyata, Y. Yamane, O. Forukimi, H. Niwa, and K. Tamaki, “Corrosion of new 13% Cr stainless steel OCTG in severe CO_2 environment,” *NACE Int.*, 1995.

[21] “V&M 13% Cr & Super 13% Cr steel grades for Sweet CO_2 corrosion service,” Vallourec Group Technical report, 2015.

[22] D. Sidorin, D. Pletcher, and B. Hedges, “The electrochemistry of 13% chromium stainless steel in oilfield brines,” *Electrochim. Acta*, vol. 50, pp. 4109–4116, 2005.

[23] H. Marchebois and H. E. L. Alami, “Sour service limits of 13% Cr and super 13% Cr stainless steels for OCTG: effect of environmental factors,” in *Corrosion Conference*, 2009, no. 9084, pp. 1–19.

[24] A. Turnbull and A. Griffiths, “Corrosion and Cracking of Weldable 13 Cr Martensitic Stainless Steels – A Review,” 2002.

[25] H. Vedage, T. a. Ramanarayanan, J. D. Mumford, and S. N. Smith, "Electrochemical Growth of Iron Sulfide Films in H 2 S-Saturated Chloride Media," *Corros. NACE*, vol. 49, no. 2, pp. 114–121, 1993.

[26] D. Rickard, "Kinetics of FeS precipitation: Part 1. Competing reaction mechanisms," *Geochim. Cosmochim. Acta*, vol. 59, no. 21, pp. 4367–4379, 1995.

[27] A.R. Lennie and D. J. Vaughan, "Spectroscopic studies of iron sulfide formation and phase relations at low temperatures," *Geochemical Soc.*, no. 5, pp. 117–131, 1996.

[28] B. N. Brown, "The Influence of Sulfides on Localized Corrosion of Mild Steel," PhD thesis, Ohio University, 2013.

[29] J. Kvarekval, "Morphology of localized corrosion attacks in sour environments," in *corrosion conference*, Nashville, USA, 2007, no. 7659, pp. 1–10.

[30] T. Laitinen, "Localized corrosion of stainless steel in chloride , sulfate and thiosulfate containing environments," *Corros. Sci.*, vol. 42, 2000.

[31] D. Enos and L. Scribner, "The potentiodynamic polarization scan,", Technical report of Solarton instruments, 1997.

[32] M. Koteeswaran, "CO_2 and H_2S corrosion in oil pipelines," Master thesis, University of Stavanger, 2010.

[33] R. O. Rihan, "Electrochemical corrosion behaviour of x52 and x60 steels in carbon dioxide containing saltwater solution," *Mater. Res.*, vol. 16, no. 1, pp. 227–236, 2013.

[34] W. Sun and S. Nesic, "A Mechanistic Model of H_2S Corrosion of Mild Steel," *NACE Int.*, no. 7655, pp. 1–26, 2007.

[35] K. J. Lee and S. Nešić, "The Effect of Trace Amount of H_2S on CO_2 Corrosion Investigated by Using the EIS technique," *Corrosion*, no. 5630, pp. 1–16, 2005.

[36] W. Sun, S. Nešić, and S. Papavinasam, "Kinetics of Iron Sulfide and Mixed Iron Sulfide/Carbonate Scale Precipitation in CO_2/ H_2S Corrosion," *NACE Int.*, no. 6644, pp. 1–26, 2006.

[37] D. Rickard and G. W. Luther, "Chemistry of iron sulfides," *Chem. Rev.*, vol. 107, no. 2,

pp. 514–562, 2007.

[38] S. N. Smith and J. . Pacheco, “Prediction of corrosion in slightly sour environments,” *Corrosion*, no. 2241, pp. 1–16, 2002.

[39] S. N. Smith and T. a. Ramanarayanan, “Scaling Phenomena in High-Temperature Aqueous and Gaseous Environments Containing Sulfur,” in *International Symposium of Corrosion Science and Engineering Proceedings*, 1989.

[40] T. A. Ramanarayanan and S. N. Smith, “Corrosion of Iron in Gaseous Environments and in Gas-Saturated Aqueous Environments,” *Science*, pp. 66–74, 1990.

[41] R. Steudel, “Mechanism for the formation of elemental sulfur from aqueous sulfide in chemical and microbiological desulfurization processes,” *Ind. Eng. Chem. Res.*, vol. 35, no. 4, pp. 1417–1423, 1996.

[42] A. Davydov, K. T. Chuang, and A. R. Sanger, “Mechanism of H_2S Oxidation by Ferric Oxide and Hydroxide Surfaces,” *J. Chem. Soc.*, vol. 5647, no. 98, pp. 4745–4752, 1998.

[43] R. Steudel and F. Physik, “Solid Sulfur Allotropes,” *Top Curr. Chem.*, no. 230, pp. 1–79, 2003.

[44] J. Zaman and A. Chakma, “Production of hydrogen and sulfur from hydrogen sulfide,” *Fuel Process. Technol.*, vol. 41, pp. 159–198, 1995.

[45] D. D. MacDonald, B. Roberts, and J. B. Hyne, “The corrosion of carbon steel by wet elemental sulphur,” *Corros. Sci.*, vol. 18, no. 5, pp. 411–425, Jan. 1978.

[46] P. Boden and S. Maldonado-Zagal, “Hydrolysis of Elemental Sulfur in Water and its Effects on the Corrosion of Mild Steel,” *Br. Corros. J.*, vol. 17, pp. 116–120, 1982.

[47] L. ZHIDE *et al.*, “Corrosion influencing factors of sour gas wells in Chuandongbei, China,” *Mater. Perform.*, 2006.

[48] H. Fang, D. Young, and N. Srdjan, “Elemental sulfur corrosion of mild steel at high concentration of sodium chloride,” in *17th international corrosion congress*, Los Vegas, USA, 2009, vol. 2592, pp. 1–16.

[49] H. Fang, B. Brown, D. Young, and M. Technology, “Investigation of elemental sulfur

corrosion mechanisms," *NACE Int.*, no. 11398, pp. 1–13, 2011.

2. ELECTROCHEMICAL AND MICROSTRUCTURAL ANALYSIS OF FeS FILMS FROM ACIDIC CHEMICAL BATH AT VARYING TEMPERATURE, pH, AND IMMERSION TIME

Preface

A version of this manuscript is accepted for publication in the International Journal of Corrosion. I am the primary author of this paper, along with the co-authors, John Shirokoff and Gary whelan. I conducted the literature review and proposed the outline of the experiments and the analysis procedure. I conducted most of the experiments and microstructural analysis. Gary Whelan, Suncor's work term student, helped us through the experimental steps and corrosion measurements. I prepared the first draft of the manuscript and subsequently revised the manuscript based on the co-authors' feedbacks and also the initial feedbacks from the journal reviewers. The co-author John Shirkokff helped in analyzing the final results, and contributed in preparing, reviewing and revising the manuscript.

Abstract

The corrosion resistance and corrosion products of 4130 alloy steel have been investigated by depositing thin films of iron sulfide synthesized from an acidic chemical bath. Tests were conducted at varying temperatures (25°C-75°C), pH levels (2-4), and immersion times (24-72 hours). The corrosion behavior was monitored by linear polarization resistance (LPR) method. X-ray Diffraction (XRD), Energy Dispersive X-ray Spectroscopy (EDX), and Scanning Electron Microscopy (SEM) have been applied to characterize the corrosion products. The results show that along with the formation of an iron sulfide protective film on the alloy surface, increasing temperature, increasing immersion time, and decreasing pH all directly increase the corrosion rate of steel in the tested experimental conditions. It was also concluded that increasing temperature causes an initial increase of the corrosion rate followed by a large decrease due to transformation of the iron sulfide crystalline structure.

Keywords: 4130 alloy steel, SEM, EDX, XRD, LPR, chemical bath deposition.

2.1. Introduction

The corrosion of steel in aqueous environments containing hydrogen sulfide, H_2S, is of great interest to the oil and gas industry[1-5]. Unlike carbon dioxide corrosion, H_2S corrosion always involves the formation of corrosion products that are predominantly iron sulfide, FeS, compounds with various phases. These corrosion product films should be characterized to illustrate the corrosion mechanism. It has been reported that the

formation of the FeS generally controls the H_2S corrosion[6]. However, there is still debate on how the initial corrosion product layers form.

It is well known that surface scale formation is one of the most important factors that influences the corrosion rate [7]. The scale slows down the corrosion process by presenting a diffusion barrier for the species involved in the corrosion process and by covering and preventing the underlying steel from further dissolution. The scale growth depends primarily on the kinetics of scale formation [8].

H_2S corrosion on the metal surface is also strongly dependent on the type of corrosion product films formed on the surface of the metal during the corrosion process. The precipitation rate or the formation of these films depends on various environmental factors and the concentration of species. The stability, protectiveness, and adherence of these films determine the nature and the rate of corrosion [9-10]. It is important to note that in contrast to one single type of iron carbonate formed in CO_2 corrosion, many types of FeS may form during H_2S corrosion such as amorphous ferrous sulfide, mackinawite, cubic ferrous sulfide, smythite, greigite, pyrrhotite, troilite, pyrite and marcasite [11-18].

In aqueous solutions of H_2S, two mechanisms were proposed for the formation of FeS films, namely, dissolution of iron followed by precipitation of FeS and sulfide ion adsorption followed by direct film formation [19].

The first proposed theory is a possible mechanism for FeS formation in that the FeS layer is formed by precipitation only when its concentration reaches the solubility limit, analogous to how precipitation equilibrium governs the mechanism of iron carbonate formation. However, if this is to be true, the kinetics of FeS formation must be much

faster than that of iron carbonate. In cases where FeS is highly under-saturated in the bulk, it can still be formed on the steel surface. This is suspected to be due to the high surface pH caused by consumption of hydronium ions by corrosion as well as local high ferrous ion concentration, resulting in a supersaturation of FeS on the steel surface. Therefore, FeS forms relatively fast on the steel surface, irrespective of the bulk conditions [20-22]. Another possible theory has been proposed by Shoesmith, et al., which describes that the first layer of mackinawite is generated by a direct, solid-state reaction between the steel surface and H_2S [2][19]. Mackinawite then grows with time. The corrosion product layer growth rate depends upon the corrosion rate as well as the water chemistry with regards to pH, temperature, etc. It has been found that when the thickness of FeS reaches a critical value, this corrosion product layer cracks due to the development of internal stresses [6], [23]. More corrosive species such as H_2S or hydrogen ions diffuse through the now porous FeS layer and attack the steel surface. More FeS is then formed either by solid-state reaction between steel and H_2S akin to what happened initially, or precipitation of FeS due to local FeS supersaturation. This direct, solid-state reaction theory is supported by other research [24-25].

How FeS initially forms is pertinent, because it can help to better predict the H_2S corrosion. However, until now research efforts have not achieved agreement on this subject. The situation is complicated by the variety of types of FeS that can be formed. Depending on the conditions relating to the corrosion environments: mackinawite, pyrrhotite, greigite, smythite, marcasite and pyrite are the six naturally occurring FeS minerals [5], [19].

Most of the previous studies in this area are conducted at high temperatures and usually in gaseous H_2S environment. In the present study, all the experiments are performed at lower temperature in an aqueous solution because the real temperature of some oil and gas production and pipelines are below 100°C. In this study, FeS films have been synthesized on the metal alloy surface without the presence of H_2S in the solution. Rather, FeS was formed by chemical bath deposition of iron and sulfur ions at acidic pH levels under varying environmental conditions.

2.2 Experimental procedure

2.2.1. Material and sample preparation

According to NACE MR0175/ISO 15156, the most common steel alloys for tubular and tubular components in sour service is UNS G41XX0, formerly AISI 41XX [26]. 4130 Steel is among the most common of these alloys used in industry. This steel typically consist of 0.80-1.1 Cr, 0.15-0.25 Mo, 0.28-0.33 C, 0.40-0.60 Mn, 0.035 P, 0.040 S, 0.15-0.35 Si and balance Fe. The working electrode was machined from the parent material into cylinders having dimensions of approximately 9 mm, length and diameter. Prior to the experiments, all specimens were polished with Coated Abrasive Manufacturers Institute (CAMI) grit designations 320, 600, 1000 corresponding to average particle diameters 36.0, 16.0, and 10.3 microns and finally 6 micron grit silicon carbide paper, and then cleansed with deionized water until a homogenous surface was observed. Following this the specimens were quickly dried using cold air to avoid oxidation.

2.2.2. Electrolyte solution preparation and synthesis of FeS films

Due to the inherent safety concerns associated with H_2S gas, an alternative method of FeS film deposition was employed [27]. The alternative method provided an acidic electrolyte solution which has the potential to form thin FeS layer on the steel surface like what happens in the sour oil pipeline.

This acidic chemical bath contains 6.25g iron (II) chloride (0.15 M), 12.60g urea (1 M) and 31.55g thioacetamide (2 M). Deionized water was used as the solvent in every experiment. Each reagent was mixed with 210 ml of deionized water, stirred with a magnetic stir rod for 30 minutes, and mixed together under stirring for an additional two hours to achieve a clear solution.

The mechanism of FeS formation in this acidic bath is the slow release of iron and sulfur ions within solution followed by the deposition of these ions on the alloy surface. The iron and sulfur ions are provided from iron (II) chloride and thioacetamide respectively. The formation of FeS films from this acidic bath is dependent on whether the deposition rate of the ionic product of iron and sulfur is higher than solubility of FeS. Adding urea to the solution adjusted the balance between hydrolysis and deposition. The proposed reactions for this mechanism is described as follow [27]:

$$FeCl_2 \rightarrow Fe^{2+} + 2\ Cl^- \quad (2.1)$$

$$CH_3CSNH_2 + H_2O \leftrightarrow S^{2-} + CH_3CONH_2 + 2H^+ \quad (2.2)$$

$$CO(NH_2)_2 + H_2O \leftrightarrow 2NH_3 + CO_2 \quad (2.3)$$

$$NH_3 + H_2O \leftrightarrow NH_4^+ + OH^- \quad (2.4)$$

$$Fe^{2+} + S^{2-} \leftrightarrow FeS \quad (2.5)$$

$$Fe^{2+} + CH_3CSNH_2 + CO(NH_2)_2 + 2H_2O \rightarrow FeS + CH_3CONH_2 + 2NH_4^+ + CO_2 \quad (2.6)$$

Finally, the overall reaction would be written as:

2.2.3. Corrosion tests

Experiments were conducted in a multi-port glass cell with a three electrodes setup at atmospheric pressure based on the ASTM G5-94 standard for potentiostatic anodic polarization measurements [28]. A graphite rod was used as the counter electrode (CE) and saturated silver/ silver chloride (Ag/AgCl) was used as the reference electrode (RE). In order to investigate the electrochemical characteristic of the corrosion films formed on the steel alloy, the specimens subjected to corrosion were used as working electrodes (WE).

An Ivium Compactstat Potentiostat monitoring system was used to perform electrochemical corrosion measurements. Linear Polarization Resistance (LPR) technique was used to investigate the corrosion rate. The applied potential range for the LPR measurements were from -0.02V to 0.02V with a scanning rate of 0.125mV/s. All the measurement were conducted by setting the potentiostat to take measurements at 0.5, 1, 2, 4, … to 24, 48 or 72 hours depending on the test. Prior to start of each test the sample

was immersed in the solution for 55 minutes in accordance with ASTM G5-82 [28]. The pH was adjusted by adding deoxygenated hydrochloric acid.

Table 2.1 describes the experimental conditions. Three series of experiments were conducted to investigate the effect of temperature, immersion time and pH on the corrosion behavior of FeS films.

Table 2.1. Experimental conditions

Condition no.	Temperature (°C)	pH	Immersion time (Hour)
1	50	4	24
2	50	4	48
3	50	4	72
4	25	4	24
5	50	4	24
6	75	4	24
7	50	2	24
8	50	3	24
9	50	4	24

2.2.4. Surface morphology observation and corrosion product analysis

Upon completion of corrosion testing, morphological characterization of the surface was conducted using a FEI Quanta 400 Scanning Electronic Microscope (SEM) with Bruker Energy dispersive X-ray (EDX) spectroscopy. The SEM was operating at 15 kV, with a

working distance of 15 mm, and beam current of 13 nA. The crystal structure and chemical composition of the corrosion products were characterized by X-ray diffraction (XRD) using a Rigaku Ultima IV X-ray diffractometer operating at 40 kV and 44 mA, and SEM-EDX to confirm the chemical elements.

2.3. Results and discussion

2.3.1 Effect of immersion time on the corrosion mechanism and products

Figure 2.1. shows the effect of 24, 48 and 72 hours of immersion time on the corrosion rate of the specimens at 50°C and pH 4. During a corrosion process the rate of the reaction is determined by the corrosion mechanism. Growth of a corrosion film limits the rate of further corrosion by acting as a diffusion barrier for the species involved in the process. Gradually the corrosion rate decreases and the underlying steel is protected from further dissolution [8], [19].

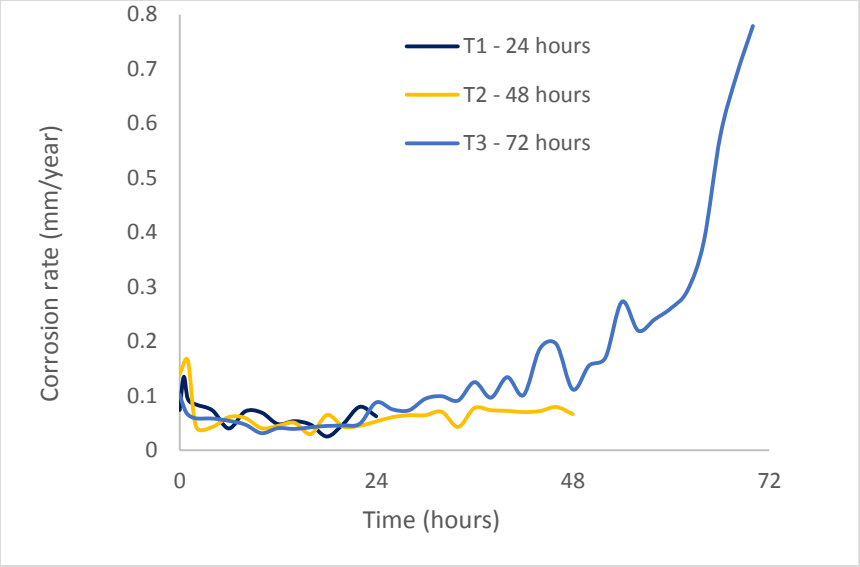

Figure 2.1. Corrosion rate with time at pH 4, 50°C

Figure 2.1. indicates that in this experiment the results of LPR measurements did not agree well with the idea of a decrement of corrosion rate by increase of exposure time to the solution. It shows that corrosion rate is increasing gradually by increasing the immersion time which could be explained as follows:

1. The corrosion rate is significantly greater than the rate of film formation on the surface.

2. The corrosion product has weak adherence to the alloy surface causing it to detach and expose the unprotected alloy to the corrosive solution and increase the possibility of localize corrosion on the surface.

The diffraction spectra in Figure 2.2, were search-matched to the XRD computer database (i.e. contains powder diffraction files (PDF) from the joint committee on powder diffraction standards (JCPDS) and international center for diffraction data (ICDD)).

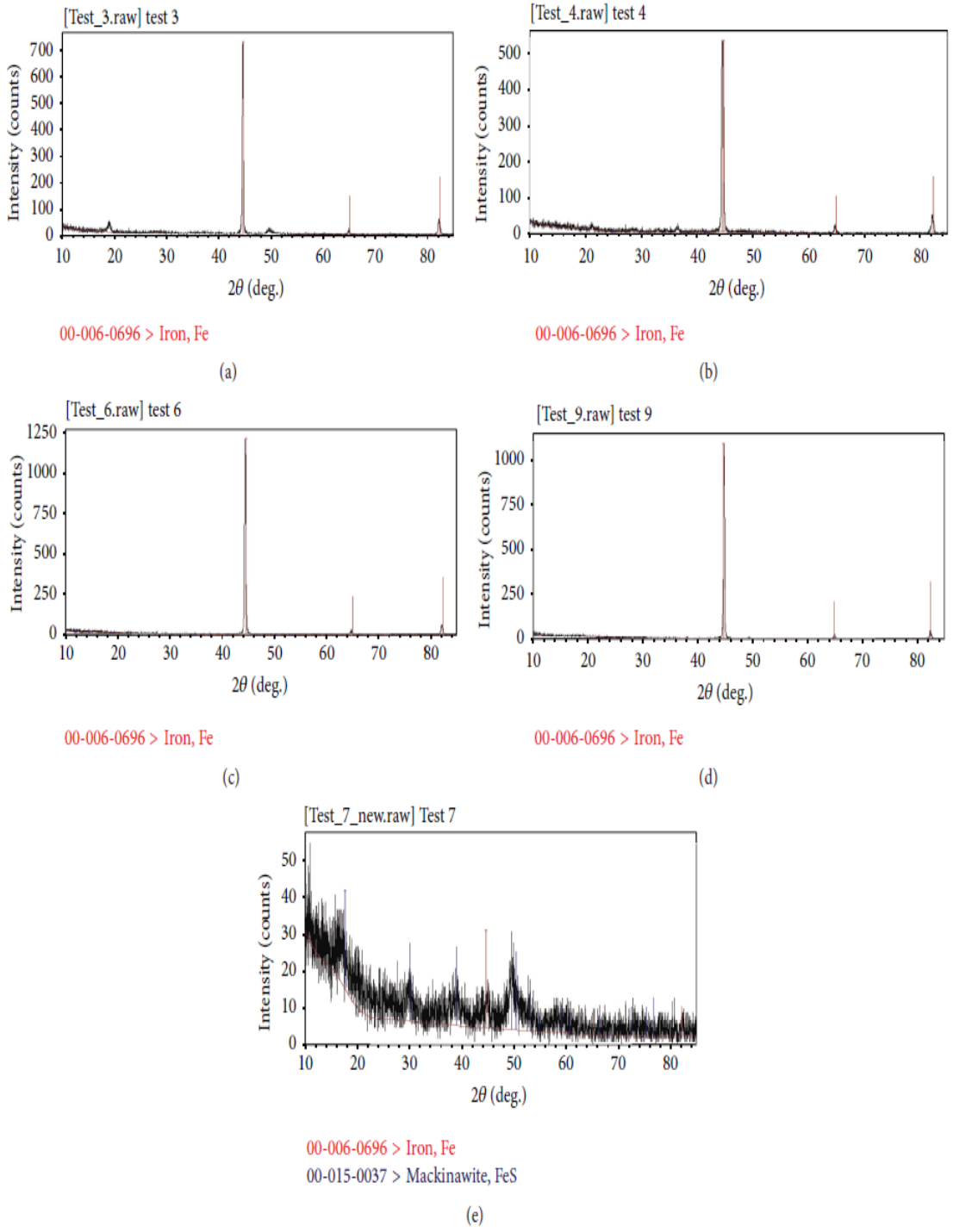

Figure 2.2. P-XRD analysis on the 4130 alloy surface at: a) 50°C, 4 pH and 48 hours, b) 25°C, 4 pH and 24 hours , c) 50°C, 2 pH and 24 hours , d) initial condition (uncorroded sample) and e) 75°C, 4 pH and 24 hours.

Figure 2.2 (a-d) identified 006-0696 iron Fe (alpha-Fe body-centered cubic (bcc) crystal type), and Figure 2.2 (e) identified both 006-0696 iron Fe (alpha-Fe bcc) and 015-0037 mackinawite FeS (tetragonal FeS crystal type). These PDF numbers and names appear in the top right corner of each diffraction spectra and corresponding line positions are superimposed onto the spectral peaks in each figure.

Figure 2.2 shows the results of crystal structure characterization of the steel alloy surfaces with powder (P)-XRD. From Figure 2.2 (a-c) it is apparent that XRD results primarily indicated elemental Fe consistent with the uncorroded sample in Figure 2.2 (d), this is likely a result of inadequate film thickness for detection by a P-XRD spectrometer. The thin nature of the corrosion film on the surface of the steel alloy is consistent with literature discussing the deposition of FeS using the indicated chemical bath alternative to H_2S exposure [24].

As shown in Figure 2.2 (e) there was a small amount of mackinawite detected by the P-XRD spectrometer on the surface of the sample exposed to 75°C for 24 hours at 4 pH. This result suggests that the film thickness is increased at high temperatures. In lieu of thin film XRD analysis, P-XRD may be able to detect thicker corrosion layers formed at relatively high temperatures.

Figure 2.3 shows the SEM images of corrosion product films formed under varying immersion times. After 24 hour immersion time, a uniform layer of corrosion product, consisting of small tetragonal mackinawite, covered the surface [29].

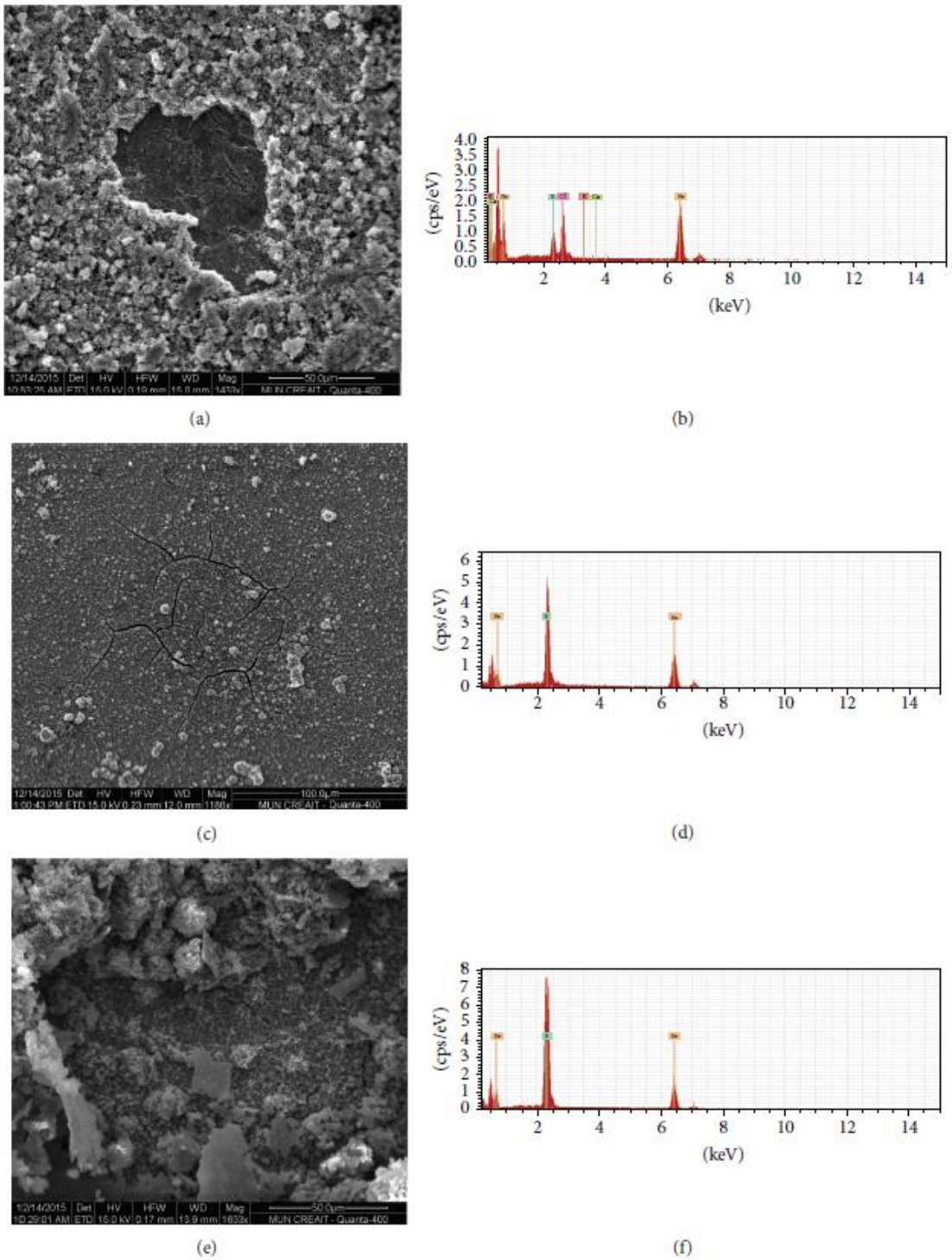

Figure 2.3. SEM analysis of corrosion products of 4130 alloy after a) 24, c) 48 and e) 72 hours immersion at pH4, 50°C and EDX analysis of corrosion products of 4130 alloy after b) 24, d) 48 and f) 72 hours immersion at pH4, 50°C.

As shown in Figure 2.3. (a) this thick corrosion layer is loose and full of blister and cracks, causing the corrosion rate to accelerate by increasing the diffusion of electrochemical reaction species such as Fe^{2+} through the alloy surface. As has been mentioned in other research, this initial mackinawite layer is easily cracked and peel off due to stress as a result of the volume effect [30]. This failure of the initial corrosion layer will gradually increase the corrosion rate and expose more unprotected area to the solution.

Figure 2.3 (b). shows the EDX analysis results of corrosion product films after 24 hours immersion. These results indicated that most of the corrosion products are iron-rich compounds such as mackinawite, which generally has lower corrosion resistance compared to sulfur-rich compounds such as troilite. The corrosion resistance of FeS follows a sequence of mackinawite < troilite, <pyrrhotite < pyrite[24].

After 48 hours immersion, the corrosion scale cracks become more severe and hexagonal crystals form beside the cracks as shown in Figure 2.3 (c). The EDX results of these hexagonal crystals indicate high sulfur content in their chemical composition as shown in Figure 2.3 (d).

Figure 2.3 (e) shows that after 72 hours of immersion, the initial corrosion product film has cracked and peeled off the surface of the specimen and a newly formed corrosion scale has been integrated. Larger, hexagonal shaped corrosion products formed on top of the new scale as mainly troilite crystals formed near the end of the 72 hours.

Generally, it could be said that by increase of immersion time more corrosion resistant products such as troilite replaced the initially formed mackinawite on the alloy surface. This is supported by the EDX results that indicate the major corrosion product varied from iron-rich mackinawite to sulfur-rich troilite, in Figure 2.3 (b, d and f). Despite the nucleation of stable troilite crystals on the metal surface the results of LPR measurements showed that between 48 and 72 hours the corrosion rate dramatically increased from 0.0662 to 0.779. This increase could be explained by localized fracture of the corrosion film due to weak adhesion of the scale on the surface. This provides a path for sulfide to penetrate and attack the substrate of metal surface.

2.3.2 Effect of temperature on the corrosion mechanism and products

Figure 2.4. shows the effect of increasing temperature on the corrosion rate of specimens over the course of 24 hours at pH 4.

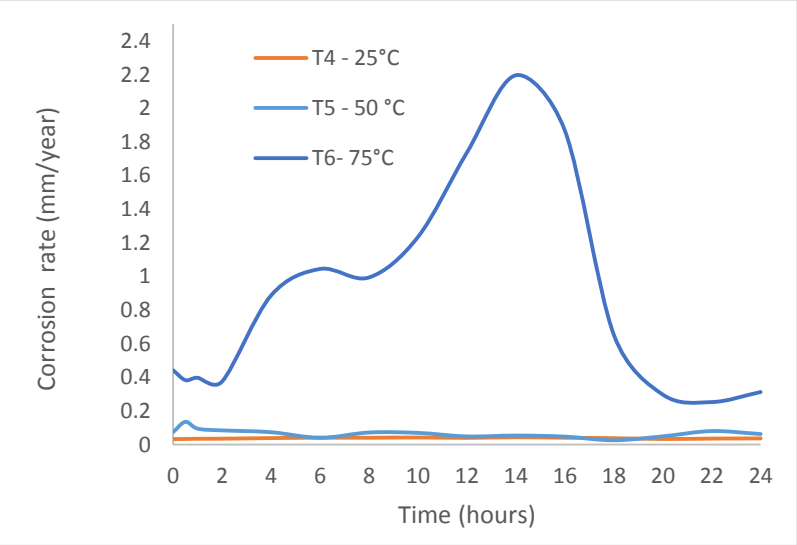

Figure 2.4. Corrosion rate with temperature at pH 4, 24 hours.

It can be observed that during first 12 hours of increasing temperature from 25°C to 75°C, the corrosion rate dramatically increased which can be explained by following reasons:

1. Increasing the temperature could accelerate the diffusion of species involved in electrochemical reactions.

2. Temperature could affect the concentration of corrosion species by preferentially evaporating one or more species out of the solution, which could affect the corrosion reaction.

It has been confirmed by previous research that temperature generally accelerates most of the chemical, electrochemical and transporting processes occurring during the corrosion process and also both cathodic reactions and anodic currents which were measured increased with increasing temperature [31].

During the final 12 hours of testing at 75°C the corrosion rate significantly decrease from 2.2 to 0.25 mm/year, which could be related to transformation of mackinawite crystalline structure to a more resistant troilite crystalline structure. The SEM image in Figure 2.5 shows significant fracturing of the surface film at 75°C which explains the initial higher corrosion rate due to the diffusion of species into non-protective mackinawite followed by the decreased corrosion rate due to formation of the protective troilite crystalline structure on the alloy surface.

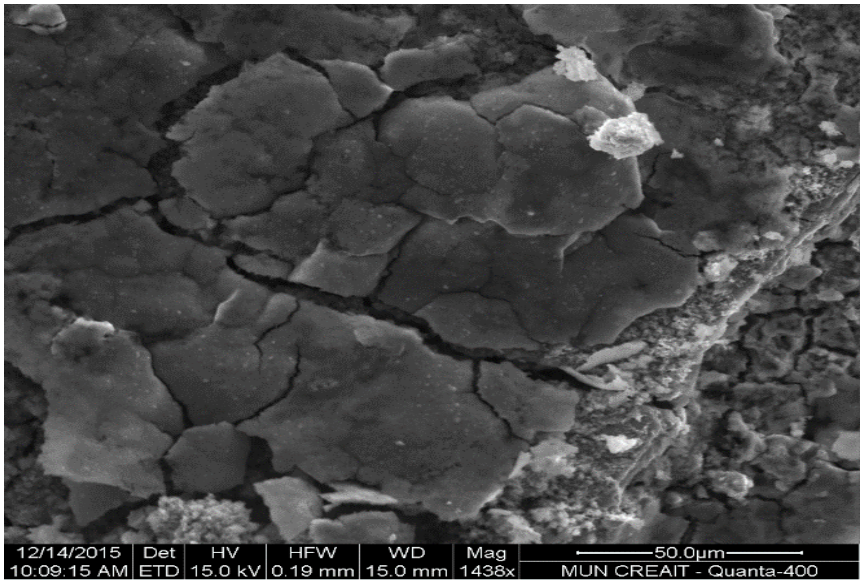

Figure 2.5. SEM image of corrosion products on surface of 4130 alloy after 24 hours immersion at pH 4, and 75°C.

2.3.3 Effect of pH on the corrosion mechanism and products

Figure 2.6 shows the effect of pH on the corrosion rate of specimens immersed for 24 hours at 50°C.

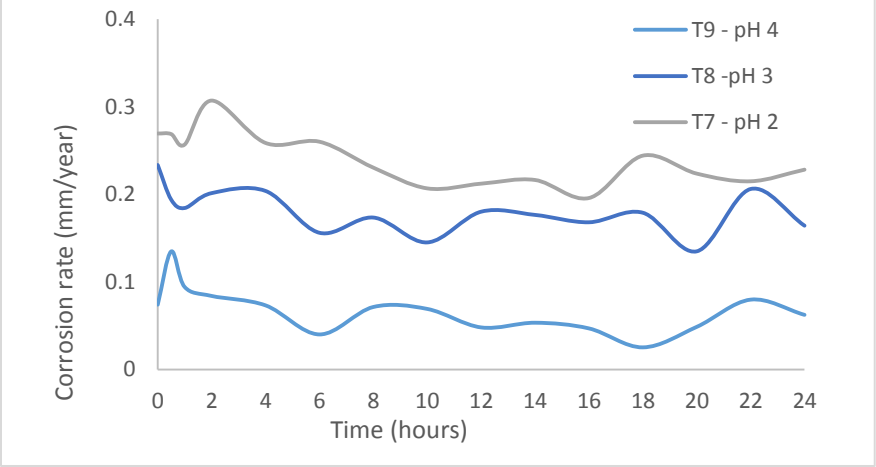

Figure 2.6. Corrosion rate with pH at 50°C, 24 hours.

The results show that decreasing pH from 4 to 2 slightly increases the corrosion rate. The protective nature and composition of the corrosion product depend greatly on the pH of the solution. At lower values of pH (<3), iron is dissolved and FeS is mostly inhibited from precipitating on the metal surface due to a very high solubility of FeS phases [32]. Figure 2.7 (a) shows the SEM image of corrosion products on the surface of a specimen after 24 hours at pH 2 and 50 °C.

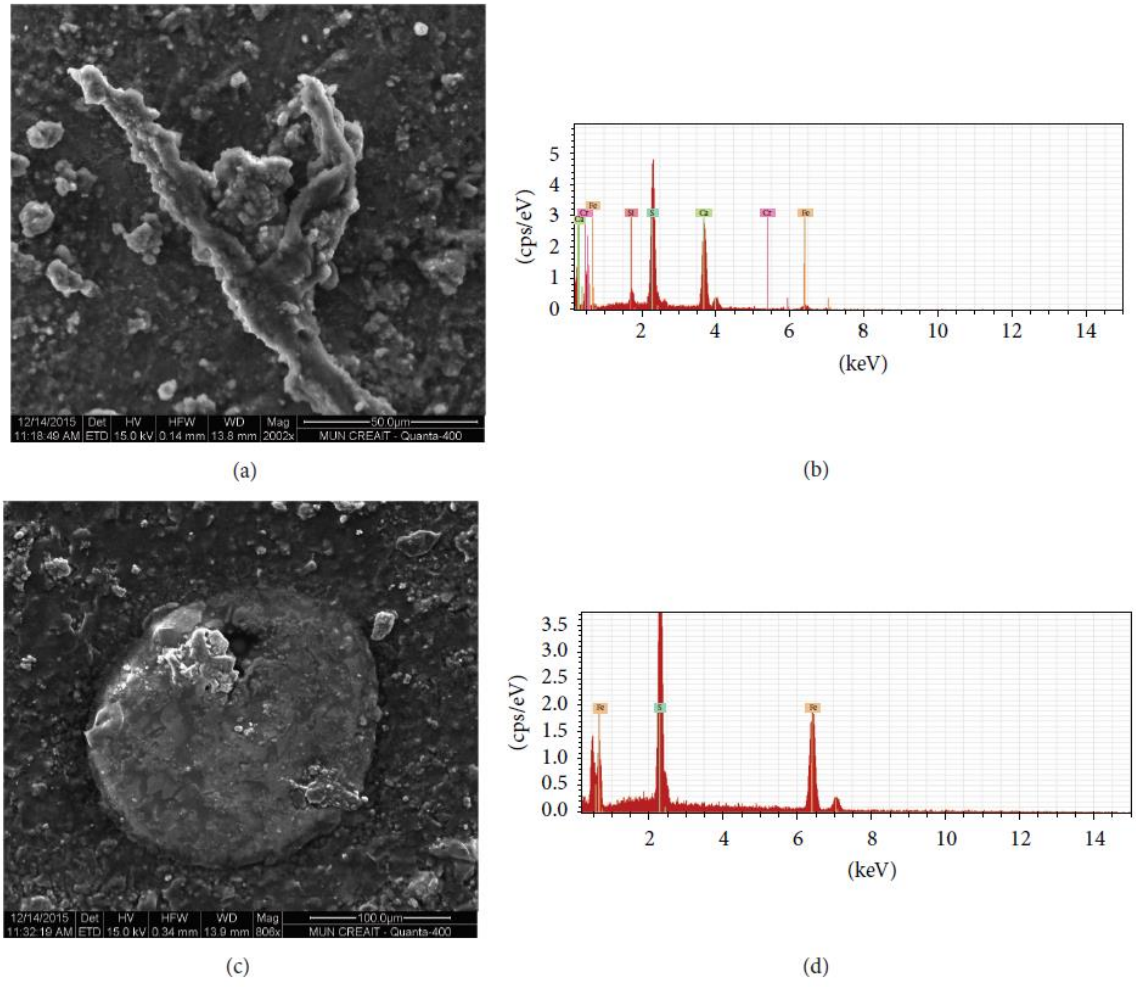

Figure 2.7. SEM images of corrosion products on surface of 4130 alloy after 24 hours immersion at 50°C, pH 2: (a), (c)and EDX analysis of corrosion products on surface of 4130 alloy after 24 hours immersion at 50°C, pH 2: (b), (d).

As can be observed, the corrosion products are loose and detached from the surface. This could result in the products being easily removed by shear stress. The EDX results as shown in Figure 2.7 (b) indicate a high presence of sulfur compounds and a low presence of iron compounds on the surface.

The SEM results in Figure 2.7(c) of the specimen immersed in the solution at pH 2 also shows the presence of a pit on the surface. This is another reason for the higher corrosion rates seen at low pH. The corrosion pit shown in Figure 2.7(c) has a brittle cap covering the substrate. EDX analysis indicates that this cap is primarily sulfide as shown in Figure 2.7 (d). At pH 3, the top surface layer displayed a flaky structure as seen in Figure 2.8.

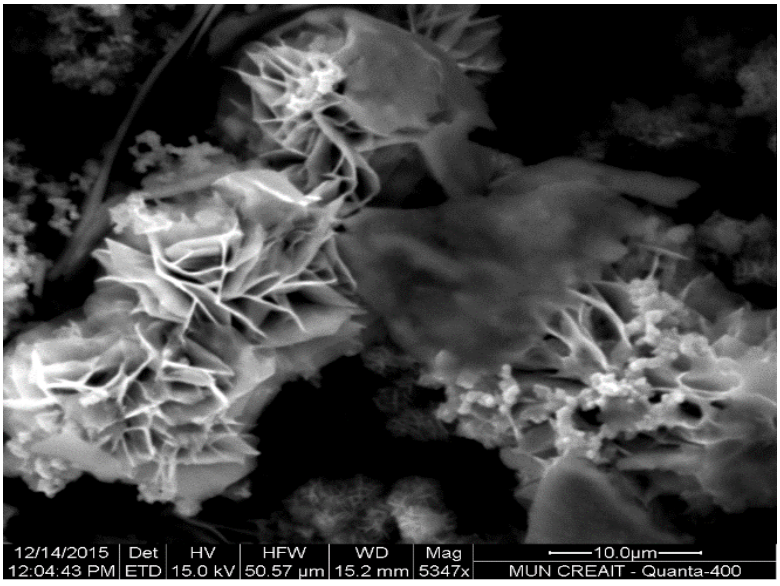

Figure 2.8. SEM image of corrosion products on surface of 4130 alloy after 24 hours immersion at pH 3, and 50°C.

Parts of the layer had spalled off and revealed the presence of much smaller crystallites under the outer layer. It is likely that this layer is the result of the immediate precipitation of Fe^{2+} released by corrosion [32]. At pH values from 3 to 4, an inhibitive effect of the

corrosion mechanism is seen due to the formation of a marcasite FeS protective film on the electrode surface. At pH 3, small crystals were observed on areas where the outer layer had spalled off as shown in Figure 2.8. At pH 4, the surface was mostly covered with a much denser layer as shown in Figure 2.9.

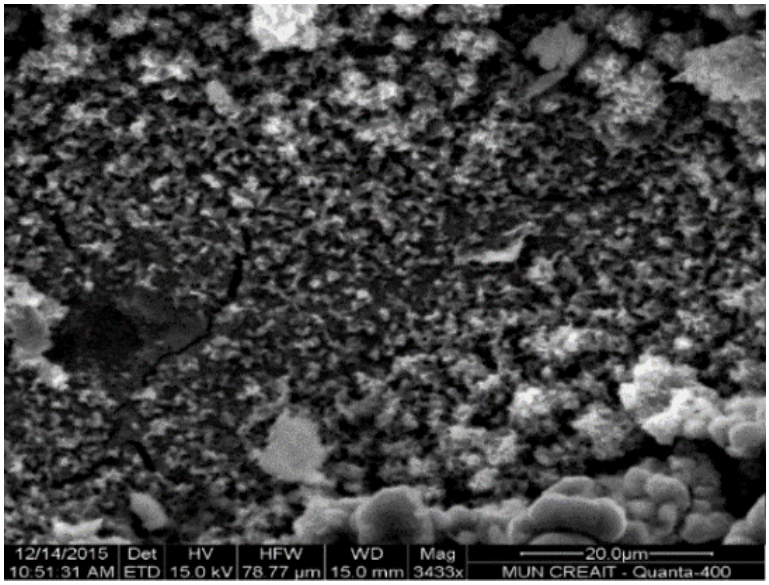

Figure 2.9. SEM image of corrosion products on surface of 4130 alloy after 24 hours immersion at pH 4, and 50°C.

2.4. Conclusions

The results of this research indicated that acidic chemical bath deposition could be successfully applied to investigate the formation and growth of FeS thin films under varying experimental conditions. Due to the inherent safety concerns associated with sour corrosion experiments in laboratories, this acidic chemical bath deposition method could be applied as a substitute for H_2S in certain experiments to characterize formation and transformation of FeS corrosion products.

Other primary findings of this research are:

- Increase of immersion time gradually increases the corrosion rate of 4130 chromium alloy steel in this experiment, resulting from localize fracture of corrosion layer despite transformation of FeS crystalline structures from iron-rich mackinawite to sulfur-rich troilite compounds during the corrosion process.
- Increase of pH directly decreases the corrosion rate of 4130 alloy steel in this experiment resulting from the formation of a more resistant FeS film at higher values of pH.
- Increase of temperature from 25°C to 75°C causes an increase in the corrosion rate of 4130 alloy steel, likewise resulting from the transformation of FeS crystalline structure during the corrosion process.

2.5. References

[1] D. W. Shoesmith, M. G. P. Taylor, and J. Bailey and D. G. Owen, "The formation of ferrous monosulfide polymorphs during the corrosion of iron by aqueous hydrogen sulfide at 21°C," Electrochem. Soc, vol. 127, pp. 1007–1015, 1980.

[2] D. W. Shoesmith, "Formation, transformation and dissolution of phases formed on surfaces," Electrochem. Soc. Meet., Ottawa, Nov 27, 1981.

[3] S. N. Smith and E. J. Wright, "Prediction of minimum H_2S levels required for slightly sour corrosion," Proc. Conf. on Corrosion, NACE Int., Paper no. 11, 1994.

[4] S. N. Smith and E. J. Wright, "Prediction of corrosion in slightly sour environments," CORROSION/2004, NACE Int., Paper no. 02241, 2002.

[5] J. S. Smith and J. D. A. Miller, "Nature of sulfides and their corrosive effect on ferrous

metals, a review," Br. Corros. J., vol. 10, pp. 136–143, 1975.

[6] H. Fang, "Investigation of localized corrosion of carbon steel in H_2S environments," PhD Thesis, Ohio University, 2012.

[7] W. Sun and S. Nesic, "A mechanistic model of H_2S corrosion of mild steel," CORROSION/2007, NACE Int., Paper no. 07655, pp. 1–26, 2007.

[8] W. Sun, S. Nesic, and S. Papavinasan, "Kinetics of iron sulfide and mixed iron sulfide/carbonate scale precipitation in CO_2/H_2S Corrosion," CORROSION/2007, NACE Int., Paper no. 06644 , 2007.

[9] M. Koteeswaran, "CO_2 and H_2S Corrosion in oil pipelines," Master Thesis, Stavanger, June, 2010.

[10] W. Sun, "Kinetics of iron carbonate and iron sulfide scale formation in CO_2/H_2S Corrosion," PhD Thesis, Ohio University, 2006.

[11] P. Taylor, "The stereochemistry of iron sulfides- a structural rationale for the crystallization of some metastable phases from aqueous solution," Am. Mineral., vol. 65, pp. 1026–1030, 1980.

[12] M. Bonis, M. Girgis, K. Goerz, and R. MacDonald, "Weight loss corrosion with H_2S: using past operations for designing future facilities," CORROSION/2006, NACE Int., Paper no. 06122, 2006.

[13] D. Rickard and G. W. Luther, Chemistry of iron sulfides, Chem. Rev., vol. 107, Paper no. 2. 2007.

[14] A. R. Lennie and D. J. Vaughan, "Spectroscopic studies of iron sulfide formation and phase relations at low temperatures," Miner. Spectrosc., Special Publ., vol. 5, pp. 117–131, 1996.

[15] L. Smith and B. Craig, "Practical corrosion control measures for elemental sulfur," CORROSION/2005, NACE Int., Paper no. 05646, pp. 1–20, 2005.

[16] B. N. Brown, "The influence of sulfides on localized corrosion of mild steel," PhD Thesis, Ohio University, December, 2013.

[17] T. Laitinen, “Localized corrosion of stainless steel in chloride, sulfate and thiosulfate containing environments,” Corrosion Sci., vol. 42, no. 3, pp. 421–441, 2000.

[18] J. Kvarekval, “Morphology of localized corrosion attacks in sour environments,” CORROSION/2007, NACE Int., Paper no.07659, 2007.

[19] K. J. Lee, “A mechanistic modeling of CO_2 corrosion of mild steel in the presence of H_2S,” PhD Thesis, Ohio University, November, 2004.

[20] N. G. Harmandas and P. G. Koutsoukos, “The formation of iron sulfides in aqueous solutions,” J. Cryst. Growth, vol. 167, pp. 719–724, 1996.

[21] J. Amri and J. Kvarekvål, “Simulation of solid state growth of iron sulfide in sour corrosion conditions,” CORROSION/2011, NACE Int., Paper no. 11076, 2011.

[22] N. S. Obuka et al., “Review of corrosion kinetics and thermodynamics of CO_2 and H_2S corrosion effects and associated prediction/evaluation on oil and gas pipeline system,” Int. J. Sci. Technol. Res., vol. 1, no. 4, pp. 156–162, 2012.

[23] A. G. Wikjord, T. E. Rummery, F. E. Doern, and D. G. Owen, “Corrosion and deposition during the exposure of carbon steel to hydrogen sulfide-water solutions,” Corrosion Sci., vol. 20, no.5, pp. 651–671, 1980.

[24] S. N. Smith, “A proposed mechanism for corrosion in slightly sour oil and gas production,” Proc. 12th Int. Corrosion Congr., NACE Int., vol. 4, pp. 2695–2706, 1993.

[25] D. Rickard, “Kinetics of FeS precipitation: part 1. competing reaction mechanisms,” Geochim. Cosmochim. Acta, vol. 59, no. 21, pp. 4367–4379, 1995.

[26] NACE MR0175 / ISO 15156-1 Petroleum and natural gas industries — "Materials for use in H_2S containing environments in oil and gas production", 2001.

[27] M. Saeed Akhtar, A. Alenad, and M. Azad Malik, “Synthesis of mackinawite FeS thin films from acidic chemical baths,” Mater. Sci. Semicond. Proc., vol. 32, pp. 1–5, 2015.

[28] ASTM-G5-82, “Standard reference method for making potentiostatic and potentiodynamic anodic polarisation measurements.,” Annu. B. ASTM Stand., vol. 03.02, Reapproved as ASTM-65–87 and as ASTM- 65–94, pp. 511–521, 1982.

[29] P. Bai, S. Zheng, H. Zhao, Y. Ding, J. Wu, C. Chen, "Investigations of the diverse corrosion products on steel in a hydrogen sulfide environment", Corrosion Sci., vol. 87 pp. 397–406, 2014.

[30] M. Liu, J. Wang, W. Ke, and E. H. Han, "Corrosion behavior of X52 anti-H_2S pipeline steel exposed to high H_2S concentration solutions at 90 °C," J. Mater. Sci. Technol., vol. 30, no. 5, pp. 504–510, 2014.

[31] Y. Zheng, B. Brown, and S. Nesic, "Electrochemical study and modeling of H_2S corrosion of mild steel," CORROSION/2013, NACE Int., Paper no. 2406, pp. 1–22, 2013.

[32] B. Valery, "Effect of Pre-exposure of Sulfur and Iron Sulfide on H_2S Corrosion at Different Temperatures," Master Thesis, University of Stavanger, June, pp. 1–68, 2011.

3. EFFECT OF ELEMENTAL SULFUR AND SULFIDE ON CORROSION BEHAVIOR OF CHROMIUM- MOLYBDENUM ALLOY STEEL FOR TUBING AND TUBULAR COMPONENTS IN OIL AND GAS INDUSTRY

Preface

A version of this manuscript is accepted for publication in the Materials journal (MDPI). I am the primary author of this paper, along with the co-authors, John Shirokoff. I conducted the literature review and proposed the outline of the experiments and the analysis procedure. I conducted most of the experiments and microstructural analysis. I prepared the first draft of the manuscript and subsequently revised the manuscript based on the co-author's feedbacks and also the initial feedbacks from the journal reviewers. The co-author John Shirkokff helped in analyzing the final results, and contributed in preparing, reviewing and revising the manuscript.

Abstract

The chemical degradation of alloy components in sulfur-containing environments is a major concern in oil and gas production. This paper discusses the effect of elemental

sulfur and its simplest anion, sulfide, on the corrosion of Cr-Mo low alloy steel at pH 2 and 5 during 10, 20 and 30 hours immersion in two different solutions. 4130 Cr-Mo low alloy steel is widely used as tubing and tubular components in sour services. According to the previous research in aqueous conditions, contact of solid sulfur with alloy steel can initiate catastrophic corrosion problems. The corrosion behavior was monitored by the potentiodynamic polarization technique during the experiments. Energy dispersive x-ray spectroscopy (EDS), and scanning electron microscopy (SEM) have been applied to characterize the corrosion product layers after each experiment. The results show that under the same experimental conditions, the corrosion resistance of Cr-Mo low alloy in the presence of elemental sulfur is significantly lower than its resistance in the presence of sulfide ions.

Keywords: corrosion behavior, elemental sulfur, sulfide, 4130 Cr-Mo low alloy, potentiodynamic polarization

3.1. Introduction

For more than 40 years elemental sulfur deposition in pipelines and facilities has become a major concern in the sour oil and gas industry [1]. In conjunction with reservoir souring, the incidence of sulfur corrosion will likely increase. It is known from prior research that the presence of dry elemental sulfur in contact with carbon steel is not considered as a corrosion threat to steel; however, by adding water to the system, the corrosion process may be dramatically accelerated [2].

Elemental sulfur usually appears in an aqueous system due to the oxidation of sulfide species where the possible reaction for the formation of elemental sulfur (S_8) may involve

$$8\ H_2S\ (aq) + 16\ M^{n+}\ (aq) \rightarrow S_8\ (s) + 16\ H^+\ (aq) + 16\ M^{(n-1)+}\ (aq) \quad (3.1)$$

$$8\ H_2S\ (aq) + 4\ O_2\ (g) \rightarrow S_8\ (s) + 8\ H_2O\ (l) \quad (3.2)$$

high oxidation state metals or oxygen [3]:

MacDonald et al. hypothesized that an electrochemical reaction between iron and polysulfide could be the driving force for a corrosion process where elemental sulfur is present [4]:

$$(x-1)\ Fe\ (s) + S_{y-1}\ S^{2-}\ (aq) + 2\ H^+\ (aq) \rightarrow (x-1)\ FeS\ (s) + H_2S\ (g) + S_{y-x}\ (s) \quad (3.3)$$

In recent years, Fang et al. investigated the corrosion behavior of carbon steel at different temperatures with molten covering sulfur on the steel surface [5], [6]. These investigations comprehensively studied the sulfur hydrolysis and direct sulfur/iron reaction, with either an electrically insulating or conductive barrier placed between the sulfur droplet and the metal surface.

The investigation of Fang et al. proved that the electrical connection and physical proximity between sulfur and steel are critical characteristics for elemental sulfur corrosion of mild steel. They also identified that an electrochemical reaction is the likely mechanism of elemental sulfur corrosion of mild steel. However, there are few

electrochemical investigations on the corrosion behavior of an alloy steel such as 4130 in the presence of elemental sulfur. In this paper, the effect of elemental sulfur and its anion on corrosion mechanism and the behavior of the Cr-Mo low alloy steel were investigated at varying pH levels and immersion time through corrosion simulation tests and electrochemical measurements.

3.2. Experimental procedure

3.2.1. Material and sample preparation

According to NACE MR0175/ISO 15156, the most common steel alloy for tubular and tubular components in sour service is UNS G41XX0, formerly AISI 41XX [7]. 4130 Steel is among the most common low alloys used in the oil and gas industry. This steel typically consists of 0.80-1.1 Cr, 0.15-0.25 Mo, 0.28-0.33 C, 0.40-0.60 Mn, 0.035 P, 0.040 S, 0.15-0.35 Si and balance Fe. The working electrode was machined from the parent material into cylinders having dimensions of approximately 9 mm length and 9 mm diameter. Prior to the experiments, all specimens were polished with Coated Abrasive Manufacturers Institute (CAMI) grit designations 320, 600 and 1000, corresponding to average particle diameters 36.0, 16.0 and 10.3 microns and finally 6-micron grit silicon carbide paper, and then cleansed with deionized water until a homogeneous surface was observed. Following this, the specimens were quickly dried using cold air to avoid oxidation.

After preparing the samples, they were transferred into a multi-port glass cell which was filled with 3.5% sodium chloride solution. The pH was adjusted by adding deoxygenated hydrochloric acid or sodium hydroxide. Prior to the start of each electrochemical test, the sample was immersed in the solution for 55 minutes in accordance with ASTM G5-82 [8].

3.2.2. Direct sulfur/ iron and sulfide/ iron reactions preparation

Two series of experiments have been performed to investigate the effects of elemental sulfur (S_8) and its simplest anion, sulfide (S^{2-}), on the corrosion behavior of Cr-Mo low alloy steel at varying pH and immersion times. In the first series of experiments, all of the tests were carried out in a multi-port glass cell which was filled with solved thioacetamide (2M) in 420 ml de-ionized water. According to the literature and authors' previous studies [9, 10], addition of thioacetamide into the water would produce free sulfide ions through the bulk solution. Decomposition of thioacetamide is an irreversible reaction which has been considered as the sulfur source, generating S^{2-} by a hydrolytic method [11–14]. Equation (3.5) shows the presence of dissolved free sulfides in de-ionized water which are super active to react with samples. Table 3.1 describes the experimental conditions of the first series of experiments.

$$CH_3CSNH_2 + H_2O \leftrightarrow S^{2-} + CH_3CONH_2 + 2H^+ \quad (3.4)$$

In the second series, a similar method to the method of Fang et al.with maximum uniform coverage of adherent sulfur to the coupon surface was employed for all of the tests [1, 5, 15]. In this series of experiments, samples' surfaces were covered with sublimed elemental sulfur 99.9999% (ACROS) deposited onto polished samples. Table 3.2 describes the experimental conditions of the second series of experiments.

Table 3.1. Experimental condition of the first series

Condition No.	T (°C)	pH	Immersion Time (h)
1	80	2	10
2	80	2	20
3	80	2	30
4	80	5	10
5	80	5	20
6	80	5	30

Table 3.2. Experimental condition of the second series

Condition No.	T (°C)	PH	Immersion Time (h)
7	80	2	10
8	80	2	20
9	80	2	30
10	80	5	10
11	80	5	20
12	80	5	30

3.2.3. Electrochemical measurements

Electrochemical corrosion experiments, and in particular, the potentiodynamic polarization scan, can provide considerable information on the corrosion rate, pitting susceptibility and passivity as well as the cathodic behavior of an electrochemical system [16]. During this study, experiments were conducted in a multi-port glass cell with a three electrodes setup at atmospheric pressure based on the ASTM G5-82 standard for potentiodynamic anodic polarization measurements [8].

A graphite rod was used as the counter electrode (CE) and saturated silver/ silver chloride (Ag/AgCl) was used as the reference electrode (RE).Also as was mentioned in the material and sample preparation, 4130 low alloy steel was used as the working electrode (WE).

An Ivium Compactstat Potentiostat monitoring system was used to perform electrochemical corrosion measurements. The potentiodynamic polarization technique was applied to investigate the corrosion behavior. The applied scan rate for this measurements was 0.125 mV/s.

3.2.4. Surface morphology observation and corrosion product layers analysis

Upon completion of corrosion testing, morphological characterization of the surface was conducted using a FEI Quanta 400 scanning electronic microscope (SEM) with Bruker energy dispersive x-ray (EDS) spectroscopy. The SEM was operating at 15 kV, with a working distance of 15 mm, and beam current of 13 nA.

3.3. Results and discussion

3.3.1. First series of experiments; Effect of sulfide (S^{2-}) on corrosion mechanism of Cr-Mo low alloy steel

As was mentioned in the experimental procedure in order to investigate the effect of sulfide (S^{2-}) on the corrosion behavior of 4130 alloy, the samples were immersed into the solution containing solved thioacetamide (2M) in 420 ml de-ionized water for 10, 20 and 30 hours at 80 °C, pH 2 and 5.

3.3.1.1. Corrosion behavior of Cr-Mo low alloy steel

The potentiodynamic curves of 4130 Cr-Mo low alloy steel in thioacetamide solution at different immersion times: 10, 20 and 30 hours at 80 °C, pH 2 are illustrated in Figure 1. The scan rate was 0.125 mV/s.

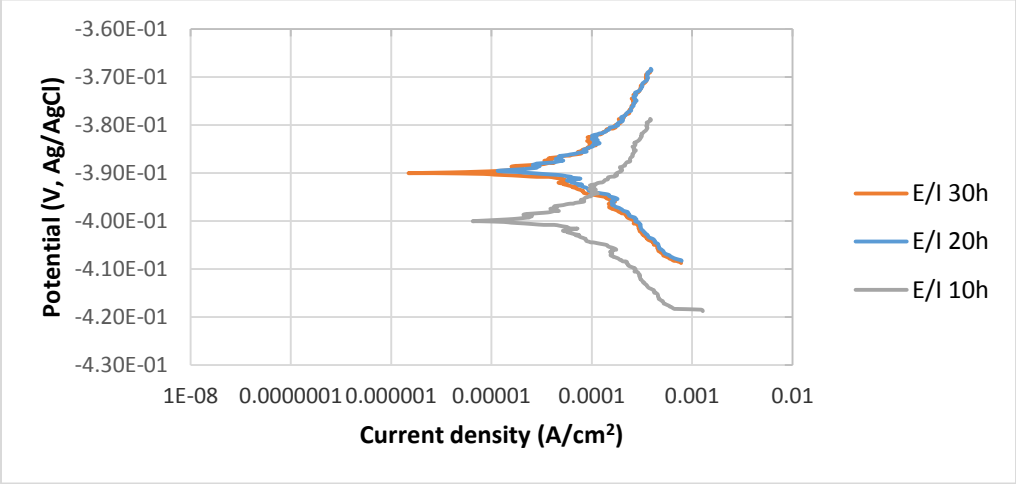

Figure 3.1. The potentiodynamic curves of 4130 Cr-Mo low alloy steel in thioacetamide solution at different immersion times: 10, 20 and 30 hours at 80 °C, pH 2.

Figure 3.1.indicates the stable behavior of anodic curves with increasing the immersion time from 10 to 30 hours at 80 °C, pH 2. It illustrates that the corrosion potential, E_{corr}, at pH 2 for 20 and 30 hours immersion time is almost the same and more positive than that of 10 hours immersion in the solution; however, the values of difference are not significant. It can be also observed that the current density of 10 hours immersion is higher than those of 20 and 30 hours immersion.

Figure 3.2.shows the stable behavior of anodic curves with increasing the immersion time from 10 to 30 hours at 80 °C, pH 5. The potentiodynamic polarization curves indicate that E_{corr} of 10 hours immersion was relatively more positive than that of 30 hours immersion which was more positive than that of 20 hours. The current density of 10 hours immersion is slightly lower than that of 30 hours immersion time which is significantly higher than the current density of 20 hours immersion in the solution.

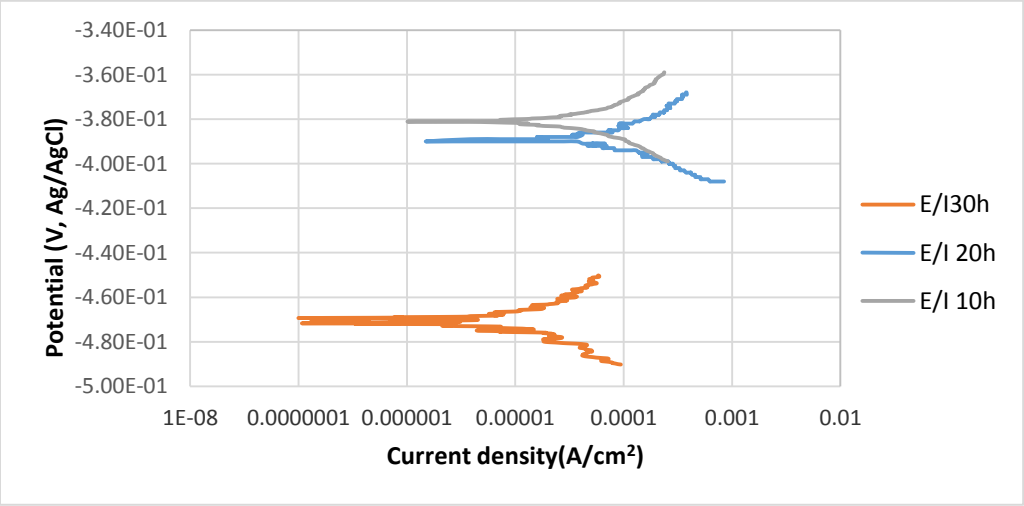

Figure 3.2. The potentiodynamic curves of 4130 Cr-Mo low alloy steel in thioacetamide solution at different immersion times: 10, 20 and 30 hours at 80 °C, pH 5.

During a corrosion process, the rate of the reactions is determined by the corrosion mechanism. The growth of a corrosion product layer limits the rate of further corrosion by acting as a diffusion barrier for the species involved in the process [17, 18]. After 20 hours immersion at pH 5, the formation of a protective corrosion product layer prevented the further corrosion of the sample surface; however, after 30 hours immersion, the corrosion current density significantly increased, which may be related to the breaking down of the protective corrosion product layer on the alloy surface. The values of anodic (β_a) and cathodic (β_c) Tafel slopes of the samples of each experiment were obtained by potentiostat as illustrated in Table 3.3.

Table 3.3. The values of anodic (β_a) and cathodic (β_c) Tafel slopes of first series

Experiment	β_a (mV·decade^{-1})	β_c (mV·decade^{-1})
1	0.022	0.019
2	0.029	0.020
3	0.020	0.019
4	0.034	0.023
5	0.021	0.018
6	0.028	0.020

3.3.1.2. Corrosion rate of Cr-Mo low alloy steel

The corrosion current (i_{corr}) was calculated using the following equations [19]:

$$i_{corr} = \frac{B}{R_P} \quad (3.5)$$

Where:

i_{corr} is the corrosion current density in A.m^{-2};

R_P is the polarization resistance in $\Omega.m^2$ and B is the proportionality constant in

$$B = \frac{\beta_a \beta_c}{2.3\ (\beta_a + \beta_c)} \quad (3.6)$$

mV.decade^{-1}:

which can be calculated by the given values of anodic (β_a) and cathodic (β_c) Tafel slopes of the samples of each experiment. Finally, the corrosion rate (CR) was calculated using equation (3.8):

$$CR = \frac{i_{corr}\ w}{\rho\ F} \quad (3.7)$$

Where:

w is the equivalent weight of 4130 alloy,

F is Faraday constant, and ρ is the density of 4130 alloy.

Table 3.4. The corrosion rate of the first series

Experiment	**1**	**2**	**6**	**4**	**5**	**6**
pH	2	2	2	5	5	5
Corrosion Rate (CR) (mm/year)	0.368	0.325	0.318	0.066	0.044	0.224

As can be observed in Table 3.4, in thioacetamide solution the corrosion rate of Cr-Mo low alloy at pH 2 is greater than that of pH 5, which is usually related to the formation of a corrosion protective layer at higher pH. At pH 2, iron is dissolved and iron sulfide is not significantly precipitated on the surface of the alloy due to the high solubility of iron sulfide phases at pH values less than 2[20–22]. In this case, sulfide exhibits only the accelerating effect on the dissolution of iron. At pH 5, the inhibitive effect of sulfide is seen due to the formation of iron sulfide protective film on the alloy surface [16].

Table 3.4 shows that the corrosion rate has a maximum of 0.368 mm/y after 10 hours immersion at pH 2 which slightly decreases to 0.318 mm/y after 30 hours immersion. The corrosion rates of pH 5 indicate a small decrease and a large increase during 20 and after 30 hours immersion respectively due to formation and breakdown of the corrosion product layer. These results are consistent with data obtained from the potentiodynamic polarization technique.

3.3.2. Second series of experiments; Effect of elemental sulfur (S_8) on corrosion mechanism of Cr-Mo low alloy steel

As was mentioned in the experimental procedure, in order to investigate the effect of elemental sulfur (S_8) on the corrosion behavior of 4130 Cr-Mo low alloy, the surfaces of the samples were covered by melted elemental sulfur 99.999% (ACROS) and then immersed in a glass cell which was filled with the 3.5% sodium chloride solution.

3.3.2. 1. Corrosion behavior of Cr-Mo low alloy steel

The potentiodynamic curves of 4130 Cr-Mo low alloy steel covered with elemental sulfur in the 3.5% sodium chloride solution at different immersion times: 10, 20 and 30 hours at 80 °C, pH 2, are illustrated in Figure 3.3. The scan rate was 0.125 mV/s. Figure 3.3 presents that E_{corr} at pH 2 for 20 hours immersion time is more positive than that of 30 hours immersion in the solution; however, the difference is not significant. It can be observed that the current density of 30 hours immersion is higher than that of 20 hours immersion.

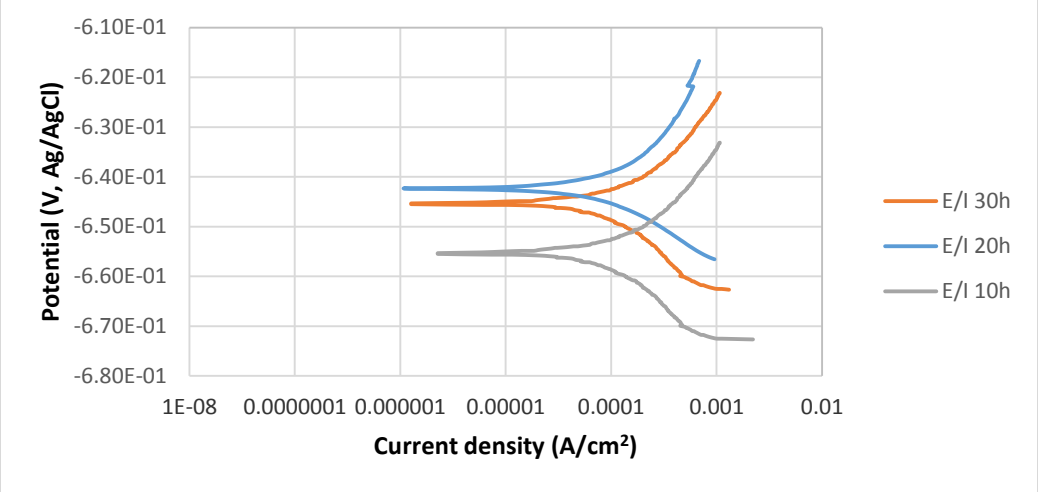

Figure 3.3. The potentiodynamic curves of 4130 Cr-Mo low alloy steel covered with elemental sulfur in 3.5% sodium chloride solution at different immersion times: 10, 20 and 30 hours at 80 °C, pH 2.

Figure 3.3 also shows that E_{corr} at pH 2 for 10 hours immersion time is the most negative one. It can be observed that current density of 10 hours immersion is higher than that 20 and 30 hours immersion.

Figure 3.4 shows the stable behavior of anodic curves of samples covered with elemental sulfur with increasing the immersion time from 10 to 30 hours at 80 °C and pH 5. The potentiodynamic polarization curves indicate that E_{corr} of 30 hours immersion is more positive than that of 20 hours immersion in the 3.5% sodium chloride solution. It can be observed that current density of 20 hours immersion is higher than that of 30 hours immersion. The values of anodic (β_a) and cathodic (β_c) Tafel slopes of the samples of each experiments were determined as illustrated in Table 3.5.

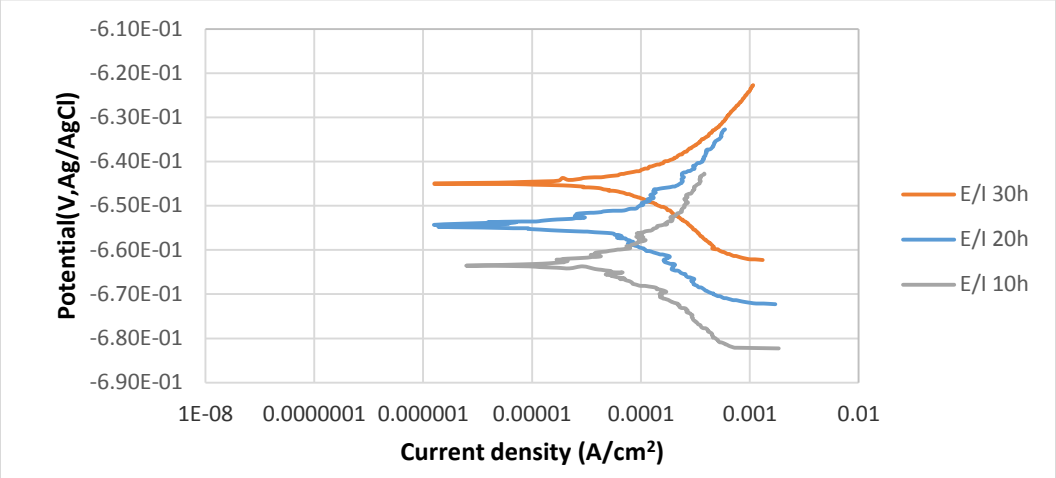

Figure 3.4. The potentiodynamic curves of 4130 Cr-Mo low alloy steel covered with elemental sulfur in 3.5% sodium chloride solution at different immersion times: 10, 20 and 30 hours at pH 5.

Table 3.5. The values of anodic (β_a) and cathodic (β_C) Tafel slopes of second series

Experiment	β_a (mV·Decade^{-1})	β_C (mV·Decade^{-1})
7	0.032	0.015
8	0.030	0.013
9	0.023	0.020

10	0.022	0.021
11	0.022	0.019
12	0.020	0.019

3.3.2.2. Corrosion rate of Cr-Mo low alloy steel

The corrosion rates of the second series of the experiments were calculated with the same method as the first series. Table 3.6 indicates the corrosion rate of each experiment.

Table 3.6. The corrosion rates of second series

Experiment	**7**	**8**	**9**	**10**	**11**	**12**
pH	2	2	2	5	5	5
Corrosion Rate (CR) (mm/year)	0.615	0.605	0.595	0.381	0.367	0.318

As Table 3.6 indicated, generally the corrosion rates of Cr-Mo low alloy in the presence of elemental sulfur are greater than those in the presence of sulfide ions. Also, it can be observed that at pH 2 the rates of corrosion are higher than those of pH 5, which is due to the formation of protective corrosion product layers on the alloy surface at pH greater than 2. The corrosion rate after 10 hours immersion at pH 2 has a maximum of 0.615 mm/y which slightly decreased to 0.595 mm/y after 30 hours immersion. The corrosion rates of pH 5 gradually decreased by increasing the immersion time due to the formation of protective corrosion product layer. These results are consistent with data obtained from the potentiodynamic polarization technique.

3.3.3. Analysis of corrosion product layers on the surface of the alloy

Figure 3.5 shows the SEM micrograph of the corrosion product layers that form on the surface of each sample at pH 2 under 10, 20 and 30 hours immersion time in thioacetamide solution. Figure 3.5 shows that by increasing the immersion time, a thin corrosion product layer gradually covered the alloy surface and protected it from further corrosion. EDS results indicate that this corrosion product layer contains iron and sulfur and so, likely, compounds of iron sulfide.

The EDS spectrum of Figure.a illustrates that once the corrosion product layer formed on the sample surface, in some areas sulfur element was observed as the predominant constituent with a high ratio compared to iron elements. The same features have been reported by F. Alabbas et al [23].

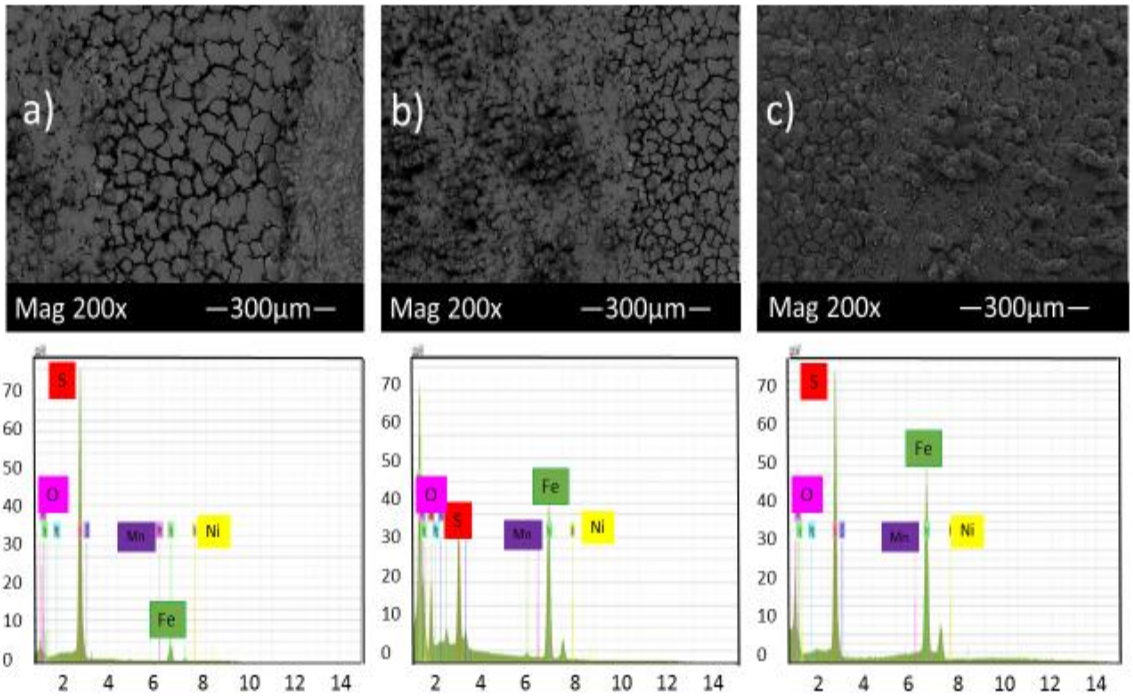

Figure 3.5. SEM micrograph and EDS of the corrosion product layers that form on the surface of each sample at pH 2 under a) 10, b) 20 and c) 30 hours immersion time in thioacetamide solution.

Figure 3.6 shows the SEM micrograph of the corrosion product layers that form on the surface of each sample at pH 5 under 10, 20 and 30 hours immersion time in thioacetamide solution.

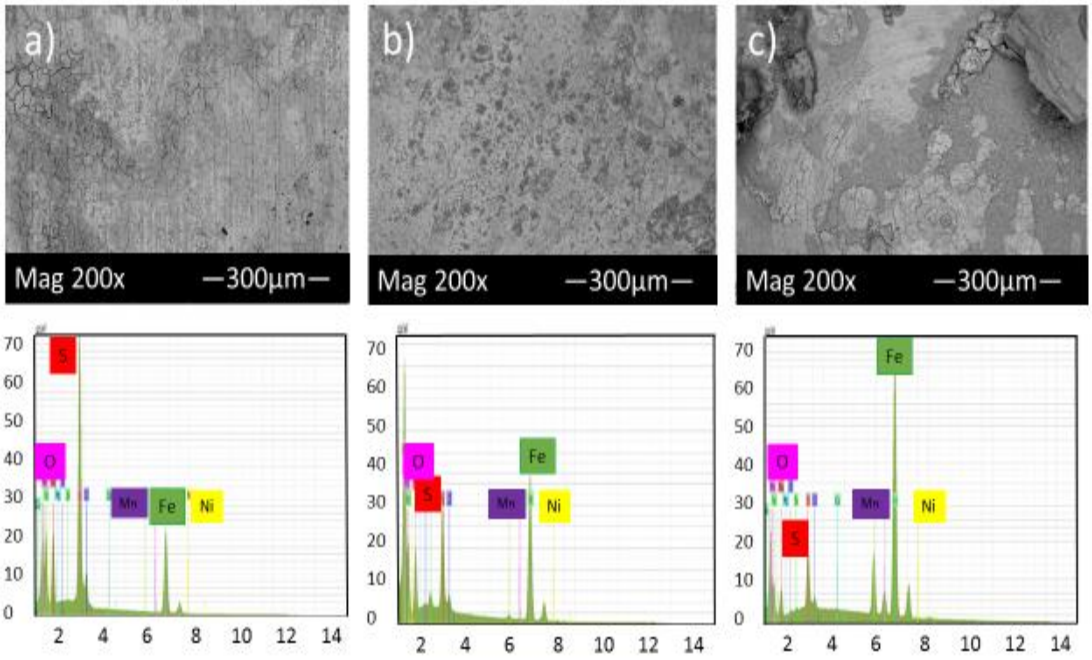

Figure 3.6. SEM micrograph and EDS of the corrosion product layers that form on the surface of each sample at pH 5 under a) 10, b) 20 and c) 30 hours immersion time in thioacetamide solution.

Figure 3.6 (a) and (b) show that generally, a much thicker film was deposited on the alloy surface at pH 5 after 10 and 20 hours immersion in thioacetamide solution. The composition of this film was shown by EDS to consist of iron and sulfur. After 30 hours immersion in the solution, the corrosion product layer was broken and exposed the sample surface to the corrosive solution.

Comparison of Figures 3.5 and 3.6 and also the cross section of the corrosion product layers shows that at pH 2, a very thin and open structure layer formed which could not display a protective role against corrosion. However, at pH 5, the corrosion product layer was more dense, adherent and protective due to a higher volume of precipitated products on the sample surface.

Higher pH would generally decrease the solubility of the corrosion products layer and consequently result in an increase of precipitation rate, faster formation of protective layers and the reduction of corrosion rates [21].

Figure 3.7 shows the SEM micrograph of the corrosion product layers that formed on the surface of each sample covered with elemental sulfur at pH 2 under 10, 20 and 30 hours immersion time.

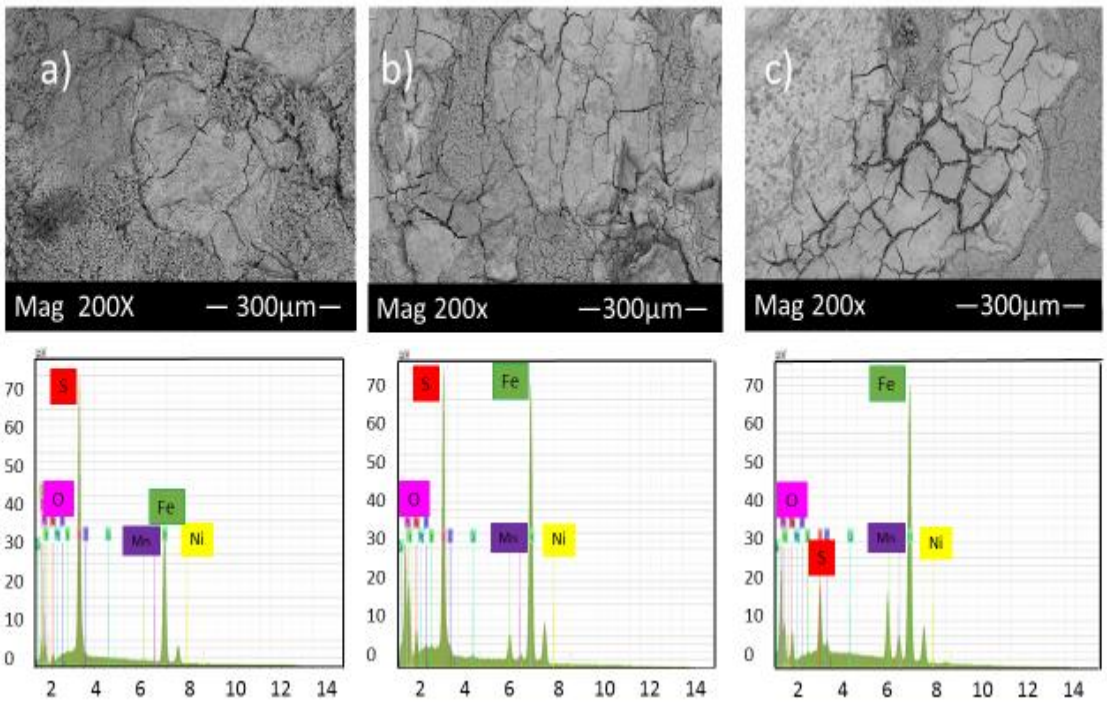

Figure 3.7. SEM micrograph and EDS of the corrosion product layers that form on the surface of each sample covered with elemental sulfur at pH 2 under a) 10, b) 20 and c) 30 hours immersion time.

Figure 3.7 illustrated that the highest percentage of cracks and pits can be observed in this experimental conditions; however, the corrosion product layers formation on the alloy surface gradually increased with time, which slightly reduced the corrosion rate. The

EDS analysis shows the presence of different values of iron and sulfur which also indicates the presence of various compounds of iron sulfide on the surface of samples.

Figure 3.8 shows the SEM micrograph of the corrosion product layers that form on the surface of each sample covered with elemental sulfur at pH 5 under 10, 20 and 30 hours immersion time.

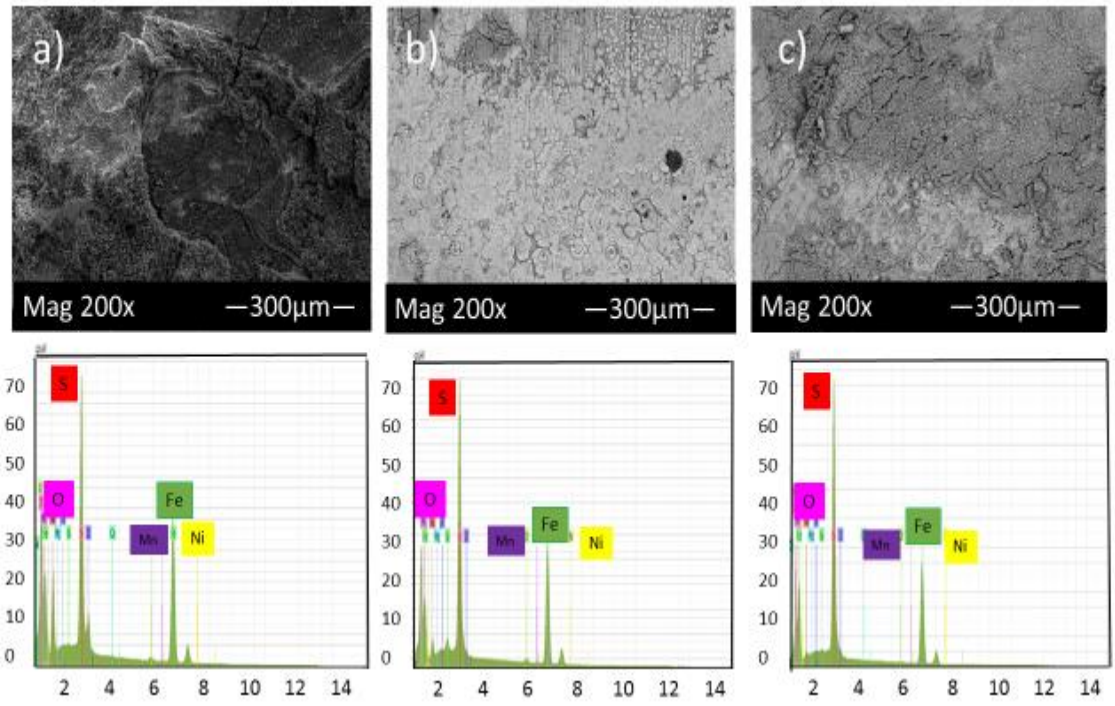

Figure 3.8. SEM micrograph of the corrosion product layers that form on the surface of each sample covered with elemental sulfur at pH 5 under a) 10, b) 20 and c) 30 hours immersion time.

Comparison of Figure 3.7 and 3.8 shows that by increasing pH from 2 to 5 the corrosion product layer became more even and continuous which is consistent with data from corrosion rate and potentiodynamic polarization tests. At pH 5 and after 30 hours immersion in the solution, the corrosion product layers became finer and compact,

indicative of good protection for the alloy compared to those of 10 and 20 hours immersion. Formation of this condensed corrosion product layer slightly prevents further corrosion and consequently decreases the corrosion rate with time.

3.3.3.1. General comparison of the corrosion product layers in two series of experiments

Figure 3.9 (a) and (b) show the cross section of corrosion product layers of the first and second series of experiments at pH 5 after 10 hours immersion time respectively.

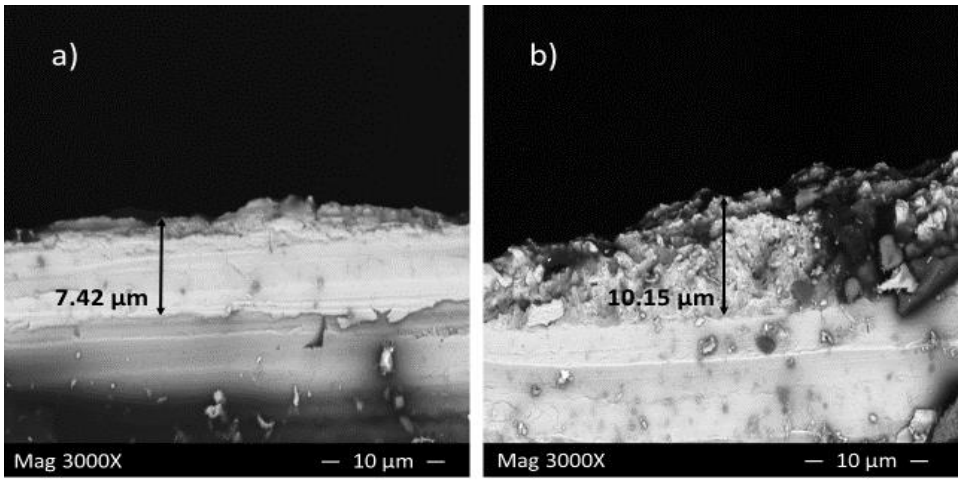

Figure 3.9. Cross section of corrosion product layer of (a) first and (b) second series of experiments at pH 5 after 10 hours immersion time.

In the presence of sulfide ions, Figure 3.9 (a), a thin, dense and adherent layer covered the sample surface with a thickness of approximately 7 µm, which provided a barrier against further corrosion; however, in the presence of elemental sulfur, Figure.3.9 (b), the top surface layer indicates a flaky structure. The thickness of this layer is about 10.15 µm

which still cannot provide enough protection due to the structure being too porous and detached from the sample surface.

The results of cross-sectional analysis verified the results from the corrosion rate calculation and potentiodynamic measurements.

XRD pattern of 4130 Cr- Mo alloy steel exposed to sulfide ions and elemental sulfur are displayed in Figure.3.10. As has been mentioned in the cross-sectional analysis, the corrosion product layer thickness is extremely low for most of the samples, which made them undetectable with XRD measurements. Figure 3.10 (a) indicates the XRD pattern for the sample covered, with elemental sulfur at pH 5 after 30 hours immersion. As can be seen, iron is the only element that was detected on the sample surface.

The XRD patterns in Figure 3.10 (b) and (c) confirmed the formation of iron sulfide compounds on the surface of the samples at pH 5 after 10 hour's immersion time in the first and second series of experiments respectively, where the corrosion product layers were thick enough to be detected by X-ray spectra.

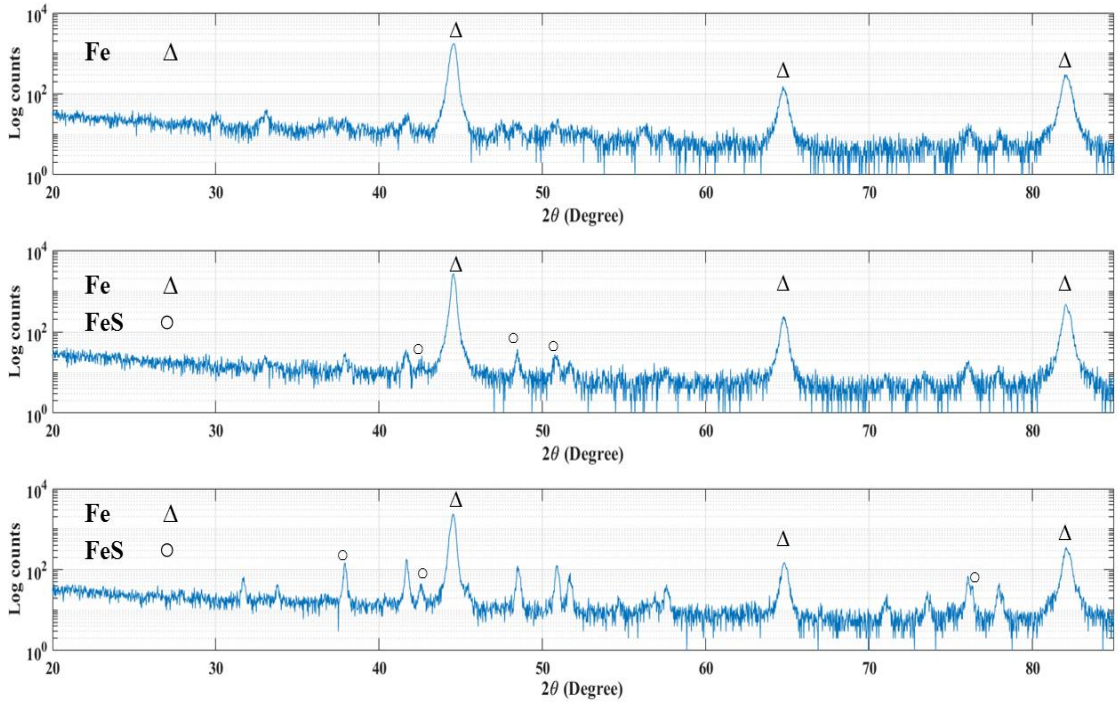

Figure 3.10. XRD pattern for the samples in a) second series of experiment at pH 5 after 30 hours immersion, b) first series of experiments at pH 5 after 10 hours immersion and c) second series of experiment at pH5 after 10 hour's immersion.

3.4. Conclusion

Corrosion resistance of Cr-Mo low alloy in the presence of elemental sulfur is significantly lower than its resistance in the presence of sulfide ions with the same experimental conditions.

Increasing the pH significantly decreases the corrosion rate of Cr-Mo low alloy steel in the presence of elemental sulfur which is due to the formation of more even and compact corrosion product layers on the alloy surface.

The effect of immersion time on the corrosion behavior of alloy is more complicated than the effect of pH. Results suggest that a number of factors such as microstructure,

composition and stability of corrosion product layers and immersion time can increase or decrease the corrosion rate.

How stable the corrosion product layers are from elemental sulfur corrosion in various aggressive environments needs to be further investigated.

3.5. References

[1] Fang, H.; Young, D.; Srdjan, N. Elemental sulfur corrosion of mild steel at high concentration of sodium chloride. In 17th international corrosion congress; Las Vegas, 2009; Vol. 2592, pp. 1–16.

[2] Bojes, J.; Lerbscher, J.; Wamburi, W.; Dilley, C. Elemental sulfur in 3- phase sour gas systems- Is condensate really your ally? In Northern area western conference; Calgary, 2010; pp. 1–22.

[3] Steudel, R. Mechanism for the formation of elemental sulfur from aqueous sulfide in chemical and microbiological desulfurization processes. Ind. Eng. Chem. Res. 1996, 35, 1417–1423.

[4] Macdonald, D. D.; Roberts, B.; Hyne, J. B. Corrosion of carbon steel by wet elemental sulfur. Corros. Sci. 1978, 18, 411–425.

[5] Fang, H.; Brown, B.; Young, D.; Nesic, S. Investigation of elemental sulfur corrosion mechanisms. NACE Int. 2011, 1–13.

[6] Fang, H. Investigation of localized corrosion of carbon steel in H_2S environments, PhD thesis, Ohio University, 2012.

[7] Petroleum and Natural Gas Industries – Materials for use in H_2S -containing Environments in Oil and Gas Production; 2005.

[8] ASTM Standard reference method for making potentiostatic and potentiodynamic anodic polarization measurements; 1982; pp. 511–521.

[9] Khaksar, L.; Whelan, G.; Shirokoff, J. Electrochemical and microstructural analysis of FeS films from acidic chemical bath at varying temperatures, pH, and Immersion Time. Int. J. Corros. 2016, 1025261.

[10] Saeed Akhtar, M.; Alenad, A.; Azad Malik, M. Synthesis of mackinawite FeS thin films from acidic chemical baths. Mater. Sci. Semicond. Process. 2015, 32, 1–5.

[11] Butler, E. A.; Peters, D. G.; Swift, E. H. Hydrolysis reactions of thioacetamide in aqueous solutions. Anal. Chem. 1958, 30, 1379–1383.

[12] Oswald, M. P.; Camiel, J. de R. Pathways in thioacetamide hydrolysis in aqueous acid: detection by kinetic analysis. J. Chem. Soc. 1974, 1832–1835.

[13] Dumbrava, A.; Badea, C.; Prodan, G.; Ciupina, V. Synthesis and characterization of cadmium sulfide obtained at room temperature. Chalcogenide Lett. 2010, 7, 111–118.

[14] Gury, F.; Mohamed, B.; Cournil, M. Precipitation dynamics of zinc sulfide multi-scale agglomerates. AIChE J. 2009, 55(10), 2553–2562.

[15] Fang, H.; Young, D.; Nešić, S. Elemental sulfur corrosion of mild steel at high concentrations of sodium chloride. In 17th international corrosion congress; Las Vegas, 2009; pp. 1–16.

[16] Enos, D. G.; Scribner, L. L. The Potentiodynamic Polarization Scan Technical Report 33. Cent. Electrochem. Sci. Eng. 1997, 1–13.

[17] Sun, W.; Nešić, S.; Papavinasam, S. Kinetics of Iron Sulfide and Mixed Iron Sulfide/Carbonate Scale Precipitation in CO_2 /H_2S Corrosion. NACE Int. 2006, 1–26.

[18] Koteeswaran, M. CO_2 and H_2S corrosion in oil pipelines, Master thesis, University of Stavanger, 2010.

[19] Rihan, R. O. Electrochemical corrosion behavior of x52 and x60 steels in carbon dioxide containing saltwater solution. Mater. Res. 2013, 16, 227–236.

[20] Sun, W.; Nesic, S. a Mechanistic Model of H_2S Corrosion of Mild Steel. NACE Int. 2007, 1–26.

[21] Sun, W. Kinetic of iron carbonate and iron sulfide scale formation in CO_2/ H_2S corrosion, PhD thesis, Ohio University, 2006.

[22] Lee, K. J. A mechanistic modeling of CO_2 corrosion of mild steel in the presence of H_2S, PhD thesis, Ohio University, 2004.

[23] Alabbas, F. M.; Williamson, C.; Bhola, S. M.; Spear, J. R.; Olson, D. L.; Mishra, B.; Kakpovbia, A. E. Microbial corrosion in pipeline steel under the influence of a sulfate-reducing consortium isolated from an oil field. J. Mater. Eng. Perform. 2013, 22, 3517–3529.

4. EFFECT OF DEPOSITED CORROSION PRODUCT LAYERS ON ELECTROCHEMICAL BEHAVIOUR OF CONVENTIONAL 13% CHROMIUM STEEL EXPOSED TO CHLORIDE CONTAINING ENVIRONMENT

Preface

A version of this manuscript is accepted for publication in the Journal of Innovation in Corrosion and Materials Science. I am the primary author of this paper, along with the co-authors, John Shirokoff. I conducted the literature review and proposed the outline of the experiments and the analysis procedure. I conducted most of the experiments and microstructural analysis. I prepared the first draft of the manuscript and subsequently revised the manuscript based on the co-author's feedbacks and also the initial feedbacks from the journal reviewers. The co-author, John Shirokoff, helped in analyzing the final results, and contributed in preparing, reviewing and revising the manuscript.

Abstract

Due to the increase in the number of sour wells in today's oil and gas industry, reservoir souring and related acidizing issues must be considered as an essential concern for material selection which significantly affect the application and performance of alloy steels. The influence of deposited corrosion product layers on the electrochemical behavior of 13% chromium stainless steel was investigated in an acidic solution to study the effect of a deposited elemental sulfur and FeS layer on the electrochemical behavior of 13% chromium steel with particular emphasis on the role of temperature, chloride concentration and morphological characterization of corrosion products. Cyclic polarization and also linear polarization resistance techniques were applied to measure the corrosion parameters such as corrosion rate, E_{corr}, E_{pit} and I_{pass} of 13% chromium steels at various temperatures and chloride concentrations. All the electrochemical measurements were performed at 25 and 75 °C with addition of 0, 10 and 20 g/L NaCl in 0.01 M hydrochloric acid solution. Surface measurement techniques such as SEM, EDS, and AFM were applied for morphological analysis of the corrosion products. The results showed that both temperature and chloride concentration had significant effects on corrosion parameters; however, these effects on the corrosion rates in the presence of elemental sulfur were significantly higher than those in the presence of an iron sulfide layer or without any initial deposited layer on the sample surface. Environmental variables, such as temperature and chloride concentration have an important role on the corrosion resistance of 13% chromium steel which can indicate either protective or destructive effects on the corrosion behavior of steel.

4.1. Introduction

Among all types of Corrosion Resistant Alloys (CRA) used in today, oil and gas industry, martensitic stainless steels (MSS) are some of the most reliable and applicable ones. These steels have a great CO_2 corrosion resistance due to the addition of a minimum of 11% chromium content to their composition. NACE and American Petroleum Institute (API) standards suggest a number of MSS for oil and gas industry applications; among all of them, 13% chromium steel is the most recommended [1].

All types of 13% chromium steels are categorized into two general groups: conventional and modified. Conventional 13% Cr steels (13Cr) are the most applicable ones in oil and gas some of which are CA6NM (UNS J91150), AISI 410(UNS S41000), and AISI 420 (UNS S42000). These alloys meet all the needs of wellhead, tubular, and downhole components except resistance to cracking in H_2S containing environments [2]. Modified 13% Cr (M13Cr) steels came from the need for increased corrosion resistance at higher temperatures, H_2S cracking resistance, and yield strength above 85 ksi (586 MPa), primarily for tubular goods and other downhole equipment. These features were provided by the addition of nickel (Ni), molybdenum (Mo), copper (Cu), and other alloying elements to the conventional ones. M13Cr meets all the essential requirements of wellhead, tubular, and downhole components and also provides higher corrosion resistance than 13Cr up to approximately 350°F (177°C) and yield strengths up to 110 ksi (758 MPa) [1].

Due to the increase in the number of sour wells in today's oil and gas industry, reservoir souring and related acidizing issues must be considered [3]. These issues would significantly affect the selection, application and performance of 13% Cr steels [4].

The corrosion of 13 % chromium steel in either sweet or sour condition, and of course the role of a passive film, a few nanometers layer which is thick and rich in chromium on the top surface, have been investigated from various aspects [4]–[6]. According to those investigations, one of the most effective factors in the corrosion process in oil and gas pipelines and especially in the sour ones, is the presence of deposited elemental sulfur produced by the H_2S corrosion process in there [7]. It is known from prior research that the presence of dry elemental sulfur in contact with carbon steel is not considered as a corrosion threat to steel; however, by adding water to the system, the corrosion process may be dramatically accelerated [8]. A literature review has shown that the nature of H_2S corrosion product layers controls the kinetics of this corrosion process from both phase type and morphology perspectives [9].

The following equations are usually the main sources of producing elemental sulfur in an aqueous system [10]:

$$8\ H_2S\ (aq) + 16\ M^{n+}\ (aq) \rightarrow S_8\ (s) + 16\ H^+\ (aq) + 16\ M^{(n-1)}\ (aq) \quad (4.1)$$

$$8\ H_2S\ (aq) + 4\ O_2\ (g) \rightarrow S_8\ (s) + 8\ H_2O \quad (4.2)$$

It is also known that an iron sulfide, FeS, layer is another main product of H_2S corrosion which can initiate some localized corrosion due to its local breakdown on the surface [11]. This breakdown could have various environmental causes such as the presence of solids, chlorides, high velocity etc. Among these reasons, chloride ions can cause initiation of localized corrosion through the FeS layer on the steel surface and consequently pitting corrosion in the steel [9]–[12].

Nose et al. proved that the corrosion resistance of M13% Cr steel is highly affected by the chloride content [13]. Evans et al conducted long-term H_2S corrosion tests of carbon steel, 13% Cr steel and a few other stainless steels to study their resistance to corrosion in various environmental conditions [14]. Although this study was almost comprehensive, due to the numerous considered stainless steel and environmental conditions, it is often difficult to utilize for practical situations. Zhao et al. reported that at 90 °C, the corrosion was controlled by the activation process; thereby, 13Cr steel was susceptible to localized attack while at 150 °C a passive layer mixing with corrosion products formed a covering layer, and the corrosion behavior indicated a uniform corrosion [15]. However other research by Yin et al. showed numerous corrosion micro-pits on the localized sites of corrosion product layers of 13Cr steel at 160 °C [16].

The overall objective of this research is to study the effect of a deposited elemental sulfur and FeS layer on the electrochemical behavior of 13% chromium steel with particular emphasis on the role of temperature, chloride concentration and morphological characterization of corrosion products.

4.2. Experimental procedure

4.2.1. Material and sample preparation

According to the industrial partner's request, the corrosion samples were made from conventional 13% Cr steel. Table 4.1. indicates the composition of grade 420 chromium stainless steel.

Table 4.1. The chemical composition of conventional 13% Cr stainless steel grade 420

C	Cr	Mn	Si	P	S	V	Fe
0.15	12	0.22	0.3	0.014	0.0035	0.041	Bal.

The working electrode was machined from the parent material into cylinders having dimensions of approximately 9 mm length and 9 mm diameter. Prior to the experiments, all specimens were polished with Coated Abrasive Manufacturers Institute (CAMI) grit designations 320, 600, 1000 corresponding to average particle diameters 36.0, 16.0, and 10.3 microns and finally 6-micron grit silicon carbide paper, and then cleansed with deionized water until a homogeneous surface was observed. Following this the specimens were quickly dried using cold air to avoid oxidation.

Three groups of samples were prepared to investigate the effect of deposited corrosion product layers on the electrochemical behavior of conventional 13% Cr steel. The corrosion behavior of the first group of samples was analyzed while its top surface was exposed to the solution with no initial corrosion product layer on it. Different chloride

concentrations of 0, 10 and 20 g/L NaCl were used in a 0.01 M hydrochloric acid solution with pH 2 at 25°C and 75°C.

For the second group of samples, the corrosion behavior was analyzed with the same experimental condition, 0, 10 and 20 g/L NaCl in a 0.01 M hydrochloric acid solution with pH 2 at 25°C and 75°C, while the working electrode was covered with a thin iron sulfide corrosion layer, FeS layer, synthesized by an acidic chemical bath [17], [18]. The mechanism of FeS formation in this acidic bath is the slow release of iron and sulfur ions within the solution followed by the deposition of these ions on the alloy surface. The iron and sulfur ions are provided from iron (II) chloride and thioacetamide respectively. The formation of FeS film from this acidic bath is dependent on whether the deposition rate of the ionic product of iron and sulfur is higher than the rate of solubility of FeS. Adding urea to the solution adjusted the balance between hydrolysis and deposition. The proposed reactions for this mechanism are described as follows [19]:

$$FeCl_2 \rightarrow Fe^{2+} + 2\,Cl^- \quad (4.3)$$

$$CH_3CSNH_2 + H_2O \leftrightarrow S^{2-} + CH_3CONH_2 + 2H^+ \quad (4.4)$$

$$CO\,(NH_2)_2 + H_2O \leftrightarrow 2NH_3 + CO_2 \quad (4.5)$$

$$NH_3 + H_2O \leftrightarrow NH_4^+ + OH^- \quad (4.6)$$

$$Fe^{2+} + S^{2-} \leftrightarrow FeS \quad (4.7)$$

Finally, the overall reaction would be written as:

$$Fe^{2+} + CH_3CSNH_2 + CO(NH_2)_2 + 2H_2O \rightarrow FeS + CH_3CONH_2 + 2NH_4 + CO_2 \qquad (4.8)$$

This series of experiments enabled the estimation of the effect of the deposited FeS layer on the electrochemical and corrosion behavior of 13% Cr stainless steel in the presence of various chloride concentrations.

Finally, the electrochemical behavior of the third group of samples was analyzed with the same experimental condition, different chloride concentrations of 0, 10 and 20 g/L in a 0.01 M hydrochloric acid solution with pH 2 at 25°C and 75°C, while the working electrode was covered by sublimed elemental sulfur 99.9999% (ACROS) [20]. These experiments indicated the effect of deposited elemental sulfur on the electrochemical and corrosion behavior of 13% Cr stainless steel with the presence of various chloride concentrations.

4.2.2. Corrosion measurements

Electrochemical corrosion measurements, and in particular, Linear Polarization Resistance (LPR), provide information about the corrosion rate of an electrochemical system [21]. In this method the polarization curves represent the evaluation of current density (i) developed on the steel surface as a function of the applied potential (E). The current density is directly related to the nature and the rate of electrochemical reactions which occur at the interface between the steel surface and the aggressive solution.

During this study, corrosion and electrochemical experiments were conducted in a multi-port glass cell with a three electrodes setup, at atmospheric pressure based on the ASTM

G5-82 standard for potentiodynamic anodic polarization measurements [22]. The applied sweep rate for these measurements was 0.5mV/s. An Ivium Compactstat Potentiostat monitoring system was used to perform electrochemical corrosion measurements. The pH was adjusted at 2 by adding deoxygenated hydrochloric acid.

Hence the polarization resistance is the ratio of the applied potential and the resulting current level, A small potential in the range of ±6 mV (which does not affect the natural corrosion process) with respect to the open circuit potential (OCP) and a scan rate of 0.125 mV/s, was applied between the elements and the resisting current was measured. This resistance can then be used to find the corrosion rate of the sample using the Stern-Geary equation [21]. The values of anodic (β_a) and cathodic (β_c) Tafel slopes of the samples of each experiment were obtained as well and then applied to calculate the final corrosion rate [18].

During the electrochemical measurements, a graphite rod was used as the counter electrode (CE) while saturated silver/ silver chloride (Ag/AgCl) was installed as the reference electrode (RE) and conventional 13% Cr steel samples were chosen as working electrodes (WE).

With regard to the high susceptibility to breakdown of corrosion product layers on the working electrode surface, the pitting tendencies of specimens in the given metal-solution system were measured using the cyclic polarization technique. Cyclic polarization is a type of polarization method which is performed in a cyclic manner. The potential is swept in a single cycle (or slightly less than one cycle), and the size of the hysteresis is

examined along with the differences between the values of the starting open circuit corrosion potential and the return passivation potential. The existence of the hysteresis is usually indicative of pitting, while the size of the loop is often related to the amount of pitting [23]. Materials exhibiting higher values of pitting potential (E_P) and protection potential (E_{pro}) are more resistant to pitting corrosion, and cyclic polarization experiments are commonly used for the purpose of selecting these materials [23]. Cyclic potentiodynamic polarization was performed by starting from a negative potential at -200 mV of corrosion potential (E_{corr}) with a sweep rate of 0.125 mV/s.

4.2.3. Surface morphological observation and corrosion product analysis

Upon completion of corrosion testing, morphological characterization of the surface was conducted using an FEI Quanta 400 scanning electronic microscope (SEM) with Bruker energy dispersive X-ray (EDS) spectroscopy. The SEM was operating at 15 kV, with a working distance of 15 mm, and beam current of 13 nA. Also an MFP-3D Atomic Force Microscope (AFM) was used to obtain more information about the corrosion products features and surface roughness on the samples surface.

4.3. Results

4.3.1. Corrosion measurements

The significant corrosion parameters such as the corrosion potential (E_{corr}), the pitting potential (E_{pit}) and the passive current density (I_{pass}) were obtained to investigate the

effect of deposited corrosion product layers on the electrochemical behavior of conventional 13% Cr steel exposed to a chloride containing environment [23].

The cyclic polarization curves of the first group of samples with different chloride concentrations of 0, 10 and 20 g/L NaCl in 0.01 M hydrochloric acid solution with pH 2 at 25°C are shown in Figure 4.1.

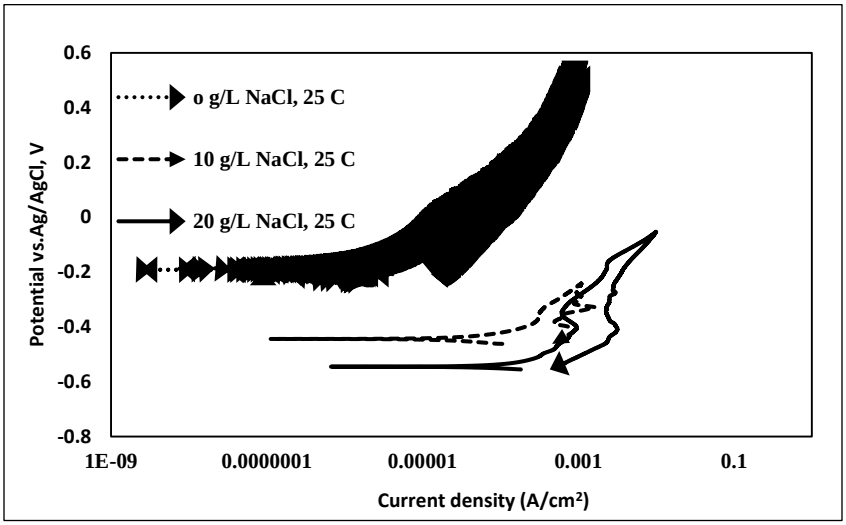

Figure 4.1. Cyclic polarization curves of the first group of samples with the addition of 0, 10 and 20 g/L NaCl at 25°C.

It can be seen that the corrosion potential (E_{corr}) and pitting potential (E_{pit}) shifted to a negative direction with an increase of chloride concentration which induced the chloride concentration effect on the pitting corrosion of 13% chromium steel. Also, the increase of current density was observed by the addition of 20 g/L NaCl to the solution which represents the increase of corrosion rate on the sample surface as well. As the chloride concentration increased from 0 to 20 g/L, the current begins to increase with potential. Such increase in current may be due to localized breakdown of the passive film by

anions, especially chloride ions [11]. The presence of these anions in the solution induced localized dissolution of the passive oxide film in the weak spots on the surface and gradually leading to exposure of the underlying sample surface that can cause the increase of the anodic current and so the formation of pits. Consequently as shown in Figure 4.2. the passive current density (I_{pass}) increased by the addition of chloride ions, which indicates the effect of the chloride ions on the acceleration of the reaction activity and eventually reduction of the pitting resistance of steel [16].

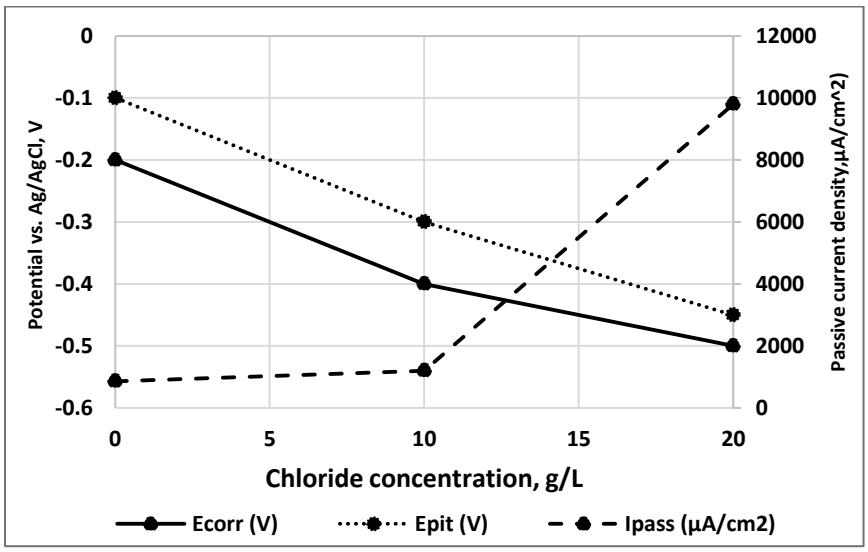

Figure 4.2. Corrosion potential (E_{corr}), pitting potential (E_{pit}) and passive current density (I_{pass}) in cyclic polarization curves of the first group of samples with the addition of various chloride concentrations at 25°C.

Figure 4.2. shows that the corrosion potential (E_{corr}) slightly shifted to the negative direction with an increase of chloride concentration and induced the susceptibility of chloride ion to be the main cause of localized corrosion of 13% Chromium steel [9].

The cyclic polarization curves of the first group of samples at 75°C are shown in Figure 4.3.

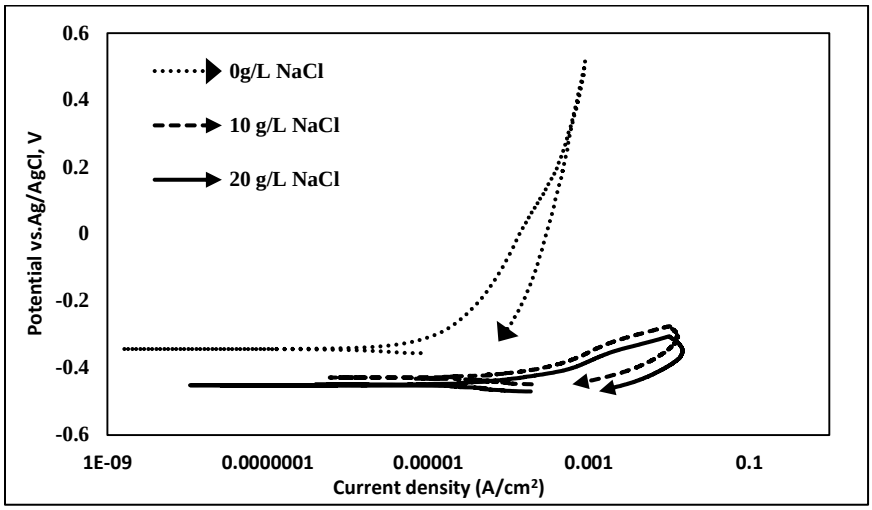

Figure 4.3. Cyclic polarization curves of the first group of samples with the addition of 0, 10 and 20 g/L NaCl at 75°C

It is clear that the curves are closer to each other at 75 °C compared to the ones at 25 °C, which means the effect of chloride concentration might be less than the sole effect of temperature. The corrosion potential (E_{corr}) shifted to a negative direction with an increase of chloride concentration and the size of the hysteresis loops slightly increased compared to that at 25 °C. Hysteresis, in the case of corrosion phenomena, describes an attribute of the polarization measurements in which the forward and reverse directions of the scan do not cover each other [24]. The size of the pitting loop provides a fair estimation of pitting tendency; a larger loop indicates a greater tendency to pitting due to the greater disruption of surface passivity and also a higher risk of localized corrosion [23]. Comparison of the size of the hysteresis in Figure 4.1 and 4.3, clarified that change

of the temperature in the constant experimental conditions can affect the passivation behavior of samples and their resistance to the anions, however, this effect does not follow a certain algorithm and affects all the corrosion parameters individually. For instance, despite the change of the hysteresis loop at 75 °C with 20 g/L NaCl, the corrosion potential does not increase and remains close to its value at 25 °C with 20 g/L NaCl. Figure 4.3. Shows a general corrosion occurred at the beginning of the measurement and gradually by addition of chloride ions to the solution, caused the formation of a small passivation region in the cyclic polarization curves with 10 and 20 g/L NaCl in the solution.

The cyclic polarization curves of the second group of samples, covered with a thin layer of iron sulfide, in 0.01 M hydrochloric acid solution with pH 2 at 25°C are presented in Figure 4.4.

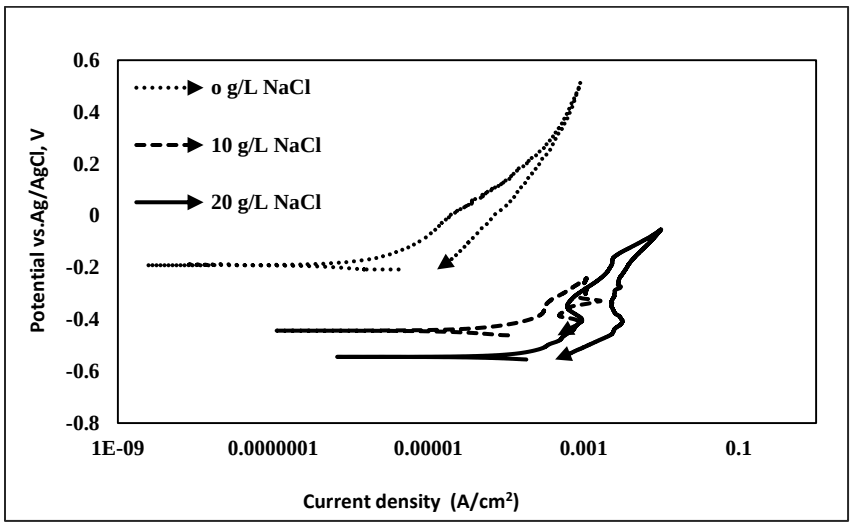

Figure 4.4. Cyclic polarization curves of the second group of samples with the addition of 0, 10 and 20 g/L NaCl at 25°C

According to the results of previous studies by the authors, an iron sulfide scale protects the surface and decreases the corrosion rate under certain conditions. This scale forms a protective barrier which slows down the corrosion process by covering and preventing the sample surface from further dissolution [17], [18], however, comparison of cyclic polarization curves with no deposited iron sulfide layer, Figure 4.1, and with the presence of deposited iron sulfide on the samples surface, Figure 4.4, showed that the deposited layer can affect the passivation behavior negatively. Figure 4.4. indicates that addition of chloride ions to the solution caused a considerable change in the size of the hysteresis loops of cyclic polarization curves. As described previously, the size of the pitting loop is a rough indication of pitting tendency: the larger the loop, the greater the tendency to pitting. This increase in pitting tendency might be related to formation of some chloride-containing composition, for example a layer of iron chloride [$FeCl_2$] on the sample surface, which is an acidic layer that affects the stability of the FeS layer and may increase the corrosion process by enabling the anodic reaction to continue. This destructive iron chloride layer significantly decreases the protective feature of the iron sulfide layer at a low temperature [25]. Further analysis has been done by EDS and SEM in the surface morphology section.

As shown in Figure 4.5, before the addition of chloride ions, the value of pitting potentials was the same as corrosion potential and consequently a low tendency for pitting in that case [23], however, after the addition of 10 and 20 g/L NaCl to the

solution, the corrosion and pitting potential gradually increased on the sample surface. Also, current density significantly increased through the sample surface may be due to the increase of solution conductivity by the addition of chloride ions to the solution beside the deposited iron sulfide layer on the surface [9].

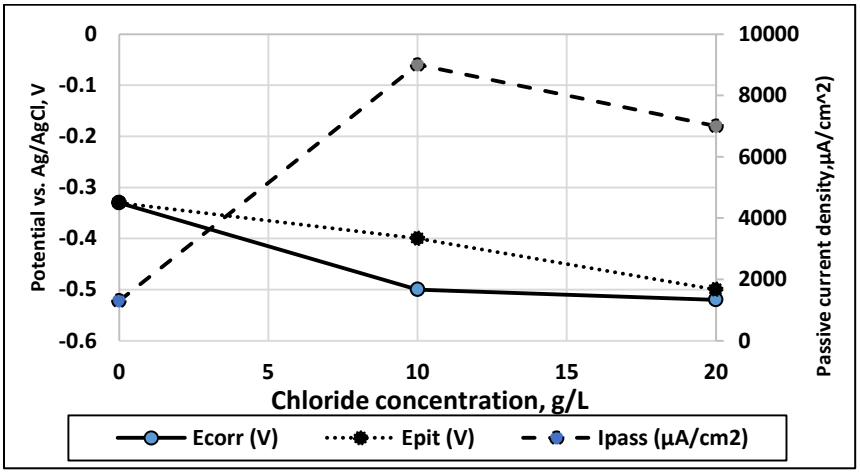

Figure 4.5. Corrosion potential (E_{corr}), pitting potential (E_{pit})and passive current density (I_{pass}) in cyclic polarization curves of the second group of samples with addition of various chloride concentrations at 25°C.

The cyclic polarization curves of the second group of samples at 75°C are shown in Figure 4.6.

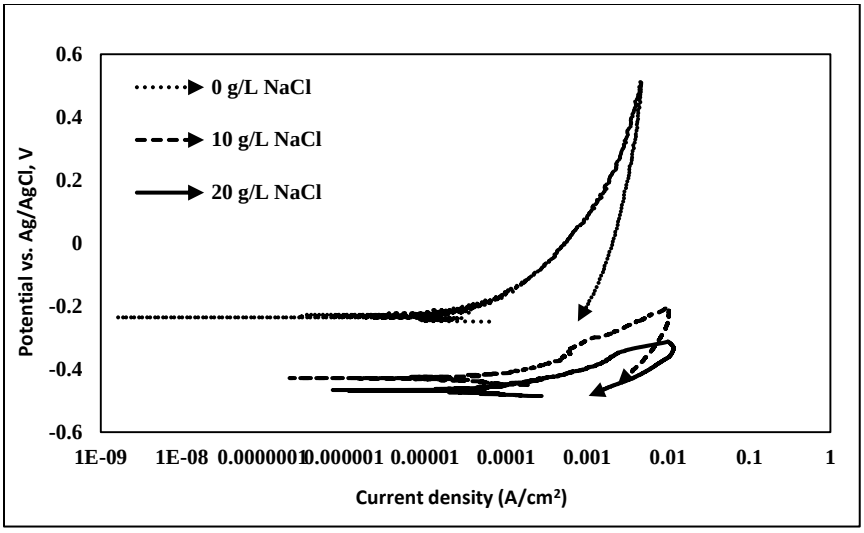

Figure 4.6. Cyclic polarization curves of the second group of samples with the addition of 0, 10 and 20 g/L NaCl at 75°C

Authors' previous studies showed that in the presence of an FeS layer on the sample surface, an increase of temperature could affect the spreading of involved species in electrochemical reactions by evaporating one or more species out of the solution, which can directly affect the corrosion reaction [17], [18]. By increasing the temperature, the general current density in the cyclic polarization curve of 0 g/L NaCl has slightly increased which accelerates the reaction activity and reduces pitting resistance which can lead to an increase in the size of the hysteresis loop, particularly before the addition of chloride ions. Therefore, it could be concluded that in the presence of an FeS corrosion layer on the sample surface, the effect of temperature is more significant than the effect of chloride ions concentration in the solution; however, the presence of chloride can certainly affect FeS layer stability and its behavior during an anodic reaction as well [25]. Also the current densities were shifted to higher values as the temperature increases which indicated a small passivation region for sample at 10 g/L NaCl and 20 g/L NaCl.

The cyclic polarization curves of the third group of samples, Covered with a thin layer of elemental sulfur, in 0.01 M hydrochloric acid solution with pH 2 at 25°C are presented in Figure 4.7.

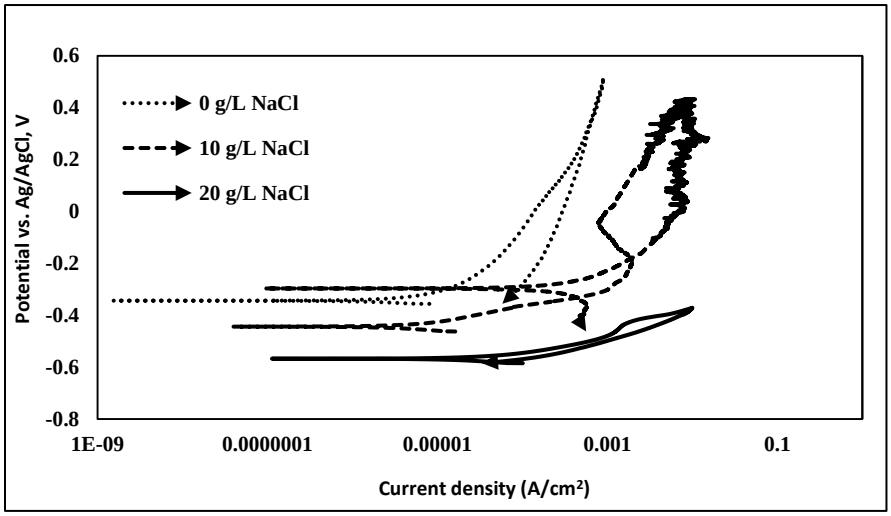

Figure 4.7. Cyclic polarization curves of the third group of samples with the addition of 0, 10 and 20 g/L NaCl at 25°C

Generally, at the start of the measurements, no chloride ions in the solution, the corrosion potential was neglectable and sample was passivated. By the addition of chloride ions to the solution, the corrosion potential slightly shifted to the negative direction; however, it was directed in a different way after addition of 10 g/L NaCl. In this case, at the beginning, the general corrosion tendency and pits propagation increased and a quite large hysteresis loop was formed. During the cathodic direction the corrosion potential slightly decreased and consequently shifted to the positive direction at the end of the curve. These observations are all related to the formation of a passive layer and its

dissolution, which determine the effect of the passive process on the corrosion behavior of the sample [16]. After the addition of 20 g/L NaCl to the solution, despite a negative increase of the corrosion potential from -0.29 to -0.57 V, the hysteresis loop became smaller and the pitting tendency decreased on the sample surface. However in this case with regard to the high values of current density, there is no chance of repassivation on the sample surface. This could happen due to the adsorption of chloride ions which generated a mass transfer barrier to the corrosive species, such as elemental sulfur on the surface [9]. As shown in Figure 4.8. the general pitting tendency slightly decreases by the addition of 20 g/L NaCl; however, there was not a strong chance of passivation process on the sample surface due to the high values of current densities.

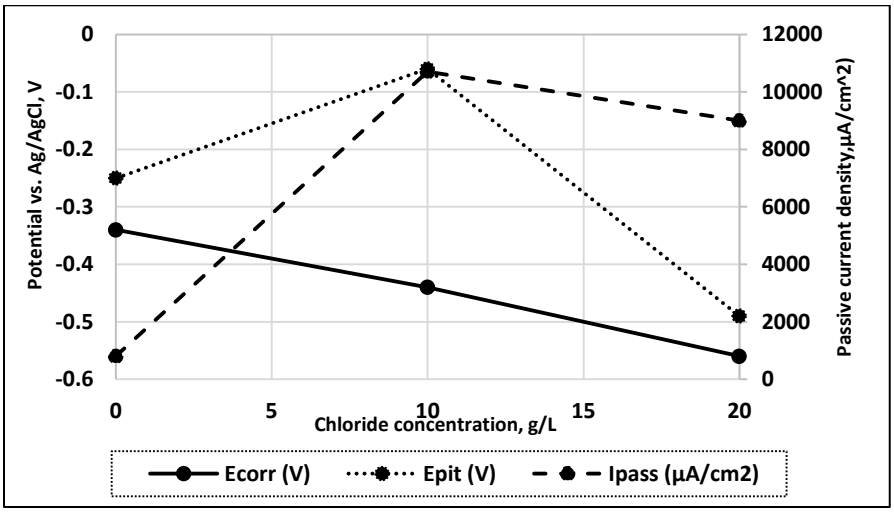

Figure 4.8. Corrosion potential (E_{corr}), pitting potential (E_{pit}), protection potential (E_{pro}), ΔE and passive current density (I_{pass}) in cyclic polarization curves of the third group of the samples with addition of various chloride concentrations at 25°C

The cyclic polarization curves of the third group of samples at 75°C are shown in Figure 4.9. It can be observed that addition of chloride ions to the solution shifted the corrosion

potential to the negative direction and slightly increased the current density which ignored the idea of passivation behavior in this regions, however, due to the presence of a small hysteresis, the increase in current density at higher potentials is attributed to initiation of the pitting or crevice corrosion on the surface but not its propagation [9].

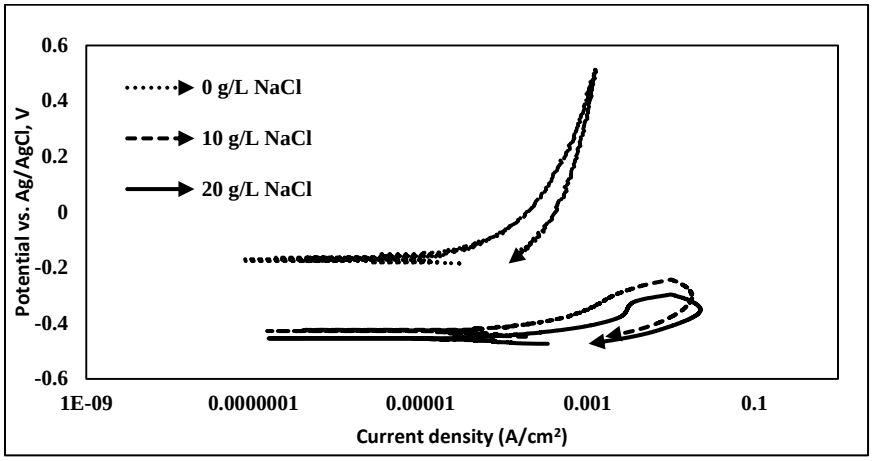

Figure 4.9. Cyclic polarization curves of the third group of samples with the addition of 0, 10 and 20 g/L NaCl at 75°C

Figure 4.9 indicates that in the presence of elemental sulfur, the role of temperature is more significant compared to its role in the first group, where the sample surface was not covered by any initial layer. The comparison of the hysteresis at 25 and 75°C with addition of 20 g/L NaCl in Figure 4.9, illustrated that in the presence of elemental sulfur, temperature affect the passivation behavior with increasing the values of current densities through the anodic reactions.

4.3.2. Surface morphological observations and corrosion product analysis

The SEM micrographs of the corrosion product layers on the surface of the first group of samples, are shown in Figure 10. As it is illustrated in Figure 4.10 a and d, there is few localized corrosion on the samples surface due to the presence of chloride ions in the electrolyte solution. By the increase of chloride concentration gradually small pits initiated and propagated on the surface, Figure 4.10 (b), (c), (e) and (f). The aggressive species such as Cl^- ions rapidly transferred to the metal surface, attacked the local corrosion products and created small pits [11].

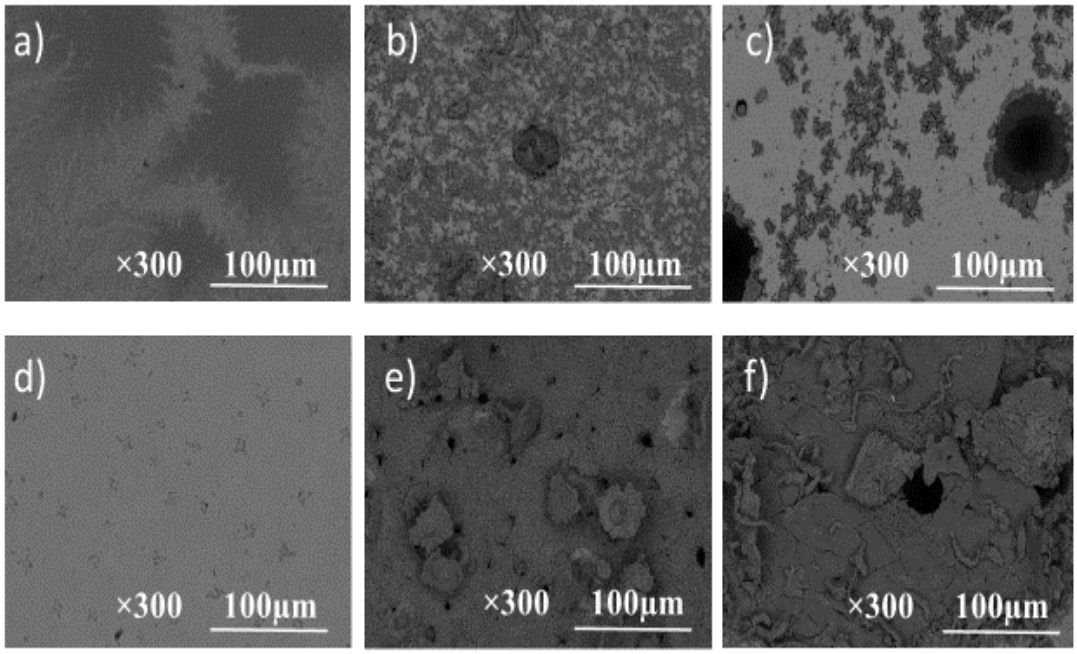

Figure 4.10. SEM micrograph of the corrosion product layers on the surfaces of the first group of samples at 25°C with (a) 0, (b) 10 and (c) 20 g/L NaCl and also at 75°C with (d) 0, (e) 10 and (f) 20 g/L NaCl

These small pits will grow and increase the current density through the sample surface; however, some of them will be repaired and passivated by the formation of corrosion products, as shown in Figure 4.10 e and f [25], [26]. According to Figure 4.10 there are not too many deposited corrosion products on the first group of samples and the few formed ones should be the products of oxidation reactions during different experimental conditions. The EDS analysis will describe these products in the following sections.

Figure 4.11 presents the SEM micrograph of the corrosion product layers on the surface of the second group of samples, where the samples' surfaces were covered with a very thin FeS layer deposited from an acidic chemical bath. More corrosion pits were formed on the surface of the samples in the second series compared to the first one, as shown in Figure 4.11 (e) and (f), which illustrated that the presence of deposited iron sulfide layer on the surface can increase the aggressiveness of the environment and adsorb more anion such as chloride, through the surface which will induce the formation of iron chloride [$FeCl_2$] on the surface of the samples. When the temperature reaches 75 °C, the corrosion product layers are almost stable, so some of the formed micro-pits on the surface do not easily repair themselves and so would continue to nucleate and grow through the layers which caused the increase of pitting tendency. The SEM analysis of the second group of samples confirms the results of cyclic polarization measurements, that in the presence of an FeS corrosion layer on the sample surface, the effect of temperature is more significant than the effect of chloride ions' concentration in the solution; however, it has been proved that the presence of chloride can certainly affect FeS layer stability and its behavior during an anodic reaction [18]. According to previous studies, formation of a

layer of iron chloride on the sample surface can affect the stability of the FeS layer on the corroded steel and enables the anodic reaction to continue [25].

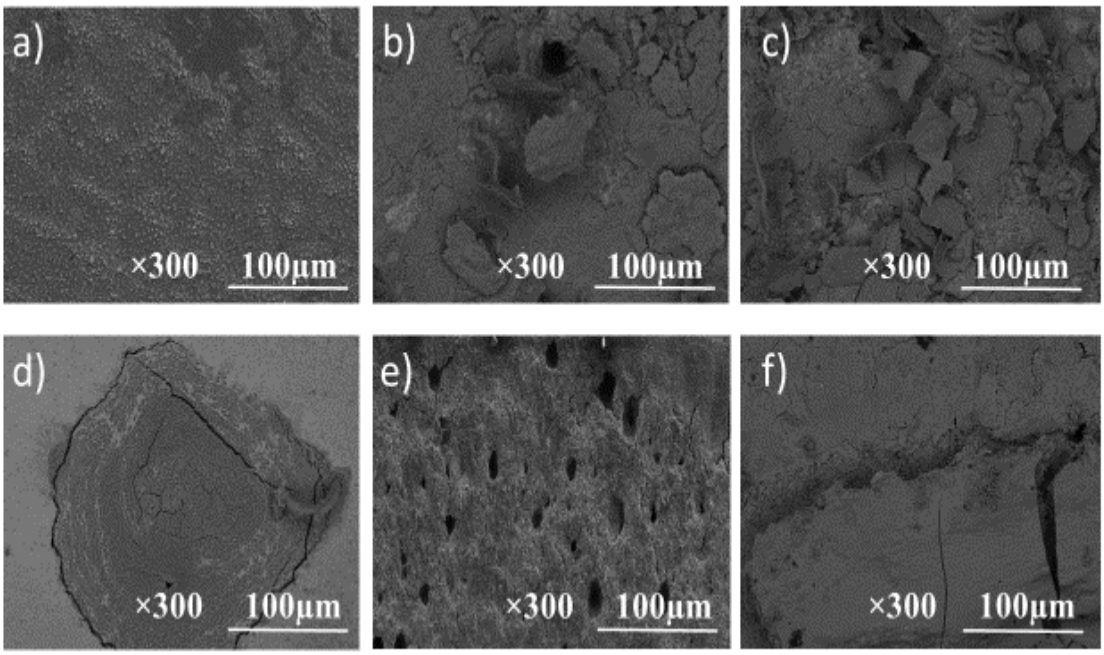

Figure 4.11. SEM micrograph of the corrosion product layers on the surfaces of the second group of samples at 25°C with (a) 0, (b) 10 and (c) 20 g/L NaCl and also at 75°C with (d) 0, (e) 10 and (f) 20 g/L NaCl.

The SEM micrograph of the corrosion product layers on the surface of the third group of samples where the samples' surfaces were covered with sublimed elemental sulfur, are shown in Figure 4.12.

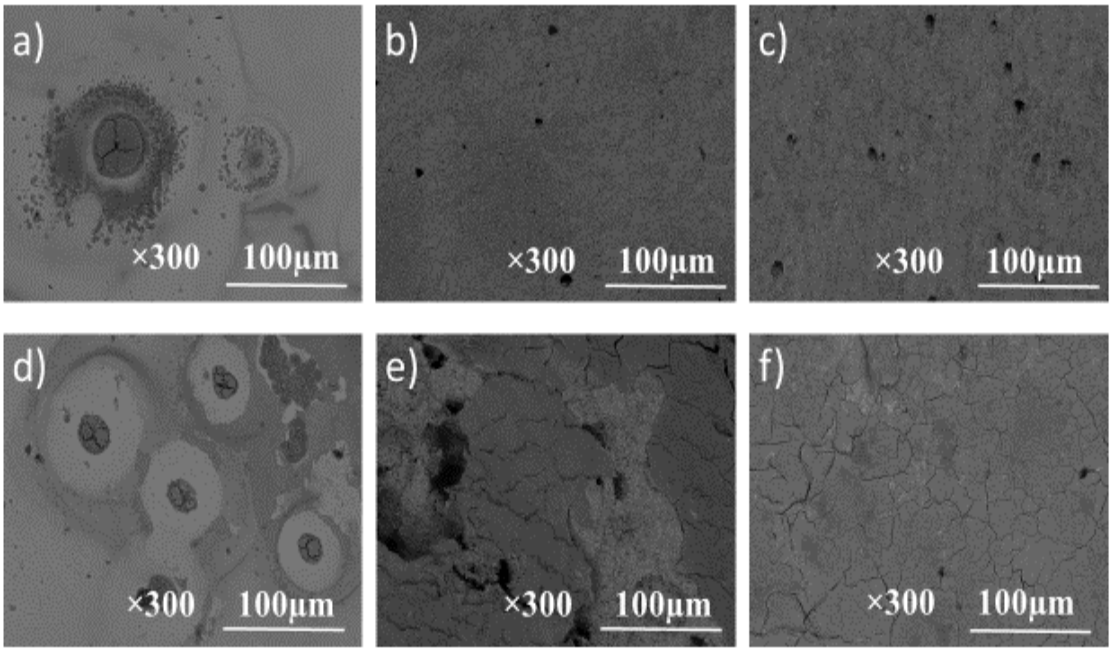

Figure 4.12. SEM micrograph of the corrosion product layers on the surfaces of the third group of samples at 25°C with (a) 0, (b) 10 and (c) 20 g/L NaCl and also at 75°C with (d) 0, (e) 10 and (f) 20 g/L NaCl

It can be observed that in Figure 4.12 (a) and (d), the presence of elemental sulfur on the top surface of samples affects formation of the corrosion products and onset of crack initiation, which seem to be accelerated by the increasing temperature [27]. Figure 4.12 (e) and (f) show that the addition of salt to the solution gradually increases the pitting tendency and disturbs the formation trend of passive layers or accelerates the cracking of passive layers, both of which result in a serious attack. Comparison of Figure 4.12 (b), (c), (e) and (f) indicates that the passivation process has more chance to occur at lower temperature, 25° C, where the corrosion product layer can easily repair itself and protect the sample surface from further corrosion. However, at higher temperature, 75°C, the

passive layer is more firm, which makes it difficult to completely dissolve the salts from the sample surface and repair itself, and so there would be more chance for micro- pits to grow through the corrosion product layer and break it down.

The EDS analysis of all the groups of samples with the highest chloride concentration at 75°C are presented in Figure 4.13.

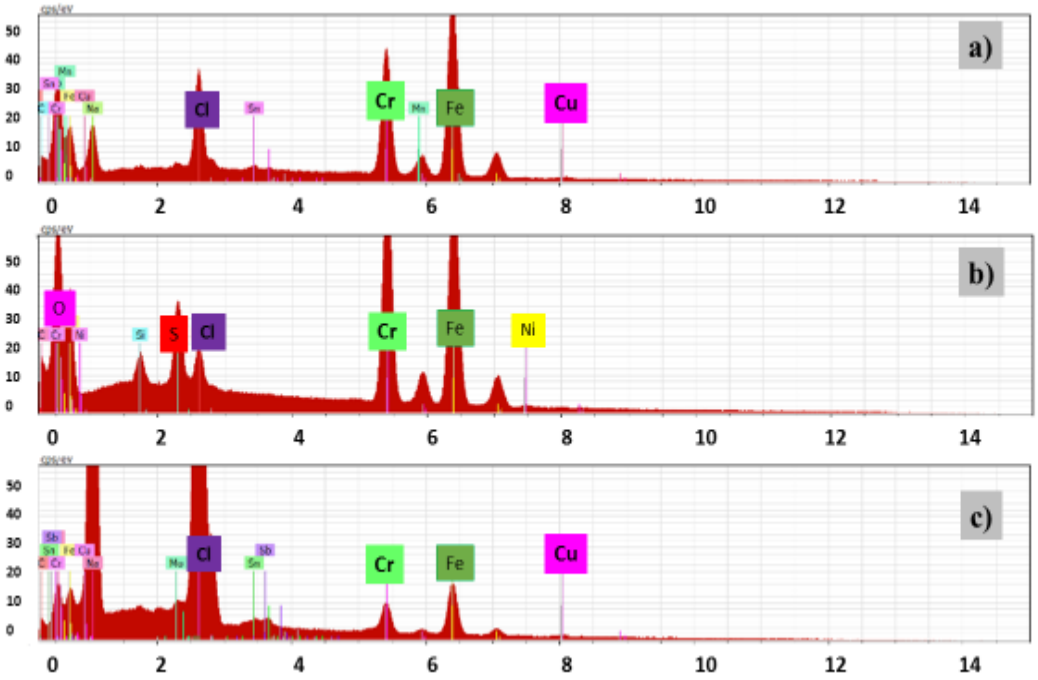

Figure 4.13. EDS analysis of the samples with the highest chloride concentration of (a) first, (b) second and (c) third groups at 75°C

For the samples covered with elemental sulfur, compared to the other two groups of samples, the stability of corrosion products significantly decreases, which could be due to the presence of a large amount of oxygen and chlorine on the sample surface. This decrease in the amount of precipitation particles on the surface might be also related to a

decrease of the scaling tendency, the precipitation rate of the scale being divided by the corrosion rate, of samples in the presence of elemental sulfur [12], [28]. In this case corrosion products are more able to dissolve into the solution instead of creating precipitation on the samples' surface. This fact also highlighted the important role of Cl^- ions in diminishing the formation trend of passive layers or accelerating the cracking of passive layers [16]. By initiation of cracks through the corrosion product layers, a higher corrosion rate will occur because of the increased mass transfer of species through the damaged area and propagation of the localized corrosion. Many locations were observed with pit penetration rates of up to 4.5 mm/year on the samples covered with elemental sulfur with 20 g/L NaCl in the solution at 75°C.

Linear polarization resistance (LPR) tests were also conducted to measure the exact corrosion rate of the samples. Figure 4.14 indicates the corrosion rate of each group of samples based on the added chloride concentration during each test. The results indicate that the corrosion resistance of 13Cr stainless steels is reduced with an increase of temperature, which is in accordance with the research by Miyata et al. [29] and Kermani et al. [30]. In addition it can be found that in the presence of elemental sulfur on a sample surface, as in the third group of samples, the effect of the increasing temperature is more significant than in other cases, Figure 4.14 (c). Also in this case it seems that the corrosion product layer at 25°C is more protective than the corrosion product layer formed at 75 °C due to the corrosion product's stability at the lower temperature [28]. Increasing the chloride concentration would gradually affect the transportation of aggressive species during the corrosion process and make an increase in the general

corrosion rate. It can also be found that the highest corrosion rates at 25 °C were observed in the presence of a FeS layer on the samples surfaces, which are 0.327, 0.403 and 0.576 by the addition of 0, 10 and 20 g/L NaCl respectively, Figure 4.14 (b). These results confirmed the observation of the previous section about the effect of chloride on the stability of a protective FeS layer. It is interesting that in the presence of elemental sulfur and with the addition of 10 g/L NaCl to the solution at 25°C, the corrosion rate of the sample is lower than all the other ones, which might be due to the passivation process on the sample surface, as discussed in the cyclic polarization section.

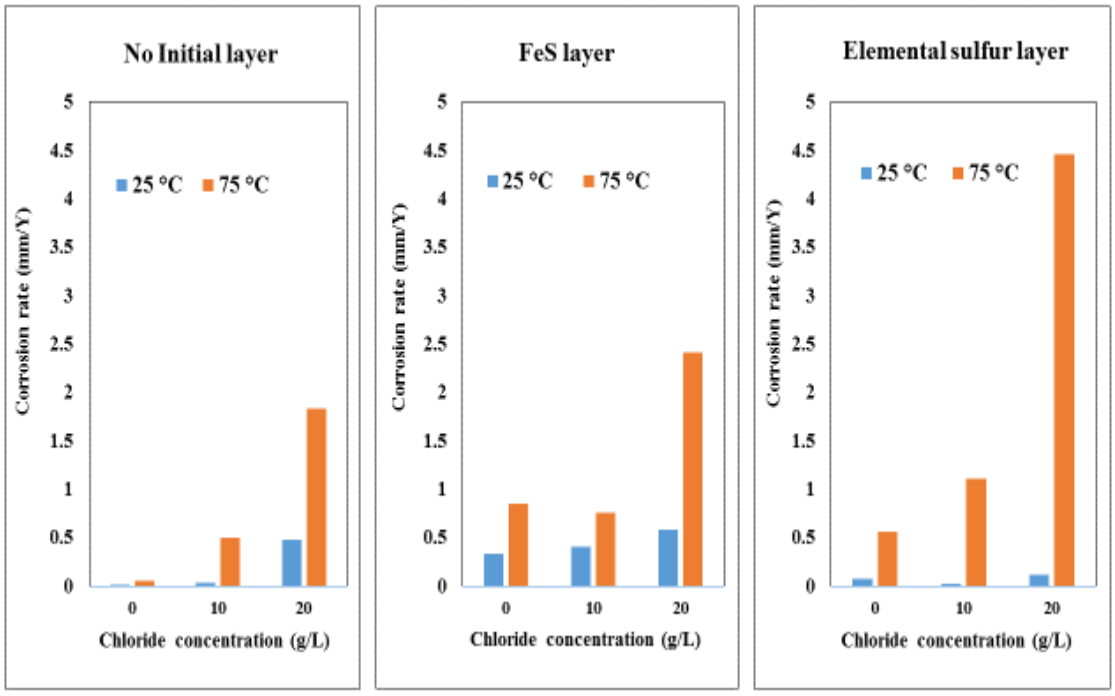

Figure 4.14. Corrosion rates of the samples with the highest chloride concentration of (a) first, (b) second and (c) third groups at 25 and 75°C

The surfaces of samples with the highest chloride concentration at 75°C were analyzed by atomic force microscopy (AFM) to investigate the surface texture as shown in Figure

4.15. According to the American National Standards Institute's B46.1 specification, surface texture is the repetitive or random deviation from the normal surface that forms the three-dimensional topography of a surface [31]. Surface texture is an important issue when the main interest is to understand the nature of surfaces. It also has a significant role in the functional performance of corrosion layers on the steel surface [32]. The roughness can be characterized by several parameters such as Roughness average (R_a) and Root mean square roughness (RMS). R_a is the arithmetic mean of the absolute value of the height of the surface profile while RMS is the mean squared absolute values of the surface roughness profile [32], which is more sensitive to peaks and valleys than the average roughness due to the squaring of the amplitude of its calculation.

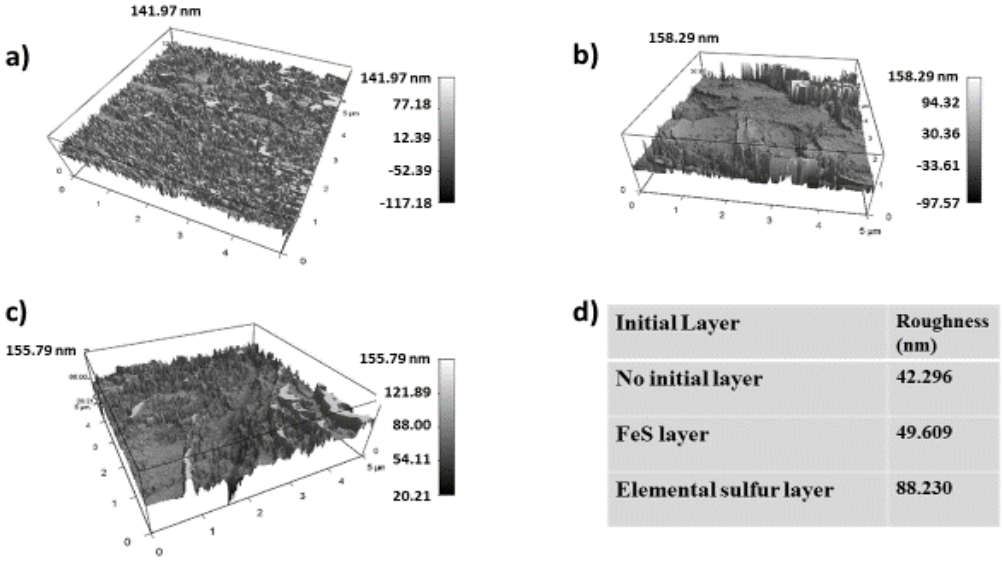

Initial Layer	Roughness (nm)
No initial layer	42.296
FeS layer	49.609
Elemental sulfur layer	88.230

Figure 4.15. AFM of the samples' surfaces with highest rates of corrosion, (a) sample with no initial layer, (b) sample with an FeS layer, (c) sample with the elemental sulfur layer and (d) the root mean square roughness of samples

The RMS values in Figure 4.15 (d) suggest that roughness of the surface slightly increases when the corrosion products which are underneath the existing layer lift and

damage the initial layer due to the internal stresses. This confirms the results of corrosion rates measurements and SEM analysis on the samples. Based on the results of AFM, it can be deduced that a rough surface with weak discontinuous corrosion product layers was formed on the surface of samples in the presence of elemental sulfur, Figure 4.15 (c), that has the highest roughness of 112.846 nm, and also the minimum of protection for the substrate surface, according to the results of LPR measurements of corrosion rates.

4.4. Conclusion

From the conducted electrochemical measurements and morphological analysis on 13% Cr steel, the following conclusions can be made:

In general, the presence of FeS and elemental sulfur deposited layers on the surface of 13% Cr steel will increase the corrosion rate, especially at a high temperature.

The role of temperature in corrosion mechanisms is more significant than the role of chloride concentration in the presence of a deposited FeS layer on the 13% Cr steel surface.

In the presence of deposited elemental sulfur, the roughness of the corrosion product layers is higher compared to that in the presence of deposited FeS layer or in the case of no initial deposited layer.

In the presence of deposited elemental sulfur, the scaling tendency on the sample surface significantly decreases compared to scaling in the presence of deposited FeS layer or cases with no initial deposited layer.

4.5. References

[1] “Corrosion resistant high Cr steel for oil and gas wells,” JFE Technical report, No. 18, 2013.

[2] “Development of sour-resistant 13%Cr oil-country tubular goods with improved CO_2-corrosion resistance", Nippon Steel Technical Report, No. 72, 1972.

[3] A. Turnbull and A. Griffiths, “Corrosion and Cracking of Weld able 13 Cr Martensitic Stainless Steels – A Review,” Technical report of national physical laboratory Teddington, UK, 2002.

[4] D. Sidorin, D. Pletcher, and B. Hedges, “The electrochemistry of 13% chromium stainless steel in oilfield brines,” Electrochim. Acta, vol. 50, pp. 4109–4116, 2005.

[5] N. Chermat-aourasse and R. Kesri, “Corrosion-Electrochemical Behavior of 13 % Chromium (Cr) Martensitic Stainless Steel in Hydrochloric Acid (HCl) Solutions,” Corros. Prot. Mater., vol. 43, no. 4, pp. 372–380, 2007.

[6] H. Marchebois and H. E. L. Alami, “Sour service limits of 13% Cr and super 13% Cr stainless steels for OCTG: effect of environmental factors,” in NACE Corrosion Conference and expo, Atlanta , USA, 2009, no. 9084, pp. 1–19.

[7] H. Fang, D. Young, and N. Srdjan, “Elemental sulfur corrosion of mild steel at high concentration of sodium chloride,” in 17th international corrosion Congress, Los Vegas, USA, 2009, vol. 2592, pp. 1–16.

[8] J. Bojes, J. Lerbscher, W. Wamburi, and C. Dilley, “Elemental sulfur in 3- phase sour gas systems- Is condensate really your ally?” in Northern area western conference, Calgary, Canada, 2010, pp. 1–22.

[9] H. Fang, “Investigation of localized corrosion of carbon steel in H_2S environments,” PhD thesis, Ohio University, Ohio, USA, 2012.

[10] R. Steudel, “Mechanism for the formation of elemental sulfur from aqueous sulfide in chemical and microbiological desulfurization processes,” Ind. Eng. Chem. Res., vol. 35, no. 4, pp. 1417–1423, 1996.

[11] B. N. Brown, “The Influence of Sulfides on Localized Corrosion of Mild Steel,” PhD thesis, Ohio university, Ohio, USA, 2013.

[12] D. Rickard, “Kinetics of FeS precipitation: Part 1. Competing reaction mechanisms,” Geochim. Cosmochim. Acta, vol. 59, no. 21, pp. 4367–4379, 1995.

[13] H. Nose, K, Asahi, “Effect of microstructure on corrosion resistance of corrosion resistance of pipeline,” Int. J. Microstruct. Mater. Prop., vol. 6, 2000.

[14] T. Evans, P. Nice, M. Schofield, and K. Waterton, “Corrosion behavior of carbon steel, low alloy steel and CRA’s in partially deaerated seawater and comingled produced water,” NACE Int. Corros., vol. 4139, 2001.

[15] H. Zhang, Y. L. Zhao, and Z. D. Jiang, “Effects of temperature on the corrosion behavior of 13%Cr martensitic stainless steel during exposure to CO_2 and chloride environment,” Mater. Lett. J., vol. 59, pp. 3370–3374, 2005.

[16] Z. F. Yin, X. Z. Wang, L. Liu, J. Q. Wu, and Y. Q. Zhang, “Characterization of Corrosion Product Layers from CO_2 Corrosion of 13%Cr Stainless Steel in Simulated Oilfield Solution,” J. Mater. Eng. Perform. vol. 20, pp. 1330–1335, 2011.

[17] L. Khaksar, G. Whelan, and J. Shirokoff, “Electrochemical and microstructural analysis of FeS films from acidic chemical bath at varying temperatures, pH, and Immersion Time,” Int. J. Corros., vol. 1025261, 2016.

[18] L. Khaksar and J. Shirokoff, “Effect of Elemental Sulfur and Sulfide on the Corrosion Behavior of Cr-Mo Low Alloy Steel for Tubing and Tubular Components in Oil and Gas Industry,” Materials (Basel). vol. 10, no. 4, p. 430, 2017.

[19] M. Saeed Akhtar, A. Alenad, and M. Azad Malik, “Synthesis of mackinawite FeS thin films from acidic chemical baths,” Mater. Sci. Semicond. Process, vol. 32, pp. 1–5, 2015.

[20] H. Fang, B. Brown, D. Young, and S. Nesic, “Investigation of elemental sulfur corrosion mechanisms,” NACE Int., pp. 1–13, 2011.

[21] D. Enos and L. Scribner, “The potentiodynamic polarization scan,” Solartrion technical report, No. 33, UK, 1997.

[22] ASTM-G5-82, “Standard reference method for making potentiostatic and potentiodynamic anodic polarization measurements.” 1982.

[23] “Basics of Corrosion Measurements,” Princeton applied research technical report, Illinois, USA, 1980.

[24] D. Silverman, “Tutorial on cyclic potentiodynamic polarization technique,” in NACE international conference, San Diego, USA, 1998.

[25] D. Brondel, R. Edwards, A. Hayman, D. Hill, and T. Semerad, “Corrosion in the Oil Industry,” Oil filed review journal, pp. 4–18, 1994.

[26] D. MacDonald, B. Roberts, and J. Hyne, “The Corrosion of Carbon Steel by Wet Elemental Sulfur,” Corros. Sci., 1978.

[27] T. Laitinen, “Localized corrosion of stainless steel in chloride, sulfate, thiosulfate containing environment,” Corros. Sci., vol. 42, pp. 421–444, 2000.

[28] W. Sun, S. Nešić, and S. Papavinasam, “Kinetic of iron sulfide and mixed iron sulfide/carbonate scale precipitation in CO_2/H_2S corrosion,” NACE Int., vol. 6644, pp. 1–26, 2006.

[29] Y. Miyata, Y. Yamane, O. Forukimi, H. Niwa, and K. Tamaki, “Corrosion of new 13% Cr stainless steel OCTG in severe CO_2 environment,” NACE Int., 1995.

[30] M. Kermani, G. Weighhill, T. Pendlington, and G. Elliot, “Operational experience of using 13%Cr tubular steels,” NACE Int., 1995.

[31] D. K. Cohen, “Introduction to ASME B46.1-2009,” Michigan metrology technical report, Michigan, USA, 2011.

[32] R.R.L. De Oliveira, D.A.C. Albuquerque, T.G.S. Cruz, F.M. Yamaji and F.L. Leite (2012). Measurement of the Nanoscale Roughness by Atomic Force Microscopy: Basic Principles and Applications, Atomic Force Microscopy - Imaging, Measuring and Manipulating Surfaces at the Atomic Scale, Dr. Victor Bellitto (Ed.), ISBN: 978-953-51-0414-8, InTech, Available from:

http://www.intechopen.com/books/atomic-force-microscopy-imaging-measuring-and-manipulating-surfaces-at-the-atomic-scale/measurement-of-the-nanoscale- roughness-by-atomic-force-microscopy-basic-principles-and-applications InTech

5. DEVELOPMENT OF ANALYTICAL MODELS FOR PREDICTION OF CORROSION RATE OF 13% CHROMIUM STEEL EXPOSED TO DIFFERENT ENVIRONMENTAL CONDITIONS

Preface

A version of this manuscript is accepted for publication in the Global Journal of Engineering Science and Researches, (GJESR). I am the primary author of this paper, along with the co-authors, John Shirokoff. I conducted the literature review and proposed the outline of the experiments, analysis procedure and modeling methods. I conducted most of the experiments and corrosion measurements. I've conducted the modeling part and prepared the first draft of the manuscript and subsequently revised the manuscript based on the co-author's feedbacks and also the initial feedbacks from the journal reviewers. The co-author John Shirokoff helped in analyzing the final results, and contributed in preparing, reviewing and revising the manuscript.

Abstract

This chapter, by experimentally investigating the influence of different corrosion product layers on the corrosion resistance of 13% chromium steel in HCl solution, describes the level of the corrosion rates induced by deposited iron sulfide and elemental sulfur layers

on the steel surface. In order to facilitate the experiment numbers, three analytic prediction methods, which are the optimal solution, curve fitting and artificial neural network, were applied to predict the corrosion rates of 13% chromium steel. Results showed that the fitness between measured and predicted corrosion rates by curve fitting indicates a good correlation between experiments and developed model, however, the minimum deviation from the measured data was obtained with artificial neural network model which is insignificant compared to the deviation of the two other models.

Keywords

13% chromium steel, Neural Network, Iron sulfide, Elemental sulfur, Corrosion

5.1.Introduction

Corrosion, either sweet corrosion generated by CO_2 or sour corrosion generated by H_2S [1], is realized as a main issue that the oil and gas industry are faced with. During the production stage, pipelines and other equipment will be corroded due to the reactions between CO_2, H_2S and Fe [2]. Pipelines designed to withstand 50 years of operation, however, under a “worst case” general corrosion rate may fail after a few months of operation due to localized corrosion. Loss of containment from a pipeline failure is a costly event as it would cause an emergency shutdown in the production of oil and gas, an emergency repair of the pipeline, and probably an environmental cleanup at the leak site [3]. In an effort to minimize pipeline failures and loss of containment, companies around the world in the oil and gas industry sponsor research programs focused on better prediction methods and better mitigation methods of localized corrosion. Normally,

prediction of these two kind of corrosion, in order to estimate the equipment lifetime, are not a simple step because the general understanding of the corrosion mechanism, especially in a certain environmental conditions, is usually below the required level to predict the accurate corrosion rate [4]. Depending on the environmental conditions, such as temperature and pH, the rate of these reactions will vary which determine the rate of corrosion process. In the literature, a number of research studies the prediction of the corrosion rate in sweet oilfields that can be classified in three general groups: mechanistic, semi-empirical and empirical models [2], [4], [5]. Among these models, by utilizing a large number of experimental CO_2 corrosion data, it was shown that the empirical model, especially one based on the Artificial Neural Network (ANN), has the highest accuracy of corrosion rate estimation, while the lowest accuracy belongs to the mechanistic model [4].

In the case of sour corrosion, it is well known that the corrosion products such as iron sulfide, formed on the steel surface immediately after a small concentration of H_2S is introduced into the system which determine the corrosion pattern with regard to the environmental conditions [6], [7]. Generally it was found that formation of corrosion products on the steel surface significantly affect the estimation of upcoming corrosion process and consequently the prediction of final corrosion rate [8].To estimate the corrosion induced by sour corrosion products, despite many studies and proposed mechanistic models that have appeared in the literature, there is still lack of a reliable and accurate predictive model which can predict the corrosion rate in the presence of H_2S corrosion products on the steel surface [9]–[11], [6]. The most recent research in this area

showed that the developed corrosion models by ANN have indicated the highest accuracy among all other predicted models [1], [12], [13].

The corrosion of 13 % chromium steel, one of the most common martensitic steel in oil and gas applications, in either sweet or sour condition, have been investigated from various aspects [14]–[16]. According to those investigations, one of the most effective factors in the corrosion process in oil and gas pipelines and especially in the sour ones, is the presence of deposited elemental sulfur produced by the H_2S corrosion process [17]. It is known from prior research that the presence of dry elemental sulfur in contact with carbon steel is not considered as a corrosion threat to steel; however, by adding water to the system, the corrosion process may be dramatically accelerated [18]. A literature review has shown that the nature of H_2S corrosion product layers controls the kinetics of this corrosion process from both phase type and morphology perspectives [6].

As aforementioned issues above, in this study we are motivated to propose several analytic approaches to predict the corrosion rate of 13% chromium steel in a simulated sour environment by considering the presence of various sour corrosion product layers on the surface of steel, which can be named as optimal solution, curve fitting and ANN. In this way, the optimal solution assumes the measured corrosion rate as an output of an initial function, therefore, solver strives to find appropriate coefficients for the initial function to minimize its error, then this initial function accuracy is improved and can be used for estimation purposes [19]. In the next proposed model, which is based on curve fitting, the measured corrosion rates in 2-D space plotted and curve fitting utilized to capture a polynomial. Thus, the obtained polynomial in proportion to input can estimate

the corrosion rates. The finial-applied approach in this study is ANN. An ANN is an information-processing pattern that is inspired by the brain's processing information system. [20]. The utilized pattern in ANN is composed of various layers, which can be classified in the following layers: input, hidden and output layers. Hidden layers are always formed from a number of hidden neurons whose output is connected to the inputs of other neuron and is therefore not visible as a network output. Typically ANN comprise some form of learning rules that mutate the weights of the connections between the layers. In the following section, the capability of each model in estimation of the corrosion rates based on environmental conditions will be discussed.

5.2. Material and methods

5.2.1. Material and sample preparation

According to industrial partner's request, the corrosion samples were made from conventional 13% Cr steel. Table 5.1 indicates composition of grade 420 chromium stainless steel. The working electrode was machined from the parent material into cylinders having dimensions of approximately 9 mm length and 9 mm diameter. It should be noted, prior to perform the experiments all specimens were polished with Coated Abrasive Manufacturers Institute (CAMI) grit designations 320, 600, 1000 corresponding to average particle diameters 36.0, 16.0, and 10.3 microns and finally 6 micron grit silicon carbide paper, and then cleansed with deionized water until a homogenous surface was observed. Thereafter, to avoid oxidation, the specimens were quickly dried by using cold air.

Table 5.1. The chemical composition of conventional 13% Cr stainless steel grade 420

C	Cr	Mn	Si	P	S	V	Fe
0.15	12	0.22	0.3	0.014	0.0035	0.041	Bal.

5.2.2. Corrosion measurements

To investigate the effect of different corrosion product layers on electrochemical behavior of conventional 13% Cr steel, three series of experiments with consideration of different environmental conditions were conducted. In the first series of experiments the corrosion behavior of each sample was analyzed while its top surface was exposed into the electrolyte solution, 0.01 M hydrochloric acid, without any initial cover on it (i.e. no initial corrosion product layer), with different environmental conditions. Table 5.2 listed the experimental conditions in first series of the experiments.

Table 5.2. The experimental conditions in first series of the experiments

Series #1 Sample No	1	2	3	4	5	6	7	8	9	10	11	12
T (◦C)	25	25	25	75	75	75	25	25	25	75	75	75
NaCl (g/L)	0	10	20	0	10	20	0	10	20	0	10	20
pH	2	2	2	2	2	2	4	4	4	4	4	4

In the second series of the experiments, behavior of corrosion was analyzed while the working electrode were initially covered by a thin iron sulfide corrosion layer (i.e. FeS

layer) synthesized by an acidic chemical bath [21]. The mechanism of FeS formation in this acidic bath is composed of first the slow release of iron and sulfur ions within solution and then the deposition of these ions on the alloy surface. The iron and sulfur ions are provided from iron (II) chloride and thioacetamide, respectively. The formation of FeS film from this acidic bath is dependent on whether the deposition rate of the ionic product of iron and sulfur is higher than solubility of FeS or not. Adding urea to the solution adjusted the balance between hydrolysis and deposition. The proposed reactions for this mechanism is described as follows [22]:

$$FeCl_2 \rightarrow Fe^{2+} + 2\ Cl^- \quad (5.1)$$

$$CH_3CSNH_2 + H_2O \leftrightarrow S^{2-} + CH_3CONH_2 + 2H^+ \quad (5.2)$$

$$CO\ (NH_2)_2 + H_2O \leftrightarrow 2NH_3 + CO_2 \quad (5.3)$$

$$NH_3 + H_2O \leftrightarrow NH_4^+ + OH^- \quad (5.4)$$

$$Fe^{2+} + S^{2-} \leftrightarrow FeS \quad (5.5)$$

Finally, the overall reaction can be written as:

$$Fe^{2+} + CH_3CSNH_2 + CO\ (NH_2)_2 + 2H_2O \rightarrow FeS + CH_3CONH_2 + 2NH_4 + CO_2 \quad (5.6)$$

This second series enabled the estimation of effect of deposited FeS layer on electrochemical and corrosion behavior of 13% Cr stainless steel in presence of various chloride concentration. Table 5.3 presents the experimental conditions in the second series of the experiments.

At the last series of experiments, the electrochemical behavior was analyzed while the electrode was initially covered by sublimed elemental sulfur 99.9999% (ACROS) [23]. This third series enabled the estimation of effect of deposited elemental sulfur on electrochemical and corrosion behavior of 13% Cr stainless steel in presence of various chloride concentrations. Table 5.4 indicates the experimental conditions in third series of the experiments.

Table 5.3. The experimental conditions in second series of the experiments

Series #1 Sample No	1	2	3	4	5	6	7	8	9	10	11	12
T (◦C)	25	25	25	75	75	75	25	25	25	75	75	75
NaCl (g/L)	0	10	20	0	10	20	0	10	20	0	10	20
pH	2	2	2	2	2	2	4	4	4	4	4	4

Table 5.4. The experimental conditions in third series of the experiments

Series #1 Sample No	1	2	3	4	5	6	7	8	9	10	11	12
T (◦C)	25	25	25	75	75	75	25	25	25	75	75	75
NaCl (g/L)	0	10	20	0	10	20	0	10	20	0	10	20
pH	2	2	2	2	2	2	4	4	4	4	4	4

During this study, corrosion experiments were conducted in a multi-port glass cell with a three electrodes setup at atmospheric pressure based on the ASTM G5-94 standard for potentiodynamic anodic polarization measurements [21]. Linear polarization resistance

(LPR) technique was used to record the general corrosion rates after each experiments. The applied sweep rate for this measurements was 0.5mV/s. An Ivium Compactstat Potentiostat monitoring system was used to perform electrochemical corrosion measurements and record the final corrosion rates. The immersion time was 24 hours for each experiment, however, prior to start of each test the sample was immersed in the solution for 55 minutes accordance with ASTM G5-82 [21]. The pH was adjusted 2 and 4 by adding deoxygenated hydrochloric acid. A graphite rod was used as the counter electrode (CE) and saturated silver/silver chloride (Ag/AgCl) was used as the reference electrode (RE) and as mentioned in material preparation section, the conventional 13% Cr steel samples was used as working electrodes (WE). Figure 5.1. illustrates our utilized experimental set up for corrosion measurements.

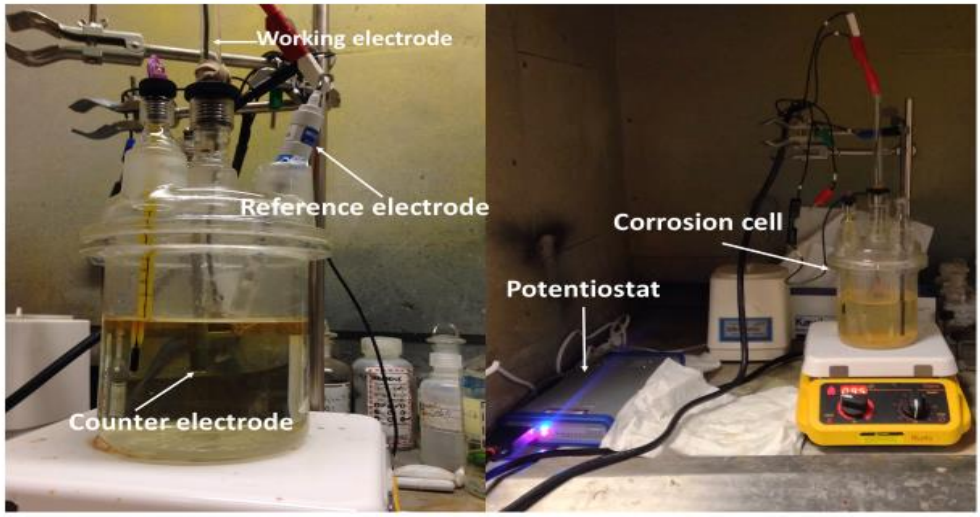

Figure 5.1. The utilized experimental set up for corrosion rate measurements

5.2.3. Optimal solution

The optimization was carried out using Microsoft Excel Solver software. Solver is part of a suite of commands with what-if analysis tools. Solver works with a group of cells that are related, either directly or indirectly, to the objective function equation in the target cell. Solver adjusts the values in the changing cells, called the adjustable cells to produce the result. Constraints are applied to restrict the range of values of the variables used in the objective function [19]. Microsoft Excel Solver tool uses the Generalized Reduced Gradient (GRG) non-linear optimization code to develop the optimal function [24].

5.2.4. Curve fitting

The polynomial curve fitting is a common task for data analysts in many fields of material science [25], [26]. However widespread application is not common largely because the use of statistics requires specialist knowledge, and no reference standards exist. The standard method to fit a curve to data is to use the least squares method [27]. In this study, due to nonlinearity of measured corrosion rates, the coefficients of a polynomial function were founded out by curve fitting method. In this regard, the measured corrosion rates were plotted and obtained data from the polynomial function were fitted to the measured results. The typical form of the utilized polynomial function can be identified as:

$$y=m_0 + m_1 * x + m_2 * x_2 + m_3 * x_3 +...+ m_9 * x_9. \quad (5.7)$$

Where m is the coefficients of a polynomial function and x is the independent variable.

5.2.5. Neural networks modeling

The most important stage in the creation of a network which enables the transfer of the input data into the output data, is the learning stage [28]. At this stage the networks parameters such as the network type, training algorithm and the number of neurons in the hidden layer of the network are modified to fit the experimental data. The number of input variables from experimental step will determine the number of input layer or in another words the number of input neurons and the number of output layers also come from the number of output variables in experimental step as well [29]. Designation of number of hidden layers between input and output layers is usually one of the most challenging part prior to create the networks because the increased number of hidden layers would not necessarily increase the networks efficiency and even may unfortunately decrease the speed of computing and make the networks much more complex. Therefore, the final efficiency of the networks would be directly affected by the interaction between neuron transfer functions and typical training patterns [4]. Further information regarding the ANN can be found in [20], [30]. Figure 5.2 outlines our utilized configuration to predict the single output, corrosion rate, based on the four input layers: corrosion product layer, pH, temperature and salt concentration, through the five hidden layers.

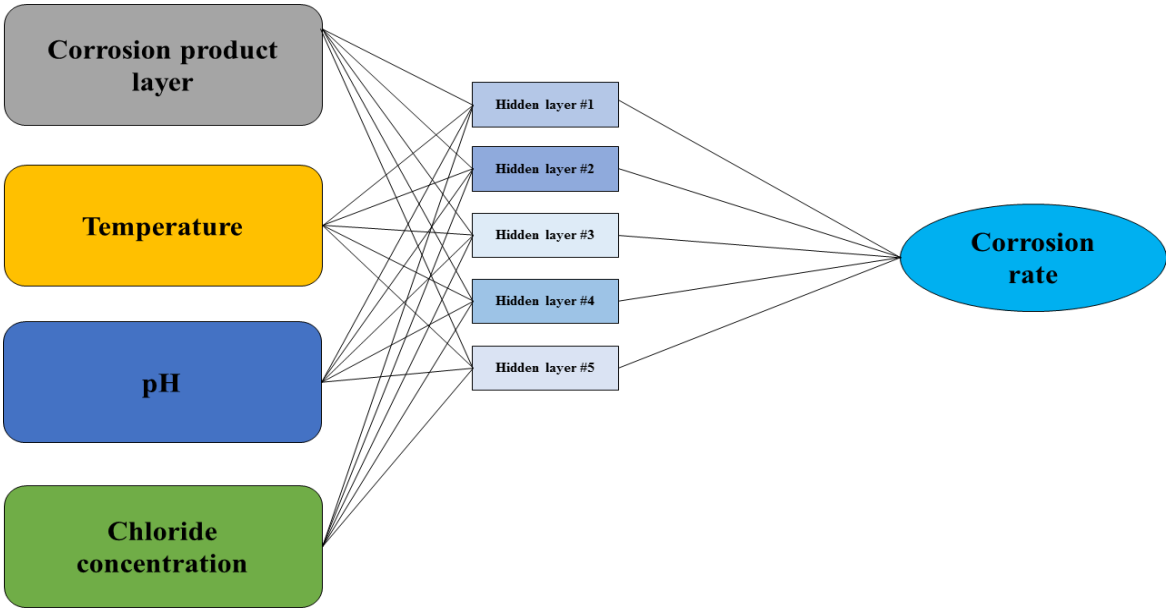

Figure 5.2. The architecture of ANN used for predicting corrosion rate

The designed network was trained by Levenberg-Marquardt algorithm, which is highly fast in computation, however, to reach the maximum performance it does require more memory in compared to the other available training algorithms [31]. Table 5.5 presents the specification of utilized ANN parameters for corrosion rate prediction purposes.

Table 5.5. The specification of utilized ANN parameters

Network Parameters	**Specification**
Hidden layer size	a) 95, b) 85, c) 80, d) 40, e) 30
Network type	Feed-Forward
Transfer function used at network layers	Tangential-sigmoidal
Performance function	Least mean of squared errors
Training algorithm	Levenberg-Marquardt

5.3. Results and Discussion

5.3.1.Corrosion measurements

The general Corrosion Rates (CR) from Linear Polarization Resistance (LPR) measurements are given in Table 5.6. According to this table, for the first group of samples, with absence of initial corrosion layer on top, it is clear that increase of temperature and chloride concentration increased amount of the corrosion rates, however, with increasing pH from 2 to 4 the corrosion rate slightly decreased which, might be related to the kinetics of precipitation and facilitate corrosion product layers formation, therefore, decreasing the corrosion rates expected [2]. For the second group of samples that were covered with a thin FeS layer, the corrosion rates are generally higher than the first group of samples. It is worth mentioning that similar to the first group of samples (i.e. with no initial corrosion layer) increase of temperature and chloride concentration increased the corrosion rates while increase of pH decreased the corrosion rates. In addition, it can be highlighted that the highest corrosion rate, 4.46 mm/ year, was observed in the presence of elemental sulfur at 75◦C after addition of 20 g/L NaCl to the solution at pH 4.

Table 5.6. The measured corrosion rates (CR) under different environmental conditions

Series #	T (◦C)	NaCl (g/L)	pH	CR (mm/y)	Series #	T (◦C)	NaCl (g/L)	pH	CR (mm/y)	Series #	T (◦C)	NaCl (g/L)	pH	CR (mm/y)
1	25	0	2	0.057	2	25	0	2	0.472	3	25	0	2	0.301
1	25	10	2	0.169	2	25	10	2	0.705	3	25	10	2	0.246
1	25	20	2	0.744	2	25	20	2	0.797	3	25	20	2	0.524
1	75	0	2	0.263	2	75	0	2	0.989	3	75	0	2	0.908
1	75	10	2	0.709	2	75	10	2	0.901	3	75	10	2	2.713
1	75	20	2	2.078	2	75	20	2	2.879	3	75	20	2	4.987
1	25	0	4	0.009	2	25	0	4	0.327	3	25	0	4	0.077
1	25	10	4	0.028	2	25	10	4	0.403	3	25	10	4	0.019
1	25	20	4	0.476	2	25	20	4	0.576	3	25	20	4	0.113
1	75	0	4	0.056	2	75	0	4	0.849	3	75	0	4	0.554
1	75	10	4	0.498	2	75	10	4	0.756	3	75	10	4	1.108
1	75	20	4	1.828	2	75	20	4	2.406	3	75	20	4	4.46

5.3.2. Optimal solution

From Table 5.6, one can see that the final corrosion rate is sensitive to all experimental parameters, i.e. the corrosion product layer, temperature, pH and chloride concentration. The complex and obscure mechanism of each parameter affects the results in microscopic and macroscopic levels, makes algebraic expressions incapable of predicting the rate of corrosion in this study. Thus, the corrosion rate is assumed to be a transcendental function of all the experimental parameters that account for the sensitivity of the

corrosion rate to the all input parameters and their interactions. The initial utilized function is given by:

$$C_R = L\,(F + a)^m\,(T + b)^n\,(P + c)^q\,(C + d)^r \quad (5.8)$$

Where F donates the film parameter, T is temperature parameter, P is the pH parameter and C is the chloride concentration parameter. L, a, m, b, n, c, q, d and r are the user defined coefficients, whose values obtained from the optimization procedure.

The goal of optimization procedure is to minimize the sum of squares of residuals. By choosing the initial value of 1 for L, m, n, q and r and 0 for a, b, c and d the model prediction for corrosion rate at each experiment is calculated and the difference between the model result and the experimental result at each experiment is recorded. The sum of squares of residuals is:

$$SS_{res} = \sum_i (y_i - f_i)^2 \quad (5.9)$$

Where y_i is the experimental corrosion rate and f_i is the predicted corrosion rate. The solver toolbox then changes the values of L, a, m, b, n, c, q, d and r to minimize the magnitude of SS_{res}. This procedure is carried out repeatedly to find the optimized values for all the coefficients simultaneously.

5.3.3. Curve fitting

In order to utilize curve fitting method for prediction purposes, we need to plot inputs and outputs in two dimension. Since the number of inputs (i.e. corrosion product layer, temperature, pH and chloride concentration) is not identical to output (i.e. Corrosion

Rate), therefore, the initial input function in terms of the 4 input parameters defined. This initial function, which is labeled as X_n, is expressed by:

$$X_n (\alpha, \beta, \gamma, \lambda) = \alpha + \beta/10 + \gamma^2 + (\gamma\lambda + 1) \quad (5.10)$$

where index of *n* is the number of experiment, α is normalized corrosion product layer parameter, which identified with three discrete values of 1, 10 and 20 that stand for the first, second and third series of experiments, respectively. β is the normalized temperature parameter in Celsius, which varied between 25 to 75 ◦C, γ is the normalized pH parameter, which is varied between 2 to 4 and λ is normalized chloride concentration parameters, which is varied between 0 to 20 g/L. Thus, thanks to defined polynomial above, input value proportion to corrosion rate calculated and equation (5.11), which is defined by curve fitting method, it can be utilized for corrosion rates prediction:

$$CR= -0.006* X_n^{\,2} + 0.136* X_n - 0.025 \quad (5.11)$$

Different degrees of polynomial from 2 to 8 were tested to find the best-fitted model. With regard to the values of R-square which indicates the closeness of the data to the fitted regression line, the best fit was obtained with polynomial of degree two. In this case the measured R-squared is 0.78 which is relatively high and so it can be assumed that the fitness of the model with the experiments is relatively reasonable. Figure 5.3. shows the curve of p (x) in MATLAB®.

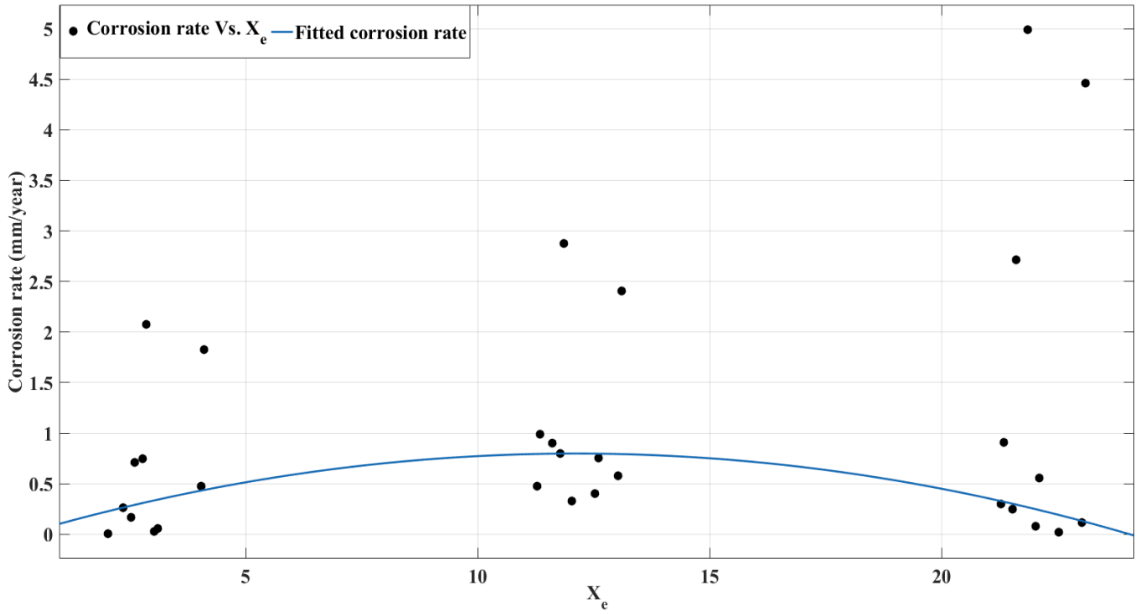

Figure 5.3. The developed model by curve fitting in MATLAB®

As displayed in Figure 5.3 the model was not able to fit with measured data in some areas, for instance, where the corrosion rates are higher than 1 mm/y. Thus, the model cannot be considered as an accurate model and still has weakness in prediction of the data.

5.3.4. Artificial neural networks

After determining the optimum ANN structure, and prior to the process of training, the whole dataset of 36 input-output pairs was randomly divided into the 30 training data set, white cell in Table 5.6 and the six validation data set, gray cells in Table. 5.6. Figure 5.4 and 5.5 demonstrate the measured values of corrosion rates and the values predicted by technique for the training and validation data set, respectively. It can be seen that in both two data sets a good prediction was achieved.

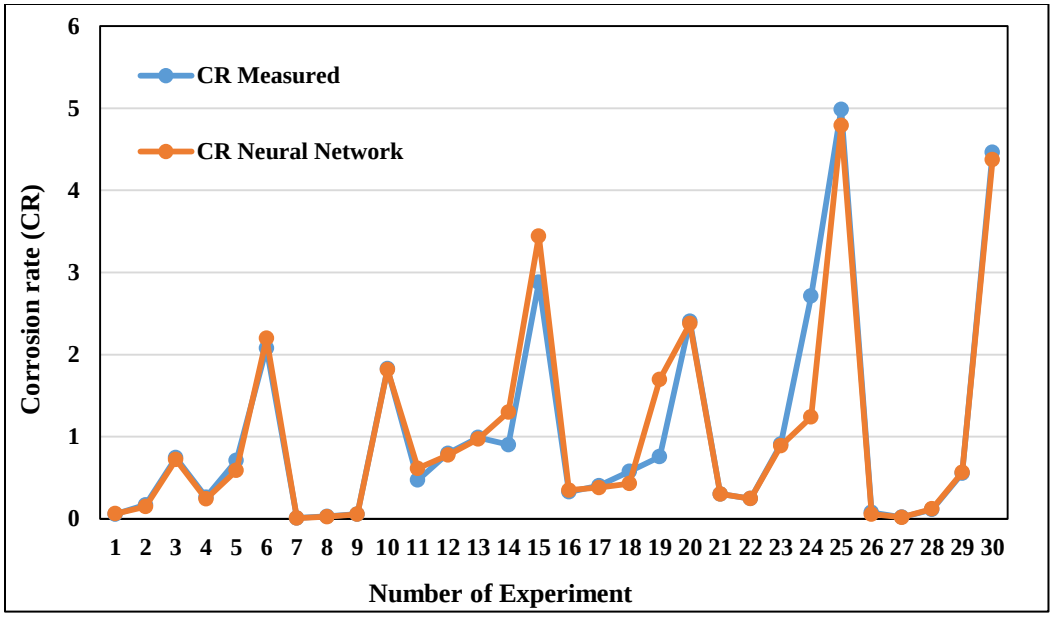

Figure 5.4. The corrosion rate (CR) amount based on measured and predicted by the ANN for the training dataset

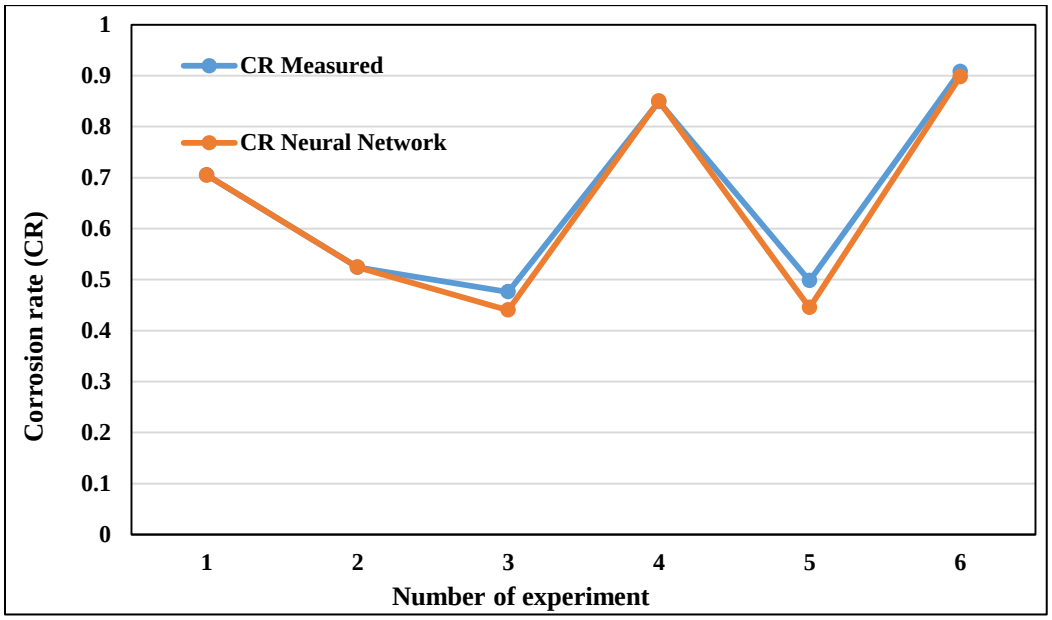

Figure 5.5. The corrosion rate (CR) amount based on measured and predicted by the ANN for the validation data set

Detailed error analysis for the training and validation datasets is presented in Table 5.7, for corrosion rates.

Table 5.7. Error analysis for the training and validation datasets

Error analysis of	Training data set	Validation data set
Maximum error	55.5%	11.8%
Minimum error	0.2%	0.06%
Average	15.5%	3.5%
Standard deviation	1.2%	0.2%

It can be concluded from Table 5.7 that the developed model has a low percentage of error for both set of training and validation datasets, which indicates the significant fitness of the model with the measured data. The small values of standard deviation also confirmed the accuracy of the predictive model.

5.3.5. Comparison of three models

Three models for prediction of corrosion rate were developed. Models are designed to predict the values of corrosion rate in different environmental conditions including various corrosion product layers, temperature, pH value and chloride ions concentration. In order to investigate the performance of each proposed model, we selected 6 data sets (i.e. utilized validation data set for the ANN computation) and their predicted corrosion rate by the optimal solution, curve fitting and ANN techniques are reported in Table 5.8. Furthermore, amount of the predicted corrosion rate error in reference to measured once demonstrated.

Table 5.8. Performance of each proposed model for validation data set

Case	CR measured	CR Optimal solution	CR curve fitting	CR neural network	%Error Optimal solution	%Error Curve fitting	%Error neural network
1	0.705	0.2697	0.795	0.7046	61.74	12.76	0.05
2	0.524	0.8659	0.2748	0.5243	65.25	47.5	0.05
3	0.476	0.2678	0.4313	0.4402	43.74	8.82	8.13
4	0.849	0.3977	0.7978	0.8502	0.3977	6.03	0.14
5	0.498	0.6769	0.3911	0.4453	35.9	21.4	11.83
6	0.908	0.702	0.320	0.8978	2.7	64.7	1.13
Average	0.66	0.53	0.50	0.64	34.95	26.86	3.55

As it is indicated in table above, the average of the error for the model developed by ANN is significantly low compared to the other two models.

Deviations from measured results are given in Figure 5.6. Maximal deviation of results predicted with optimal solution and curve fitting models compared to measured results is 0.45 and 0.58 mm/y in absolute terms, obtained in 4th and 6th instance respectively, while maximal deviation of results predicted with ANN equals 0.05 mm/y, obtained in 5th instance.

Comparison of the deviation of each model from the measured data indicates that the model developed by the ANN has the minimum general deviation and is able to predict the corrosion rate with the highest accuracy among the other models.

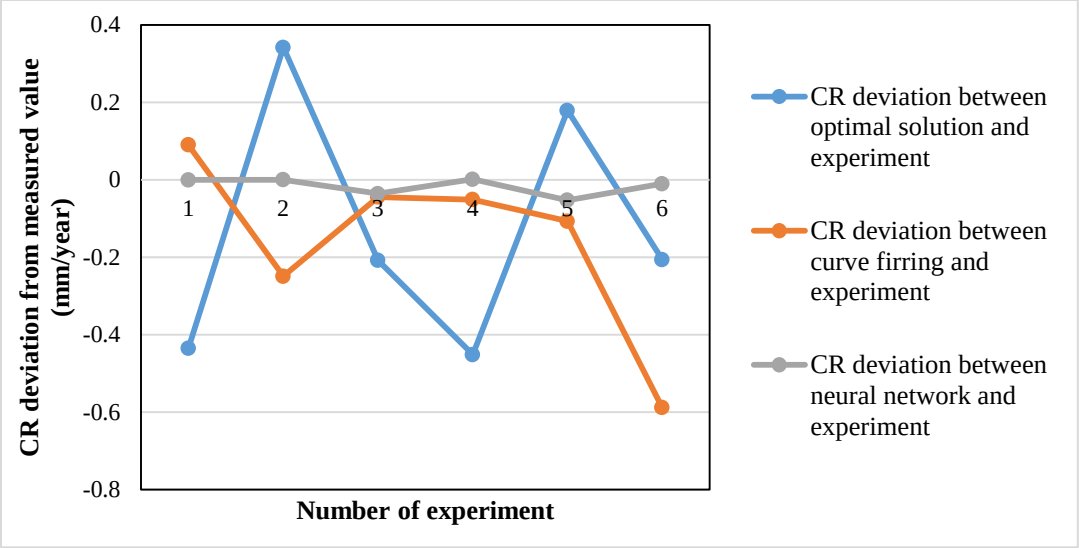

Figure 5.6. Analysis of corrosion rate (CR) difference between values obtained with models and measured results

5.4. Conclusion

From the conducted electrochemical measurements on 13% Cr steel and developed models, the following conclusions can be made:

- From the linear polarization resistance measurements, the corrosion rates for 13% chromium steels increases with the increase in chloride concentration and temperature however, it decreases with increase of pH values. This trend was observed in all series of experiments.
- Moreover from the linear polarization resistance measurements, the highest corrosion rates for 13% chromium steels were measured at the third series of experiments, in the presence of elemental sulfur at 75 ◦C, while the minimum

ones were measured at the first series of experiments, without any initial corrosion product layer on the sample surface at 25 ◦C.

- The fitness between measured and predicted corrosion rates results by curve fitting indicates a good correlation between experiments and developed model.
- The minimum deviation between predicted and measured data was obtained with ANN model, which is insignificant, compared to the deviation of the two other models from the measured data.

5.5. Acknowledgment

We acknowledge Seyedfakhreddin Nabavi for his comments on the model predicted by curve fitting and ANN.

5.6. References

[1] D. Colorado-Garrido, D. Ortega- Toledo, J. Hernandez, J. Gonzalez-Rodriguez, and J. Uruchurtu, "Neural networks for Nyquist plots prediction during corrosion inhibition of a pipeline steel," *Solid State Electrochem*, pp. 1715–1722, 2009.

[2] K. J.Lee, "A mechanistic modeling of CO_2 corrosion of mild steel in the presence of H_2S," PhD thesis, Ohio University, 2004.

[3] B. N. Brown, "The Influence of Sulfides on Localized Corrosion of Mild Steel," PhD thesis, Ohio University, 2013.

[4] S. Nesic, M. Nordsveen, N. Maxwell, and M. Vrhovac, "Probabilistic modeling of CO_2

corrosion laboratory data using neural networks," vol. 43, no. 2001, pp. 1373–1392, 2007.

[5] Y. Miyata, Y. Yamane, O. Forukimi, H. Niwa, and K. Tamaki, "Corrosion of new 13% Cr stainless steel OCTG in severe CO_2 environment," *NACE Int.*, 1995.

[6] H. Fang, "Investigation of localized corrosion of carbon steel in H_2S environments," PhD thesis, Ohio University, 2012.

[7] Y. Zheng, B. Brown, and S. Nesic, "Electrochemical study and modeling of H_2S corrosion of mild steel," *Corros. Sci.*, no. 2406, pp. 1–22, 2013.

[8] L. Khaksar and J. Shirokoff, "Effect of elemental sulfur and sulfide on the corrosion behavior of Cr-Mo low alloy steel for tubing and tubular components in oil and gas industry," *Materials (Energies)*, vol. 10, no. 4, p. 430, 2017.

[9] W. Sun and S. Nesic, "a Mechanistic model of H_2S corrosion of mild steel," *NACE Int.*, no. 7655, pp. 1–26, 2007.

[10] Y. Zheng, B. Brown, and S. Nesic, "Electrochemical study and modeling of H_2S corrosion of mild steel," *NACE Int.*, no. 2406, pp. 1–22, 2013.

[11] B. Soediono, "Kinetic of iron sulfide and mixed iron sulfide/carbonate scale precipitation in CO_2/ H_2S corrosion," *J. Chem. Inf. Model.*, vol. 53, p. 160, 1989.

[12] G. De Masi, R. Vichi, M. Gentile, R. Bruschi, and G. Gabetta, "A neural network predictive model of pipeline internal corrosion profile," in *First International Conference on Systems Informatics, Modelling and Simulation*, 2014.

[13] E. M. Rosen and D. C. Silverman, "Corrosion prediction from polarization scans using an artificial neural network integrated with an expert system," *Corrosion*, September, 1992.

[14] D. Sidorin, D. Pletcher, and B. Hedges, "The electrochemistry of 13% chromium stainless steel in oilfield brines," *Electrochim. Acta*, vol. 50, pp. 4109–4116, 2005.

[15] N. Chermat-aourasse and R. Kesri, "Corrosion-Electrochemical Behavior of 13 % Chromium (Cr) Martensitic Stainless Steel in Hydrochloric Acid (HCl) Solutions," *Corros. Prot. Mater.*, vol. 43, no. 4, pp. 372–380, 2007.

[16] H. Marchebois and H. E. L. Alami, "Sour service limits of 13% Cr and super 13% Cr

stainless steels for OCTG: effect of environmental factors," in *Corrosion Conference*, 2009, no. 9084, pp. 1–19.

[17] H. Fang, D. Young, and N. Srdjan, "Elemental sulfur corrosion of mild steel at high concentration of sodium chloride," in *17th international corrosion congress*, 2009, vol. 2592, pp. 1–16.

[18] J. Bojes, J. Lerbscher, W. Wamburi, and C. Dilley, "Elemental sulfur in 3-phase sour gas systems- Is condensate really your ally?," in *Northern area western conference*, 2010, pp. 1–22.

[19] C. Commons, *Optimization methods in management science/Operations research*. 2013.

[20] H. N. Koivo, "Neural network : Basics using Matlab neural network toolbox," 2008.

[21] L. Khaksar, G. Whelan, and J. Shirokoff, "Electrochemical and microstructural analysis of FeS films from acidic chemical bath at varying temperatures, pH, and Immersion Time," *Int. J. Corros.*, vol. 1025261, 2016.

[22] M. Saeed Akhtar, A. Alenad, and M. Azad Malik, "Synthesis of mackinawite FeS thin films from acidic chemical baths," *Mater. Sci. Semicond. Process.*, vol. 32, pp. 1–5, 2015.

[23] H. Fang, B. Brown, D. Young, and S. Nesic, "Investigation of elemental sulfur corrosion mechanisms," *NACE Int.*, no. 11398, pp. 1–13, 2011.

[24] K. Siva, N. Murugan, and V. Raghupathy, "Modelling, analysis and optimisation of weld bead parameters of nickel-based overlay deposited by plasma transferred arc surfacing," *Surf. Eng.*, vol. 1, no. 2009, pp. 174–182, 2009.

[25] A. Rajasekar, L. Rajendran, S. Maruthamuthu, N. Palaniswamy, and A. Rajendran, "Prediction of corrosion rate of steel AP5LX using curve fitting method," *Zast. Mater.*, vol. 47, pp. 47–50, 2006.

[26] Y. Shi, E. Tada, and A. Nishikata, "A Method for Determining the Corrosion Rate of a Metal under a Thin Electrolyte Film," *J. Electrochem. Soc.*, vol. 162, no. 4, pp. C135–C139, 2015.

[27] [Online] www.synergy.com/tools/curvefitting/.pdf. [Accessed: 14-June-2017].

[28] Z. Janicikova, O. Zimny, P. Kostial, “Prediction of metal corrosion by neural networks,” *Metalurgia*, vol. 52, no. 3, pp. 379–381, 2013.

[29] V. Alar, I. Žmak, B. Runje, and A. Horvatić, “Development of Models for Prediction of Corrosion and Pitting Potential on AISI 304 Stainless Steel in Different Environmental Conditions,” vol. 11, pp. 7674–7689, 2016.

[30] P. Potocnik, “Neural Networks : MATLAB examples,” 2012.

[31] “Levenberg-Marquardt backpropagation - MATLAB trainlm.” [Online]. Available: https://www.mathworks.com/help/nnet/ref/trainlm.html. [Accessed: 14-June-2017].

6. SUMMARY, CONCLUSIONS AND RECOMMENDATION

6.1. Summary

Due to the importance of corrosion on the lifetime of diverse equipment in the oil and gas industry, there have been efforts to investigate the effect and role of environmental parameters on the corrosion behavior of 4130 molybdenum steel and 13% chromium steel. A comprehensive assessment is provided to measure and monitor the corrosion process and material performance in different experimental conditions. The evolution of electrochemical behavior and main contributions in the area of corrosion assessment of alloy steels are investigated in this thesis. The effects of different environmental factors on corrosion behavior, the role of various corrosion product layers and analytical predictive models have been identified in various experimental conditions. The main ideas of the designed experiments include: (i) Electrochemical and microstructural analysis of FeS films from an acidic chemical bath at varying temperatures, pH and immersion times; (ii) Effect of elemental sulfur and sulfide on the corrosion behavior of Cr-Mo low alloy steel for tubing and tubular components in oil and gas industry; (iii) Effect of deposited corrosion product layers on electrochemical behavior of conventional 13% Cr steel exposed to a chloride containing environment, and (iv) Development of analytic models for the prediction of corrosion rate of 13% chromium steel exposed to different environmental conditions.

An acidic chemical bath is used to synthesize a thin layer of iron sulfide on the steel surface in the absence of H_2S in this work which is an experimental approach that will

benefit the oil and gas industry in terms of continuously improving corrosion resistance of material in a harsh and corrosive environment. Instead of dealing with H_2S safety issues, the utilization of the proposed technique to synthesize H_2S corrosion products layer on the steel surface simulates the real field conditions. This research also demonstrate the most accurate method for the corrosion modeling. Different analytical methods have been applied in order to predict the corrosion rate under various experimental conditions. Regarding the validation stage, the most accurate model has been identified and introduced for industrial applications. The findings from the experimental investigations are expected to highlight the fact that the complexity of data could be modeled only by a flexible network which covers all the measured data.

Finally this research aims to develop a model for the prediction of the internal corrosion rate which can also predict the influences of dissolved corrosion products, temperature, pH and chloride concentration on the corrosion rate of oil and gas pipelines.

6.2. Conclusion

The corrosion behavior of two type of steel alloys exposed to sulfide containing environment in various experimental condition were investigated. The experimental results showed how change of immersion time, pH, temperature, chloride concentration can affect the corrosion behavior of steel alloys and their final corrosion rate.

The mechanism of steel alloys corrosion in the presence of elemental sulfur was also studied in this research. The following conclusions can be obtained from the experimental results of each chapter:

6.2.1. Electrochemical and microstructural analysis of FeS films from acidic chemical bath

Considering the importance of corrosion products on the nature of corrosion behavior and the final corrosion rate, there have been efforts to simulate the production and formation of H_2S corrosion products on the alloy steel, for cases without H_2S in the experimental environment. Conducting the electrochemical and microstructural investigation of FeS in various experimental condition, provides a comprehensive idea how temperature, pH and immersion time can control the corrosion procedure.

Results show an increase of immersion time will affect the corrosion rate by increasing the likelihood of localize fracture of corrosion layers during the corrosion process. Also it could be concluded that the protective nature and composition of the corrosion products greatly depend on the pH of the solution where decreasing pH will gradually increase the corrosion rate.

Increasing the temperature could also accelerate the diffusion of species involved in electrochemical reactions and eventually affect the concentration of corrosion species by preferentially evaporating one or more species out of the solution, which could affect the final corrosion reaction.

6.2.2. Effect of elemental sulfur and sulfide on corrosion behavior of Cr-Mo low alloy steel

Regarding the presence of elemental sulfur in sour oil and gas services, numbers of experiments were conducted to analyze the electrochemical and microstructural behavior of Cr-Mo low alloy steel covered with a thin layer of elemental sulfur. According to the microscopic investigation, the texture of corrosion product layers are too porous and detached in the presence of elemental sulfur deposition. This fact leads to further corrosion of alloys steel due to the penetration of electrolyte solution through the microstructure of the steel surface. It was also illustrated that the iron sulfide corrosion product layers are more protective and adherent compared to the corrosion product layers of elemental sulfur. Results show pH plays the same role in the presence of either elemental sulfur or iron sulfide layer. At pH 2, a very thin and open structure layer formed, which could not display a protective role against corrosion, however, at pH 5, the corrosion product layer was more dense, adherent and protective due to a higher volume of precipitated products on the steel surface.

6.2.3. Effect of deposited corrosion product layers on electrochemical behavior of conventional 13% Cr steel

The martensitic stainless steels in oil and gas industry are some of the most reliable and applicable materials especially in sour service. This characteristic is obtained by the addition of a minimum of 11% chromium content to their composition. Various experiments were conducted to investigate the corrosion behavior of 13% chromium steel where its surface was pre-covered with iron sulfide or elemental sulfur. The results describe that elemental sulfur deposition could be more destructive compared to the iron sulfide deposition. In the case of iron sulfide deposition, the results prove that there is high possibility for the formation of protective corrosion layer on the surface, however, in the case of elemental sulfur deposition, this possibility reaches its minimum. In other word, the scaling tendency, the precipitation rate of the scale formed on the steel surface divided by the corrosion rate, significantly decreases in the presence of elemental sulfur and could not help to form a protective layer on the steel surface.

It is worth to note, despite the high corrosion resistance of chromium steel, its localized corrosion resistance will be affected by the addition of chloride ions to the electrolyte solution in high temperature. This fact illustrates the importance of the temperature on the process of corrosion product formation and precipitation on chromium steel in sour service, especially in the presence of elemental sulfur.

6.2.4. Development of analytic models for prediction of corrosion rate of 13% chromium steel

An analytical corrosion prediction model of 13% chromium steel in the presence of elemental sulfur and iron sulfide was developed. Three analytical approaches, optimal solution, curve fitting and artificial neural network, were examined to determine the most accurate method for the corrosion rate prediction in various experimental conditions. Regarding the percentage of error in each method, it was concluded that predicted data by the neural network has the minimum deviation from measured data among all three methods.

The model is capable of predicting the corrosion rate of iron sulfide and elemental sulfur film growth, the change in morphology of the film with respect to pH, temperature and salt concentration.

The model has been successfully validated with a number of carefully controlled corrosion experiments under different environmental parameters in elemental sulfur and iron sulfide conditions, as well as against experimental data in deposition free conditions.

The trends shown for the 13% chromium corrosion predictions agreed well with the general understanding of the corrosion process in the presence of elemental sulfur and iron sulfide films.

6.3. Recommendation

The present work investigates the electrochemical and corrosion behavior of alloy steels exposed to sulfide containing environment and also develop a corrosion rate prediction model in various environmental conditions. This study, however, can be extended further as suggested below to address the main limitations of the work, as identified in the following sections.

6.3.1. Electrochemical and microstructural analysis of FeS films from acidic chemical bath

According to this research, the only compound of iron sulfide formed in the acidic chemical bath was mackinawite. More investigation needs to be done in order to find out the experimental conditions, acidic chemical baths for which other compounds of iron sulfide will also form on the steel surface, since each kind of iron sulfide layer can significantly affect the corrosion bahviour of a given steel under environmental conditions this needs to be comprehensively investigated.

6.3.2. Effect of elemental sulfur and sulfide on the corrosion behavior of Cr-Mo low alloy steel in elevated temperature

The formation and stability of corrosion products in the presence of elemental sulfur and iron sulfide need to be investigated at elevated temperature, especially over a wider range of salt concentrations. According to this paper the trend of deposition and corrosion

product formation at elevated temperature is still confusing and there is no certain answer about how salt affects the electrochemical behavior of steel alloy in the presence of elemental sulfur.

6.3.3. Development of electrochemical investigation of conventional 13% Cr steel exposed to chloride containing environment

Numerous experiments have been conducted to investigate the localized corrosion of 13% chromium steel in sour systems. They described the effect of environmental factors on the corrosion behavior of steel however there are still lingering questions related to this topic that should be addressed such as the following questions:

How would different H_2S concentrations effect the passivation process of 13% alloy steel?

Does the surface ratio of elemental sulfur and steel specimen surface affect the corrosion behavior?

How to develop an analytical model to measure the sour corrosion of 13% chromium exposed to various environmental conditions.

6.3.4. Improvement of analytic models for prediction of corrosion rate of 13% chromium steel

New ideas can be applied to improve the developed model for further investigation. For instance, the ANN model can be improved by optimizing the network parameters such as number of hidden layers, type of hidden layers and their transfer functions, learning algorithms, changing the ratio of training and validation data. Also in order to increase the accuracy of the curve fitting and optimal solution models, conducting more experiments and increasing the number of input data for the model is recommended.